Erasmus MC
Universitair Medisch Centrum Rotterdam

Thoraxcentre

The 15th European Symposium on Ultrasound Contrast Imaging

- An ICUS Conference -

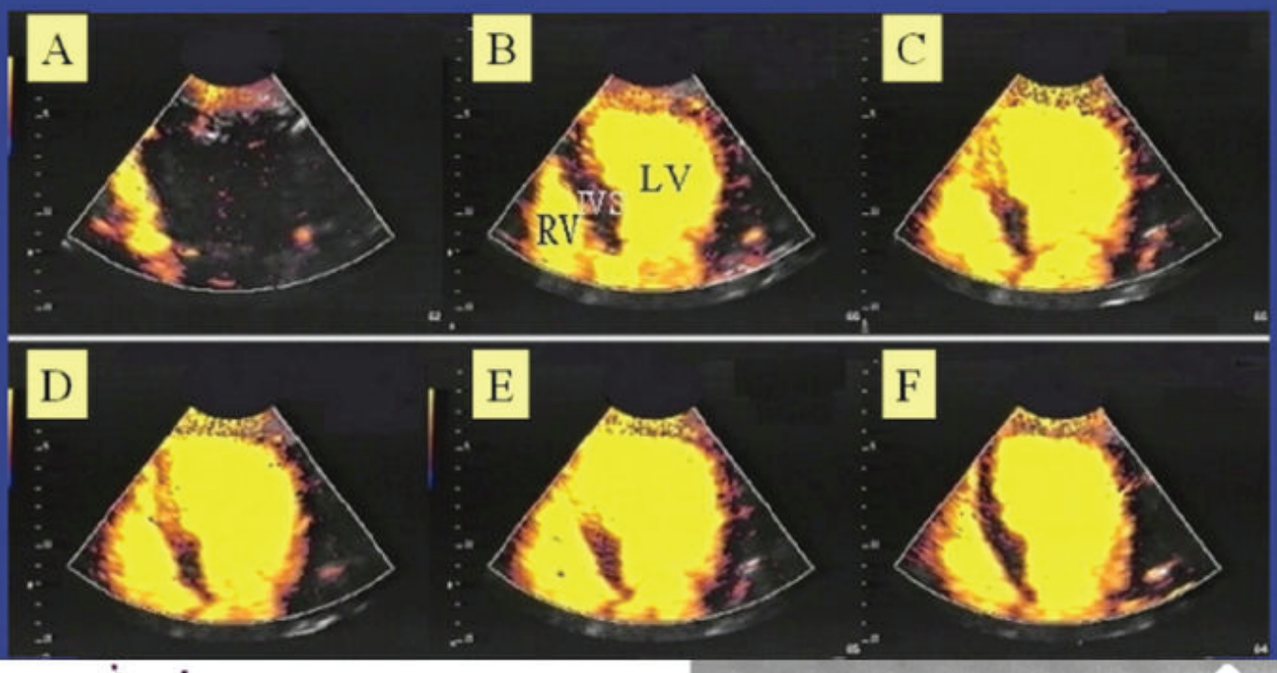

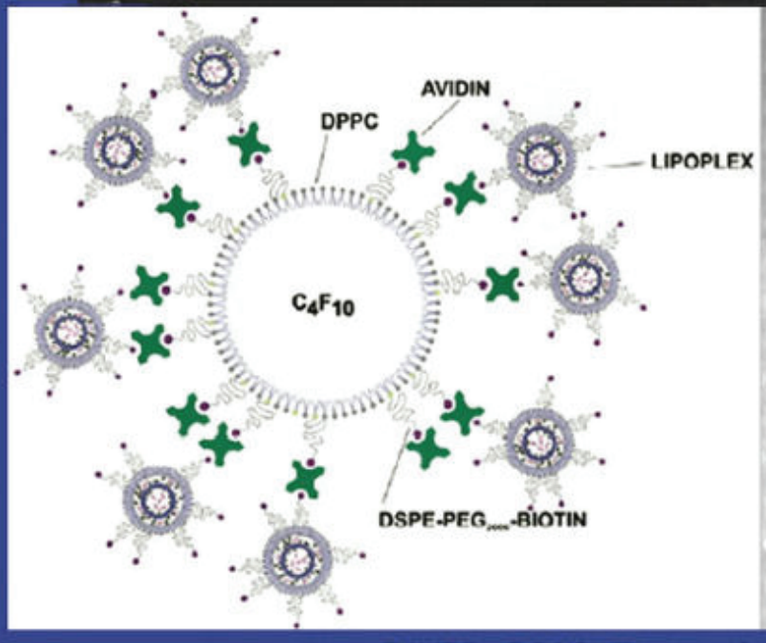

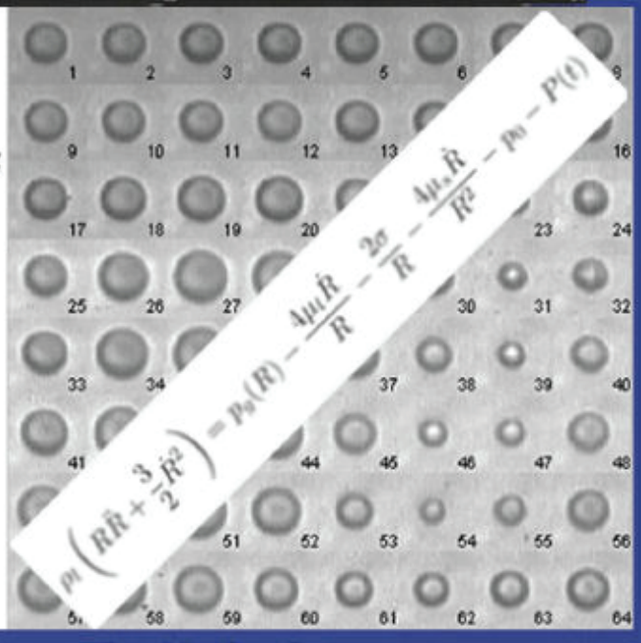

Abstract book

January, 21-22, 2010, Rotterdam, The Netherlands

Organized by Folkert ten Cate, Nico de Jong, Thomas Albrecht

Erasmus MC Rotterdam - University of Berlin

15th EUROPEAN SYMPOSIUM ON ULTRASOUND CONTRAST IMAGING
21-22 JANUARY 2010, Rotterdam, The Netherlands

WEDNESDAY, 20 January 2010

15.30 Defense Rik Vos (Erasmus University Woudestein)
Single microbubble imaging

18.00 - 20.00 Registration - Welcome Drinks – Posters ..... Hilton Hotel

THURSDAY, 21 January 2010

08.00 - 09.00 Registration

09:00 - 09:10 Introduction and opening ..... *Folkert ten Cate*

09.10 –10.40 GENERAL ULTRASOUND CONTRAST IMAGING . *Chairpersons: Folkert ten Cate / Ton van der Steen*

10.40 – 11.10 Intermission

11.10 – 12.40 ULTRASOUND CONTRAST THERAPY + MOLECULAR IMAGING *Chair: Steve Feinstein / Michel Versluis*

12.40 – 14.10 LUNCH

14.10 – 14.40 Coeur lecture ..... *Chairperson: David Cosgrove*

14.40 – 16.10 TECHNOLOGY 1 ..... *Chairpersons: Thomas Albrecht / Mark Monaghan*

16.10-16.40 Intermission

16.40 – 18.00 PROSTATE + RENAL APPLICATION ..... *Chairpersons: Hessel Wijkstra / Ferdinand Frauscher*

18.30 – 22.30 SOCIAL EVENT (Incl. Dinner buffet) 49

15th EUROPEAN SYMPOSIUM ON ULTRASOUND CONTRAST IMAGING
21-22 JANUARY 2010, Rotterdam, The Netherlands

FRIDAY, 22 January 2010

07.30 - 08.00 Registration

07.30 - 09.00 POSTER DISCUSSION A …….. .....*Moderator: Folkert ten Cate*

07.30 - 09.00 POSTER DISCUSSION B..... *Moderator: Nico de Jong*

15th EUROPEAN SYMPOSIUM ON ULTRASOUND CONTRAST IMAGING
21-22 JANUARY 2010, Rotterdam, The Netherlands

FRIDAY, 22 January 2010

Announcement of the winners of the Martin Blomley poster prize and the technical poster-prize.

3D Contrast Enhanced Stress Echocardiography

Dr Mark J Monaghan

Real-time three-dimensional stress echocardiography represents a major advance in the evaluation of ischemic heart disease. It has been performed with exercise and dobutamine with a high feasibility and good sensitivity and specificity for detection of angiographic coronary artery disease and has been combined with contrast to increase the visualization of segments at rest and during stress. Advantages of 3D for stress echocardiography include better visualization of the left ventricular apex, which is frequently foreshortened on standard two-dimensional apical images, very rapid acquisition of peak stress images before the heart rate declines in recovery, and the possibility to image segments from multiple planes using a single dataset. Disadvantages include a lower spatial resolution and lower frame rates for imaging. Moreover, only recently has 3D technology permitted side-by-side display of rest and stress images.

Contrast specific imaging modalities which have been available in 2D imaging systems for many years are now available on 3D systems. These modalities are extremely helpful in patients with sub-optimal image quality and may be used in both LVO and Low MI modes for MCE. Whilst the value of performing 3D LVO studies is pretty self evident, experience with 3D MCE is limited. It may be that this technology will be most useful during vasodilator stress studies.The incremental value of contrast to resting and stress 3D studies will be discussed in this presentation.

Why do we need to visualize microvessels in an atherosclerotic plaque? A pathologist view.

M.J.A.P. Daemen

Cardiovascular Research Institute Maastricht (CARIM) Universiteitssingel 50, 6229 ER Maastricht, The Netherlands Tel +31 43-3881766
Mat.Daemen@path.unimaas.nl

The clinical complications of atherosclerosis are caused by thrombus formation, which in turn results from rupture of an unstable atherosclerotic plaque. The formation of microvessels (angiogenesis) in an atherosclerotic plaque contributes to the development of plaques, increasing the risk of rupture. Microvessel content increases with human plaque progression and is likely stimulated by plaque hypoxia, reactive oxygen species and hypoxia inducible factor (HIF) signalling. The presence of plaque hypoxia is primarily determined by plaque inflammation (increasing oxygen demand), while the contribution of plaque thickness (reducing oxygen supply) seems to be minor. Inflammation and hypoxia are almost interchangeable and both stimuli may initiate HIF-driven angiogenesis in atherosclerosis.

Despite the scarcity of microvessels in animal models, atherogenesis is not limited in these models. This suggests that abundant plaque angiogenesis is not a requirement for atherogenesis and may be a physiological response to the pathophysiological state of the arterial wall. However, the destruction of the integrity of microvessel endothelium likely leads to intraplaque haemorrhage and plaques at increased risk for rupture. Although a causal relation between the compromised microvessel structure and atherogenesis or between angiogenic stimuli and plaque angiogenesis remains tentative, both plaque angiogenesis and plaque hypoxia represent novel targets for non-invasive imaging of plaques at risk for rupture, potentially permitting early diagnosis and/or risk prediction of patients with atherosclerosis in the near future.

Contrast enhanced ultrasound for intraductal application of contrast agent in obstructive diseases of the salivary glands

P. Zengel*1, V. Siedek*1, A. Berghaus*1, D.A. Clevert*2

**1 Department of Otorhinolaryngology, University of Munich, Germany*
**2 Department for Clinical Radiology, University of Munich, Germany*

Background: Obstructive diseases of the salivary glands are frequently caused by Sialolithiasis; however, 5-10% of the cases cannot be diagnosed by conventional radiological imaging or ultrasound. Using an intraductal application of a contrast agent may improve the ability to determine the origin and location of the impediment, help identify proper treatment, as well as allow for the tracking and evaluation of therapeutic effectiveness.

Material and Methods: The present study, performed on patients with obstructive diseases of the salivary glands, consisted of a conventional B-scan using an linear multifrequency probe (9 Mhz), followed by a second scan using an intraductal application of ultrasound contrast agent (SonoVue) on a high-end ultrasound (S2000, Siemens).

Subsequently, after completion of treatment, the procedure was repeated, and the results were compared with the subjective patient assessments.

Results: The procedure improved the accuracy of the diagnosis: in two patients a stone was detected that was not discovered by conventional ultrasound, and in five cases the duct stenosis was clearly observable which allowed the treatment to be adapted and more objectively evaluated.

Conclusion: Application of intraductal contrast agent as part of ultrasound assessment improves diagnostic capabilities in patients with obstructive salivary gland diseases and helps determine the best treatment. In comparison to MR-Sialography, the use of this method is inexpensive, fast, and reproducible, thus allowing its use as an objective measure of therapeutic effectiveness. Additionally, the examination could be applied as a periodic measure of functional recovery of the gland after conservative treatment by analysing glands parenchyma to legitimate the organ-preserving approach.

Lymphatic pathways visualization and sentinel node identification with harmonic imaging and second generation echoenhancer

R. Lanocita, L. Suman

Radiology Dpt. Fondazione "Istituto Nazionale Tumori di Milano"

Purpose: To evaluate visualization of lymphatic pathways and sentinel node after peritumoral injection of a second generation ultrasound echoenhancer.

Methods and Materials:

The study included 30 patient with indication for identification of sentinel node:

10 leg or arm melanomas;

5 penis carcinoma;

15 breast cancer.

All the patient gave written consent to the procedure. Golden standard (lymphoscintigraphy)has been used to compare results. Two different ultrasound equipments were used to identify sentinel nodes: Philips IU22 with a linear 9-3Mhz probe and an Esaote MyLab70Gold with a 9-4 linear transducer.

4.8ml of sonovue (Bracco, Milano, Italy) were injected peritumoral and the lymphatic pathways were followed until the sentinel node was visualized. At the same time and in the same site the technetium-labeled sulfur colloid was injected too and the sentinel node was found with the standard technique.

Results: There was only one case of discordance between ultrasound and scintigraphic identification. All the lymphatic ways wee explored until the first drainage node.

Conclusion: In expert hands ultrasonographic identification of sentinel node seems to be effective. Larger series of patient are needed to confirm the method.

PARAMETRIC IMAGING OF DYNAMIC VASCULAR PATTERNS OF FOCAL LIVER LESIONS IN CONTRAST-ENHANCED ULTRASOUND

Nicolas Rognin[1], Marcel Arditi[1], Laurent Mercier[1], Peter Frinking[1], François Tranquart[1]
Anass Anaye[2], Geneviève Perrenoud[2], Jean-Yves Meuwly[2]

[1] *Bracco Research S.A. – Geneva / Switzerland*
[2] *University Hospital – Lausanne / Switzerland*

Introduction: Characterization of focal liver lesions is presently the most important application of Contrast-Enhanced Ultrasound in Europe [1]. After a bolus injection of contrast agent, such a characterization is commonly guided by known Dynamic Vascular Patterns (DVP) of lesions with respect to surrounding healthy parenchyma. Figure 1(a) illustrates representative contrast-uptake kinetics as a function of time, expressed as instantaneous echo-power (arbitrary units), obtained after linearization of video signals. Hemangiomas (benign) are typically hyper-enhanced at all times, whereas hypervascular metastases (malignant) usually present a hyper-enhancement (except in possible necrotic areas) during the arterial phase followed by a hypo-enhancement in the later portal-venous phase (fast wash-out). To make these DVP signatures more conspicuous, we demonstrated in previous work [2] the clinical usefulness of subtracting, for each pixel signal, a reference signal derived from healthy parenchyma, as depicted in Figure 1(b). In this particular example, the difference signal in the hemangioma exhibits a unipolar vascular signature (strictly hyper-enhanced over time) whereas the hypervascular metastasis difference signal has a bipolar vascular signature.

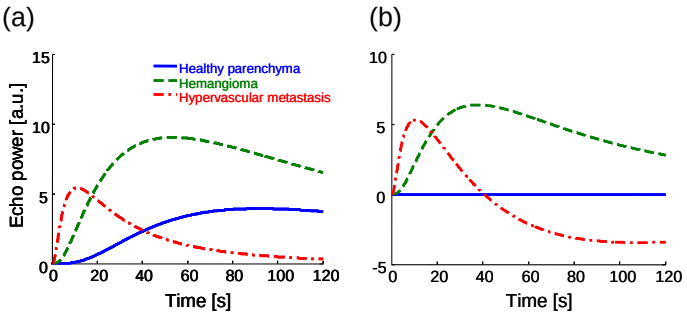

Figure 1: (a) Typical perfusion kinetics in healthy liver parenchyma (blue), in hemangioma (green) and in hypervascular metastasis (red), (b) difference signals after subtraction of the signal derived from normal parenchyma (reference).

Method: The objective of the present work was to develop a new parametric imaging technique, by mapping the vascular signatures into a single image, called DVP parametric image [3]. As summarized in Table 1, vascular signatures are categorized into four classes according to the polarities of their corresponding difference signals over time. Different color hues are used for displaying pixels in different classes: (1) green hues for unipolar positive (permanent hyper-enhanced signature); (2) blue hues for unipolar negative (permanent hypo-enhancement signature); (3) red hues for bipolar positive (hyper- followed by hypo-enhancement signature) and (4) yellow hues for bipolar negative (hypo-

followed by hyper-enhancement signature). Contrast-sequence analyses can thus be synthesized as spatial maps of vascular signatures, which may aid in the characterization of lesion types. Figure 3 shows how DVP parametric images allow facilitated lesion characterization as benign vs. malignant in four typical clinical examples, with the benign cases being colored differently from the malignant ones. The malignant lesions appear with the presence of red areas, unlike benign lesions, which appear green or green with yellow.

Table 1: Pixel classification list according to difference signal signatures with respect to healthy parenchyma.

Pixel class name	**Difference signal**	**Vascular signature**	**Color coding**	**Typically found in**
(1) unipolar positive	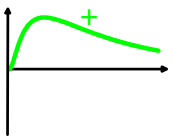	hyper-enhanced	green hues	benign lesions
(2) unipolar negative	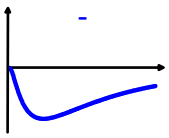	hypo-enhanced	blue hues	benign lesions
(3) bipolar positive	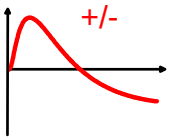	hyper-enhancement followed by hypo-enhancement	red hues	malignant lesions
(4) bipolar negative	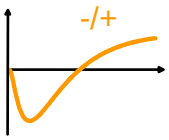	hypo-enhancement followed by hyper-enhancement	yellow hues	benign lesions

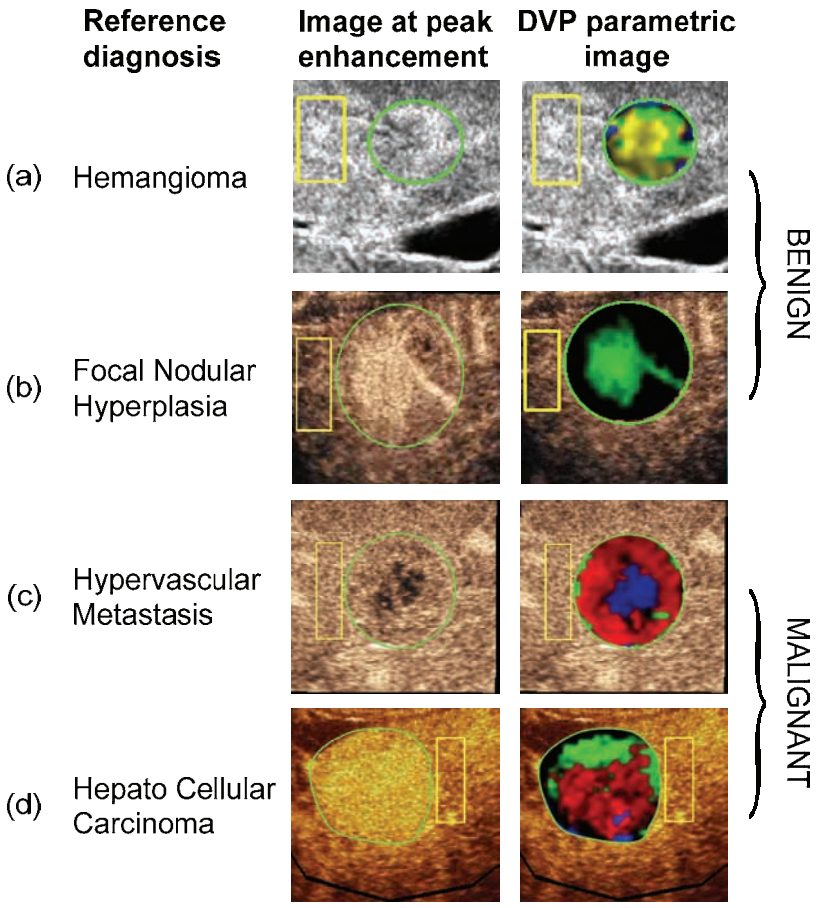

Figure 2: Typical clinical examples of DVP parametric images (right), with healthy parenchyma (reference) outlined in yellow regions of interest. Contrast images at peak enhancement (left) with Philips iU22 (a) and Siemens Sequoia 512 (b-d).

Results: The DVP parametric imaging technique was the object of a clinical assessment, including a total of 146 focal liver lesions (113 malignant and 33 benign), imaged with real-time low-MI contrast specific ultrasound after a bolus injection of 2.4 ml of SonoVue®. The reference diagnosis was provided by either CT, MRI or biopsy. The DVP parametric images were read by a blinded clinician who used the presence of red colorization as a criterion of malignancy. The resulting sensitivity and specificity were 97% and 91%, respectively.

Discussion and conclusion: The high efficacy scores obtained with DVP parametric imaging demonstrate the potential of the method for increasing confidence in characterizing focal liver lesions. They compare favorably with those published in the literature (sensitivity and specificity of 91% and 86%, respectively [4]). In addition to a very simple interpretation (the presence of red areas being an indicator of malignancy), this technique has the advantage of being less time-consuming than the usual procedure of reviewing entire sequences of contrast images (~2 minutes). In further work, automatic segmentation of normal parenchyma will be studied, as a way to reduce operator-dependent variability

in the resulting parametric maps, thus approaching true Computer-Aided Diagnosis of FLL by contrast ultrasound. In the future, 4D contrast imaging is likely to become more prevalent. As the review of such sequences may become rather tedious, the extension of DVP parametric imaging to volumetric data may represent a very valuable tool to clinicians. This aspect will be the object of a further study.

References

[1] EFSUMB Study group, "Guidelines and good clinical practice recommendations for Contrast Enhanced Ultrasound (CEUS) – Update 2008", Ultraschall in Med, 29:28-44, 2008.

[2] Rognin N., Frinking P., Messager T., Arditi M., Perrenoud G. and Meuwly J.-Y. "A New Method for Enhancing Dynamic Vascular Patterns of Focal Liver Lesions in Contrast Ultrasound", IEEE Ultrasonics Symp. Proc., 2007 © IEEE. doi: 546-549

[3] Rognin N, Mercier L, Frinking P, Arditi M, Perrenoud G, Meuwly J-Y, "Parametric imaging of dynamic vascular patterns of focal liver lesions in contrast-enhanced ultrasound", IEEE Ultrasonics Symp. Proc., 2009 © IEEE. doi: (in press).

[4] Leen E., Ceccotti P., Kalogeropoulou C., Angerson W., Moug S., Horgan P., "Prospective Multicenter Trial Evaluating a Novel Method of Characterizing Focal Liver Lesions Using Contrast-Enhanced Sonography", American Journal of Roentgenology, 186(6):1551, 2006.

The Effects of Platelet versus Fibrin Targeted Microbubbles on the Success of Ultrasound and Microbubble Mediated Thrombolysis

Feng Xie, Shunji Gao, Luke Drvol, John Lof, Omaha, NE;, UNIV NEBRASKA MED CTR, Omaha, NE; Patrick G Rafter, Philips Healthcare, Andover, MA; Evan Unger, NuvOx Pharma, Tuscon, AZ; Terry Matsunaga, Univ of Arizona, Tuscon, AZ; Thomas R Porter, UNIV NEBRASKA MED CTR, Omaha, NE

Background.

Although ultrasound and intravenous microbubbles (MB) have been used in recanalizing intravascular thrombi,the success of the technique may require targeting techniques to either platelets or fibrin. The purpose of this study was to examine the effects of platelet versus fibrin targeting on the ability of diagnostic ultrasound and MB to dissolve thrombi without the aid of a fibrinolytic agent.

Methods.

A total of 130 porcine arterial thrombi of varying age (3 or 6 hours) were treated with guided high mechanical index (MI) impulses (1.1 MI) from a three-dimensional (3D) ultrasound. Occlusive thrombi were embedded in branching silastic vessels (2 mm internal diameter) suspended in a tank containing water at 37º C. Flow within the vessel was monitored using a flow pump (MasterFlex). A tissue-mimicking phantom (TMP) of varying thickness (5-10 cm) was placed over the thrombosed vessel and the 3D (X 3-1 xMATRIX array) transducer (Philips iE 33) aligned with the thrombosed vessel using a positioning system. Diluted lipid encapsulated MB (0.5%; NuVox Pharma) that were either non-targeted or targeted to either the fibrin or glycoprotein 2b/3a receptor) were imaged with each transducer using low MI imaging (Power Modulation) at <0.2 MI which then guided the timing of the high MI impulses (>1.0) with either transducer. Total treatment time was 10 minutes. Percent thrombus dissolution (%TD) was calculated by comparison of clot mass before and after treatment.

Results.

Both non-targeted and targeted microbubbles were more effective than 3D ultrasound alone in dissolving thrombi ($p<0.05$; for both fibrin, platelet, and non-targeted microbubbles versus ultrasound alone; Figure). Platelet targeting increased the degree of thrombus dissolution of three hour old arterial thrombi at five centimeter thick TMP ($p <0.05$ when compared to non-targeted microbubbles), but were not more effective than non-targeted microbubbles at a greater TMP thickness or with older age thrombi (p=NS).

Conclusions.

Guided high MI impulses combined with platelet or fibrin- targeted microbubbles improve thrombus dissolution for fresh thrombi , but lose this effectiveness with greater attenuation of the ultrasound beam or with older age thrombi.

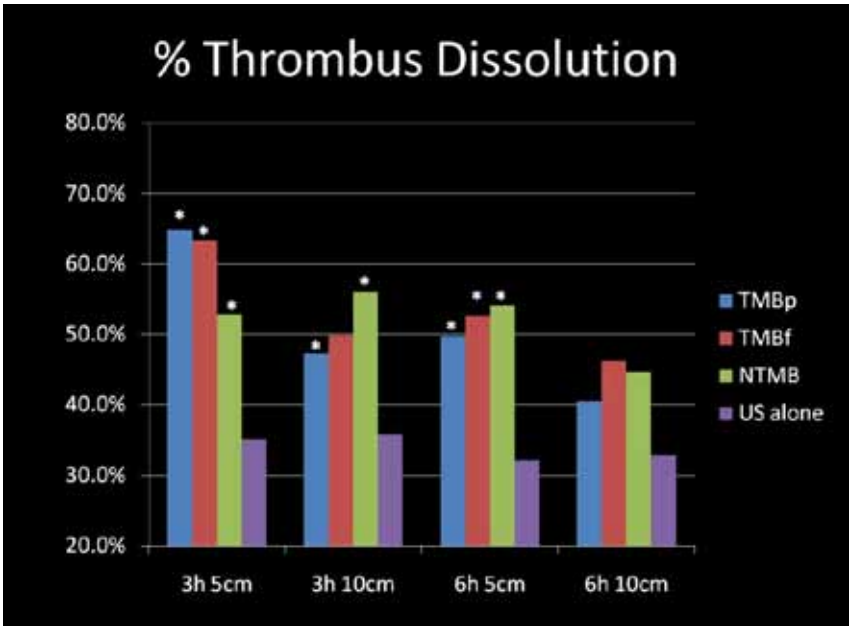

Abbreviations:
TMBp = fibrin-targeted microbubbles; TMBf = fibrin-targeted microbubbles
NTMB= non-targeted microbubbles

Directing adipose derived stem cells to the area at risk in the heart after myocardial infarction using targeted microbubbles

- Development of a new molecular therapeutic technique -

A. van Dijk[1,6], BA. Naaijkens[1,6,7], TJA. Kokhuis[2,7], M. Harteveld[2], RJP. Musters[3,6], VWM. van Hinsbergh[3,6], M. Helder[4], O. Kamp[5,6,7], N. de Jong[2,6], HWM. Niessen[1,2], LJM. Juffermans[3,5,6,7]

[1]Dept. of Pathology, VU University Medical Center, Amsterdam, the Netherlands; [2] Dept. of Biomedical Engineering, Thorax Centre, Erasmus Medical Centre, Rotterdam, the Netherlands; [3]Dept. of Physiology, VU University Medical Center, Amsterdam, the Netherlands; [4]Dept. of Orthopaedic Surgery, VU University Medical Center, Amsterdam, the Netherlands; [5]Dept. of Cardiology, VU University Medical Center, Amsterdam, the Netherlands; Institute for Cardiovascular Research, VU University Medical Center, Amsterdam, the Netherland; [7]Interuniversity Cardiology Institute of the Netherlands, Utrecht, the Netherlands

Stem cell therapy is a promising tool to restore contractile function after myocardial infarction. However, recent clinical trials show rather disappointing results with only minor improvements in cardiac function. Therefore, stem cell research needs to return from bed to bench.

The major problem with stem cell therapy is the lack of persistence of sufficient numbers of stem cells at the site of injury. Less than 3% of the cells remain at the infarction site after injection, independent of the route of administration. It is not known what exactly happens to the other cells, because it is difficult to track these cells in vivo directly after injection.

This project aims to overcome this problem by specifically targeting the stem cells to the area at risk after myocardial infarction. Adipose-derived stem cells will be coupled to contrast microbubbles, this stem cell-bubble complex will be targeted to specific molecules on endothelium of the injured vessel wall, illustrated in figure 1. This will result in larger quantities of stem cells in the area at risk, thereby improving regeneration of the heart. Besides the possibility of carrying targeting ligands on the microbubbles, the presence of microbubbles has two other main functionalities:

1) Microbubbles can be pushed towards the vessel wall using the radiation force of diagnostic ultrasound. This acoustic radiation force can also be applied to the stem cell-bubble complex, thereby facilitating the binding of the stem cell-bubble complex to the endothelium.

2) Imaging and tracking of individual stem cell-bubble complexes with contrast-enhanced ultrasound, to investigate the fate of the stem cells after injection.

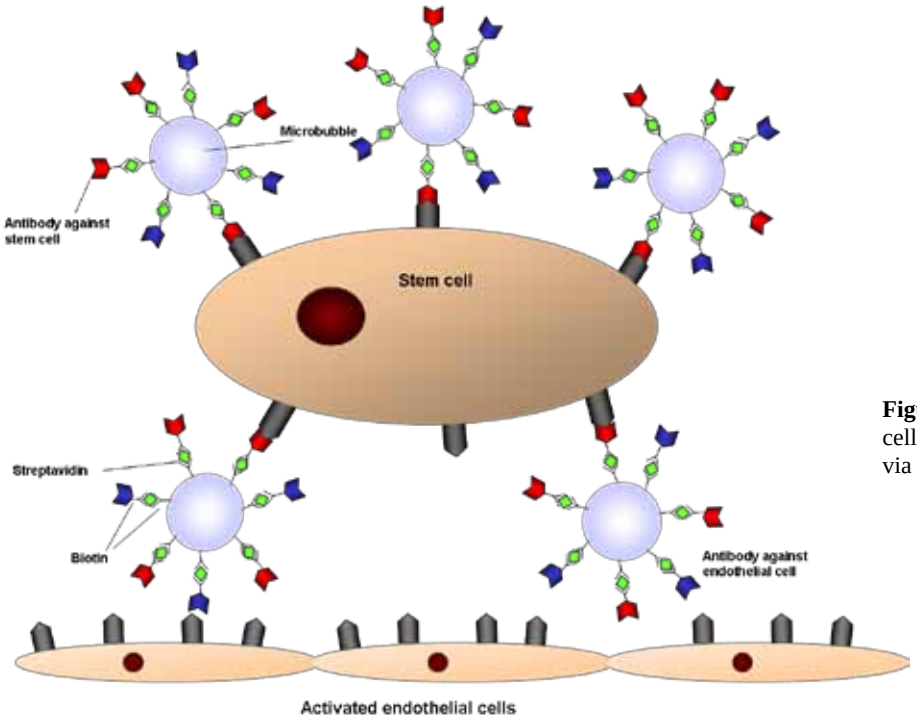

Figure 1: Schematic drawing of a stem cell coupled to activated endothelial cells via dual-targeted microbubbles

Advances in Microbubble Applications for Treatment of Brain Disease

Stephen Meairs, MD, PhD

Department of Neurology, Universitätsmedizin Mannheim
Heidelberg University, 68167 Mannheim, Germany

A promising research application with high translational capacity is ultrasound-targeted drug delivery to the brain. Most substances and drugs that would be potentially useful for treatment of a variety of brain disorders cannot be applied due to their inability to penetrate the blood-brain barrier (BBB) of the neurovascular unit (NVU). This is particularly true for large-molecule agents such as monoclonal antibodies, recombinant proteins, or gene therapeutics. Ultrasound can facilitate drug delivery into the brain. Moreover, if microbubbles are combined with ultrasound exposure, the BBB can be opened transiently by focusing ultrasound to the blood vessels with considerably lower acoustic pressures. We have recently demonstrated successful delivery of brain-derived neurotrophic factor for manipulation of endogenous stem cells using focused ultrasound and BG6895 microbubbles. Recently, highly innovative microbubbles carrying nanoparticle-loaded agents have been developed. In combination with BBB opening, this new targeting strategy will allow non-invasive therapies to the brain with substances such as immunoglobulins, viral vectors, plasmid DNA, siRNA, mRNA and high molecular weight drugs. We have applied this approach by targeting gene therapy to the brain with AAV vectors coupled to these new nanoparticles.

Although it appears that minimal tissue damage occurs at appropriate acoustic power thresholds, safety remains a concern. Our recent work demonstrates that BBB opening with ultrasound and microbubbles affects information transfer between brain cells, in particular through alterations in gap junctions. BBB opening in the rat leads to reorganization of gap junctional proteins in both cortical neurons and astrocytes, as characterized by Connexin36 and Connexin43 expression, respectively. These changes may be a cellular response to imbalances in extracellular homeostasis following blood-brain barrier leakage. Moreover, we have shown that ultrasound-mediated BBB opening leads to an increased ubiquitinylation of proteins in neuronal but not glial cells as soon as six hours after insonation. These results suggest that BBB opening with ultrasound and microcubbles induces a specific cellular stress response restricted to neuronal cells. Whether such responses are model-specific or can be reduced by further optimizations in microbubble and ultrasound parameters require further studies.

Improved treatment of ischemic stroke with ultrasound and microbubbles in combination with thrombolytic drugs shows great promise, but the optimal techniques, indications, and contraindications

have not yet been well defined. In vitro results suggesting that stabile cavitation may be more effective than inertial cavitation for clot lysis have recently found support in a new mouse ischemic stroke model employing focused ultrasound at low acoustic pressure in combination with novel therapeutic microbubbles and t-PA. Application of ultrasound and microbubbles without lytic drugs may be suited for hyperacute stroke treatment, since it appears that ultrasound may activate endogenous t-PA. Moreover, targeting thrombus with specific immunobubbles may improve the efficacy of sonothrombolysis. Another recent approach for clot lysis utilizes high intensity focused ultrasound in combination with MRI (MRgFU) for targeting and monitoring of therapy. First results demonstrate rapid lysis without thrombolytic drugs. Interestingly, this technology may have application for treatment of intracerebral hemorrhage, i.e. removal of coagulated blood. Clinical outcome following sonothrombolysis also may be related to other ultrasound bioeffects including BBB disruption, drug transport, perfusion alteration, and angiogenesis. Safety remains a major concern in the further development of ultrasound-enhanced thrombolysis and further animal work is required to define the most promising methods for translation into a human application. Here mathematical simulations may provide important information for fine tuning of ultrasound and microbubble parameters.

MOLECULAR IMAGING OF ANGIOGENESIS WITH BR55: A VEGFR2-TARGETED ULTRASOUND CONTRAST AGENT

***Sibylle Pochon*[1], *Isabelle Tardy*[1], *Thierry Bettinger*[1], *Philippe Bussat*[1], *Radhakrishna Pillai*[2], *Mathew von Wronski* [2], *Martine Theraulaz*[1], *Patricia Emmel*[1], *Nathalie Biolluz*[1], *Sylvie Pagnod-Rossiaux*[1] *and Michel Schneider*[1]**

[1]*Bracco Research S.A., Geneva, Switzerland;* [2]*Bracco Research USA, Princeton, NJ, USA*

Introduction: Angiogenesis is the growth of new capillary blood vessels. This process occurs during development, reproduction, and wound healing but also in pathological conditions like tumor growth [1]. One of the most important molecular markers of angiogenesis is the vascular endothelium growth factor receptor 2 (VEGFR2) which expression on the surface of endothelial cells has been linked to the progression and aggressiveness of many tumor types [2]. BR55 is an ultrasound contrast agent designed for the molecular imaging of human VEGFR2 (KDR). A common strategy for preparing targeted contrast agents is to couple specific biotinylated antibodies to streptavidin-functionalized microbubbles [3-6]. Although, these products are very convenient for proof-of-concept studies in animals, they are not suitable for a human use due to the risk of initiating an immune response. BR55 is a phospholipid-based contrast-agent functionalized with a KDR-specific binding peptide [7]. A phospholipid conjugate of the targeting peptide was designed to be incorporated in the microbubble membrane [8].
This study describes the evaluation of the binding efficiency of BR55 *in vitro* and its capacity for imaging angiogenesis *in vivo* in rat tumor models.

Methods: BR55 microbubbles were evaluated on recombinant proteins and on cells expressing VEGFR2 to demonstrate their binding efficiency. Specificity for the VEGF receptor-2 was determined in competition experiments. Molecular imaging of VEGFR2 was performed with BR55 in orthotopic rat tumor models using contrast-specific imaging mode at low acoustic power. Imaging experiments were performed with BR55, SonoVue® and streptavidin-functionalized microbubbles coupled to an anti-VEGFR2 antibody to compare the behavior of the three contrast agents.

Results: Although selected for the human receptor, the VEGFR2-binding peptide was also shown to recognize the rodent receptor (Flk-1). Strong binding of BR55 microbubbles was observed on the immobilized recombinant human and mouse receptors as well as on human and mouse endothelial cells. BR55 binding was competed off by VEGF and blocked by KDR- or Flk-1-specific antibodies; thereby demonstrating the specificity of the interaction.

Comparable contrast enhancement was observed in tumors at peak intensity for BR55 and SonoVue®. Then, once unbound microbubbles had cleared from the circulation, a strong enhancement of the tumor was obtained with BR55 whereas no significant microbubble accumulation was detected with SonoVue. Ten minutes after BR55 injection, the enhancement in the tumor was significantly superior to that observed in the healthy tissue. The enhancement obtained with BR55 in the tumor was not significantly different from the one observed with antibody-coupled streptavidin microbubbles.

Conclusion: BR55, a VEGFR2-targeted ultrasound contrast agent, was shown to specifically recognize the marker of angiogenesis and to be able to highlight malignant lesions by specific accumulation on the tumoral endothelium. The information provided by molecular imaging combined with the assessment of tumor perfusion may be of primary interest for characterizing tumor phenotype and monitoring tumor response to therapy.

These results validate the concept of a targeted contrast agent based on a lipopeptide construct and open the way for clinical applications.

References:

[5] P. Carmeliet "Angiogenesis in life, disease and medicine," Nature, vol. 438, pp. 932-936, 2005.

[6] D. J. Hicklin and L.M. Ellis."Role of the vascular endothelial growth factor pathway in tumor growth and angiogenesis," J. Clin. Oncol., vol. 23(5), pp. 1011-27, 2005.

[3] G. Korpanty , J. G. Carbon, P. A. Grayburn, et al. "Monitoring response to anticancer therapy by targeting microbubbles to tumor vasculature," Clin. Cancer Res., vol. 13, pp. 323-330, 2007.

[4] J. K. Willmann, R. Paulmurugan, K. Chen, et al. "US imaging of tumor angiogenesis with microbubbles targeted to vascular endothelial growth factor receptor type 2 in mice," Radiology; vol. 246, pp. 508-518, 2008.

[5] M. Palmowski, B. Morgenstern, P. Hauff, et al. "Pharmacodynamics of streptavidin-coated cyanoacrylate microbubbles designed for molecular ultrasound imaging," Invest. Radiol., vol. 43, pp. 162-169, 2008.

[6] A. Lyshchik, A. C. Fleischer, J. Huamani, et al. "Molecular imaging of vascular endothelial growth factor receptor 2 expression using targeted contrast-enhanced high-frequency ultrasonography," J. Ultrasound Med., vol. 26, pp. 1575-1586, 2007.

[7] A. Shrivastava, M. A. von Wronski, A. K. Sato, et al. "A distinct strategy to generate high-affinity peptide binders to receptor tyrosine kinases," Protein Engineering, Design & Selection, vol. 18, pp. 417–424, 2005.

[8] Pillai R, Marinelli E, Fan H et al. A phospholipid-PEG2000-conjugate of a KDR-targeting heterodimer peptide for contrast enhanced ultrasound imaging of angiogenesis. Bioconjugate Chem. Submitted forpublication.

Tumor cell killing efficiency of doxorubicin-liposome loaded microbubbles after ultrasound exposure

***Lentacker I.*, Geers B., Demeester J., De Smedt S.C., Sanders N.N.**

Ghent Research Group on nanomedicine, Department of pharmaceutical sciences, Ghent University, Harelbekestraat 72, 9000 Gent, Belgium

Aim

The aim of this study was to design doxorubicin (DOX)-liposome loaded microbubbles and evaluate their tumor cell killing efficiency in vitro.

Results

DOX-liposome loaded microbubbles were prepared by attaching Doxil-like liposomes to the surface of lipid microbubbles via avidin-biotin interaction **(Figure 1)**.

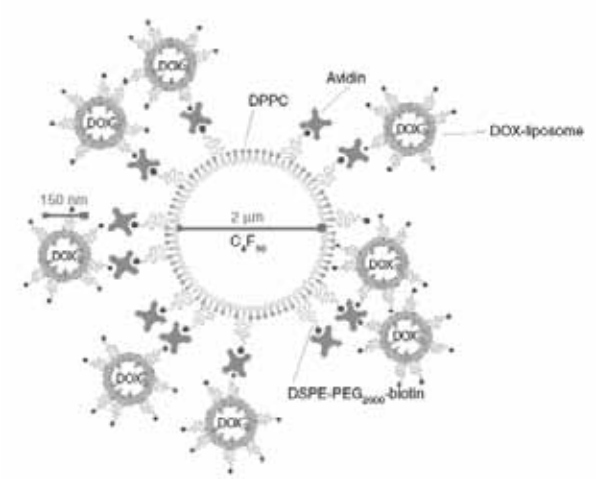

Figure 1

Melanoma cells were seeded in Opticells and exposed to DOX-liposomes and DOX-liposome loaded microbubbles without and with ultrasound exposure (USE) (1MHz, 50%DC, 30s). Exposure of the cells to DOX-liposome loaded microbubbles resulted in a much higher tumor cell killing efficiency than exposure to DOX-liposomes (**Figure 2**). We did not see an outspoken improvement of cell killing by DOX-liposomes when ultrasound was applied.

We also studied the intracellular localization of DOX after 4 hours incubation time with DOX-liposomes or DOX-liposome loaded microbubbles and USE. The DOX was almost exclusively present in the nuclei of cells treated with DOX-liposome loaded microbubbles, whereas the DOX was found in both, cytoplasm and nucleus of cells treated with DOX-liposomes (**Figure 3**). Additional experiments revealed that at least two different mechanisms are responsable for the high tumor cell killing efficiency of DOX-liposome loaded microbubbles after USE. During implosion of the microbubbles, liposomes

are damaged and free DOX is released, which is immediately taken up through cell membrane perforations.

Reference

Lentacker I., Geers B., Demeester J., De Smedt S.C., Sanders N.N. Design and evaluation of doxorubicin containing microbubbles: cytotoxicity and mechanisms involved. Molecular Therapy advance online publication. July 21th 2009. Doi: 10.1038/mt.2009.160

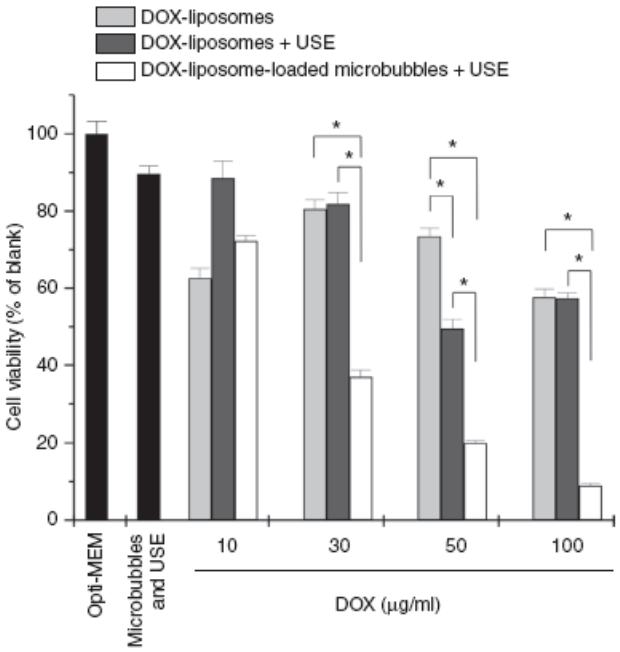

Figure 2

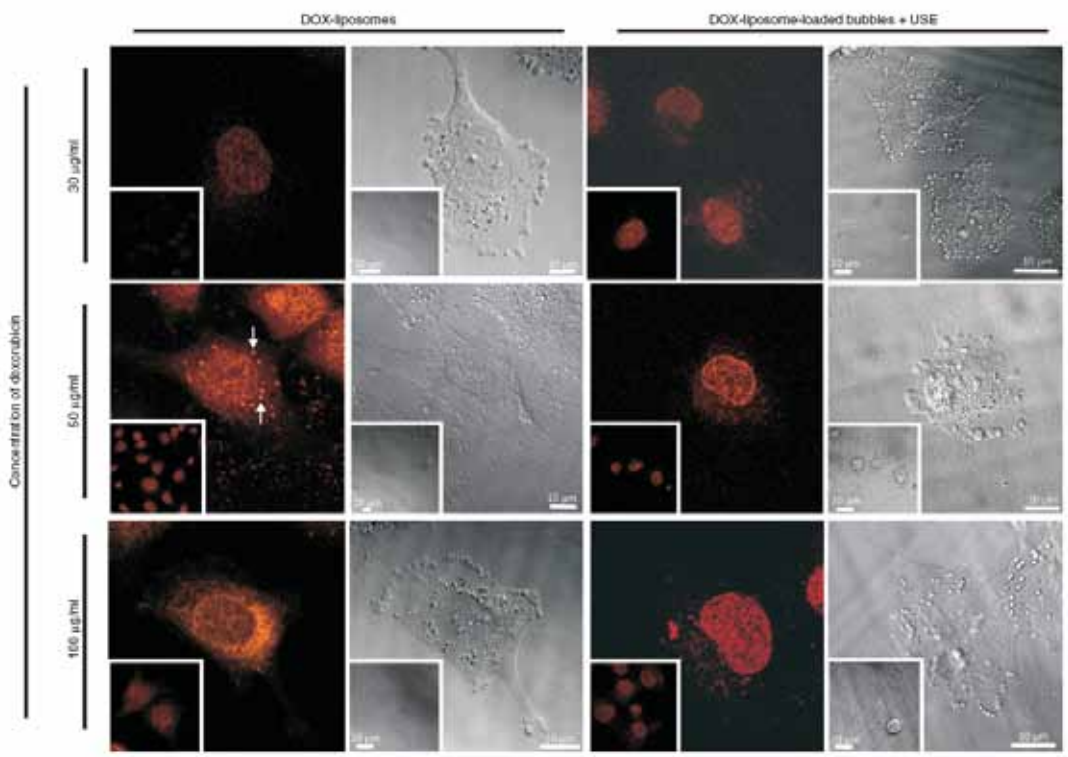

Figure 3

Role of CEUS in Endovascular Aneurysm Repair (EVAR) procedures and during the follow-up

D.A. Clevert

Department of Radiology, Klinikum Grosshadern, University of Munich, Munich, Germany

Abnormalities of the abdominal aorta may represent a diagnostic challenge in patients both with acute and chronic clinical symptoms. In addition to the examination using color coded duplex ultrasound, contrast enhanced ultrasound (CEUS) with low-mechanical-index (low MI) may contribute in achieving a precise diagnosis. Most of these patients will be treated by endovascular aneurysm repair. Endoleaks following endovascular aneurysm repair (EVAR) are common. Contrast-enhanced ultrasound (CEUS) is a promising new method for the diagnosis and follow-up of endoleaks. CEUS with SonoVue® allows a rapid and noninvasive diagnosis in the follow-up after EVAR. The sensitivity and specificity of conventional ultrasound, compared to the MS-CTA is estimated up to 33-63% and 63-93%. These values can be increased through the use of CEUS in up to 98-100% (sensitivity) and 82-93% (specificity).
This presentation describes the etiology, classification and importance of different abnormalities of the abdominal types and endoleaks. The value of CEUS in this clinical scenario will be discussed.

Convertible Liquid Droplets for Ultrasound Contrast

Nikita Reznik1, Ross Williams2, Naomi Matsuura1,2 and Peter N. Burns1,2

[1]University of Toronto, Toronto, Canada
[2]S*unnybrook Health Sciences Centre, Toronto, Canada*

One of the strengths of microbubbles is that their relatively large size confines them to the intravascular space, offering many opportunities to make measurements that are difficult to achieve with the diffusible tracers for other imaging modalities. But their size also creates some important limitations in their potential application. For example, bubbles cannot be used to sense changes in vascular permeability, nor be usefully associated with ligands which target sites outside the vascular system. Furthermore, potentiation of ablative therapies like HIFU with bubbles is complicated by the fact that the bubbles fill the perfused space in normal tissue at the same time that they are present in the target lesion.

Although it is quite difficult to make bubbles as small as the 200nm or so required for extravasation, it is possible to make emulsions of liquid droplets of this size with relative ease. Such droplets, even of low acoustic velocity liquids such as perfluorocarbons (PFC), scatter only weakly and have been shown to behave linearly at least up to about 50MHz (1). They would therefore need to be present in high concentrations in tissue or blood to be detectable and are thus are not promising as ultrasound contrast agents. However, if droplets are made of PFC liquids that have a boiling point near that of the ambient temperature, they can be vaporised by exposure to ultrasound energy. Thus nano- (or, more accurately, submicron-) droplets could be injected, diffuse selectively into tissue fed by hyperpermeable vessels such as tumour vessels, then be converted into vapour by ultrasound activation. The resulting gas may be detectable using conventional pulse-echo, by acoustic emission or, if we are lucky, by nonlinear resonant oscillation. If this goal could be achieved, droplets could be attached by ligands to extravascular targets which could then be detected or might be activated into gas which potentiates ultrasound therapy at the focus of the HIFU beam without affecting thermal absorption elsewhere in tissue. Our investigations centre on the objective of formulating and understanding the physical behaviour of activated droplets. We study the size, stability and echogenicity of the microbubbles newly created from emulsions of differing PFC liquids, coated with a surfactant shell. We use optical and acoustic methods to study properties which are needed for successful nonlinear ultrasound imaging in the first second after conversion.

Methods

Droplets of dodecafluoropentane (DDFP) coated with fluorosurfactant (Zonyl FSP), with diameter of 415 ± 20 nm, were vaporised in a 200 μm polyethylene tube with a single 10-cycle pulse from a focused 7.5 MHz transducer. Subsequent acoustic detection was performed with a series of 10-cycle pulses at 1.75 MHz and peak negative pressure (Pneg) of 120 kPa, at times from 1ms to 1s after

excitation. Converted droplets were also studied under a microscope (4 pixels per micron resolution) connected to a camera (which in Rotterdam we must call low speed) operating at 1000 fps for time periods of up to 1s after excitation.

Results

Echoes from droplets excited at Pneg > 1.7 MPa showed a significant increase in power at both the fundamental (1.75MHz) and second harmonic (3.5MHz) bands 1ms after excitation, indicating phase conversion and subsequent resonant oscillation (Fig. 2). Typical power spectra of low intensity detection pulse echoes from the droplet sample before and after excitation are shown in Fig. 3. There is a significant increase in both the fundamental (1.75 MHz) and the 2nd harmonic (3.5 MHz) component of the detected signal. In addition, the signal spectrum changes over time during the 1s time interval after excitation. The power spectrum of the echo detected 200 ms after excitation exhibits a further increase in the fundamental component. However, the power in the 2nd harmonic band is reduced. The characteristic increase in power of the fundamental band and decrease in power at the harmonic band is apparent in approximately the first 100 ms. After this initial evolution, the signal appears to be relatively stable for the following 900 ms. Fig. 4 shows the relative integrated backscatter from the droplet sample and pulse-inversion imaging power as a function of time. It is apparent that while the acoustic cross section is increased, integrated pulse-inversion power seems to decrease. The overall increase in echogenicity

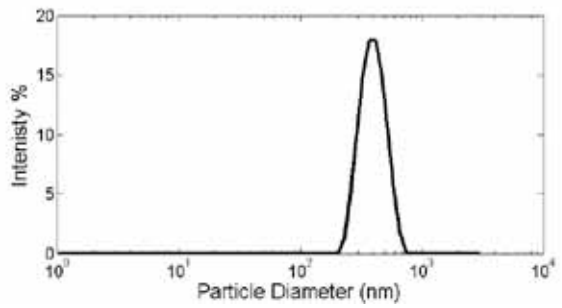

Figure 1. Size distribution of the droplet suspensions measure with dynamic light scattering. Mean droplet diameter prior to

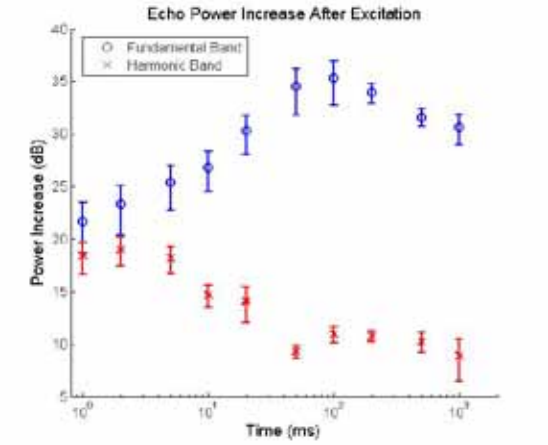

Figure 2. Power in the fundamental and harmonic bands of the scattered detection signal and different time points.

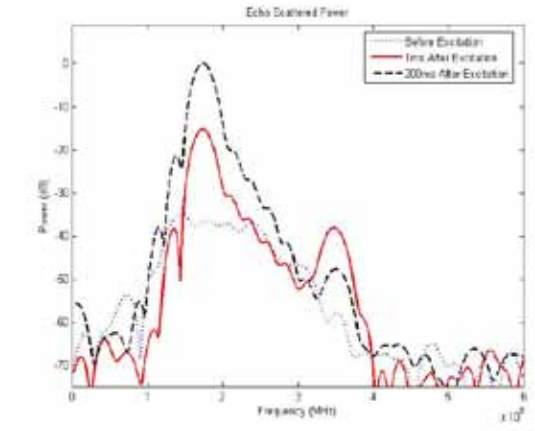

Figure 3. Power spectra of the low intensity detection signal scattered from the droplet sample before and after excitation.

suggests inception of ultrasound scatterers such as microbubbles in the sample as a result of the high intensity excitation ultrasound pulse. The increase in the 2nd harmonic band suggests the the newly created bubbles oscillate nonlinearly. Change in the scattered echo over time is characteristic of evolution in size distribution of the bubble populations. The decrease in the nonlinear response of the bubbles suggests that bubbles might grow through their resonance size, associated with the frequency of the detection pulse (1.75 MHz). Optical observations will be shown which seem to confirm this.

The ability of post-conversion droplets to scatter ultrasound non-linearly allows use of contrast specific imaging techniques, such as pulse inversion imaging, along with high intensity acoustic excitation for droplet detection in diagnostic applications. Moreover, simultaneous acoustic cross section increase and power decrease in the 2nd harmonic band in the first 1 s after conversion is different from the usual behaviour of commercially available microbubble contrast agents. Such characteristic behaviour might be used to develop an imaging technique with both regular and nonlinear B-mode for converted-droplet-specific imaging.

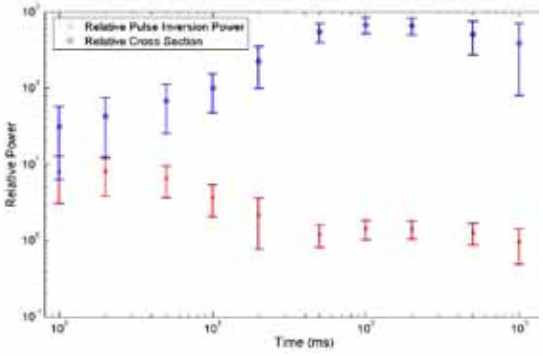

Figure 4. Relative acoustic cross section and pulse-inversion processed echo power as a function of time for post-conversion droplet sample.

Discussion

Suspensions of submicron DDFP droplets were successfully stabilised by fluorosurfactant coating through the process of high pressure emulsification. Droplets remain in liquid form when raised to 37°C in a superheated state.

External agitation by high intensity ultrasound pulse triggers the droplets to undergo phase change, expanding by approximately 5 times in diameter, effectively converting into microbubbles. In the first 100 ms after vaporisation, the bubbles experience additional size increase due to uptake of dissolved gas from the surround liquid, causing a further 4x increase in the bubble diameter. After the initial growth, the bubbles were shown to remain stable for time periods of at least 900 ms, rendering them sufficiently stable to be applicable for diagnostic ultrasound imaging.

Post-conversion droplets experience a significant increase in echogenicity. Vaporised droplets were shown to scatter ultrasound both in the fundamental and the harmonic bands of the incident pulse, enabling their detection with nonlinear imaging techniques. Furthermore, bubble growth due to uptake of gas from the host liquid induces a characteristic change in acoustic properties of the bubbles, increasing the acoustic cross-section while simultaneously decreasing nonlinear scattering power. Converted droplets may not only increase contrast in the regions of interest on an ultrasound image, but might also be selectively detected with a converted droplet specific imaging technique.

STEM CELL TRACKING USING ULTRASOUND

Flordeliza S. Villanueva , Huili Fu, Jianjun Wang, Xioping Leng, Andrew Fisher, and Xucai Chen

Center for Ultrasound Molecular Imaging and Therapeutics
University of Pittsburgh Medical Center , Pittsburgh, PA

BACKGROUND: The acute and long-term location and viability of stem cells (SCs) used in reparative cardiovascular therapies is poorly understood due to the limited methods available for safely and non-invasively serially tracking the cells *in vivo*. It is hypothesized that ultrasonic SC tracking is achievable using mesenchymal stem cell (MSC)-internalized, slowly degrading, polymer microbubbles (MBs).

METHODS: Human-bone marrow derived MSCs were cultured to confluence and dwelled with perfluorocarbon gas-filled Bodipy-labeled polymeric microbubbles for 14 hours, washed to remove free MBs, and trypsinized for acoustic testing in suspension. MB-labeling of MSCs was confirmed by confocal microscopy. Acoustic activity was confirmed by spectral analysis of free MB, control MSCs (not exposed to MBs), and MB-labeled MSCs responding to 2.5MHz tone-burst ultrasound at various powers and with second harmonic and contrast pulse sequence (CPS) imaging at 7MHz and a mechanical index of 0.97. Video intensity was averaged over 25 frames per capture. A LIVE/DEAD Viability kit and flow cytometry were subsequently used to confirm viability.

RESULTS: Spectral analysis of signals from free MB and MB-labeled MSC suspensions demonstrated non-linear acoustic behavior attributable to their sustained gas content. Control MSCs displayed only low linear acoustic behavior. Confocal microscopy exhibited several MBs associated to most MSCs. Flow cytometry confirmed viability of 95% of MB-MSC complexes, which was no different from control MSCs. Video intensity of MB-labeled MSCs was significantly higher than control MSCs in both harmonic (18.10±6.82 vs. 2.42±1.21, respectively, $p<0.01$) and CPS (18.98±2.93 vs. 0.39±0.20, respectively, $p<0.005$) images.

CONCLUSIONS: Using a polymer contrast agent microbubble label, we have developed a method for visualizing MSCs with non-linear clinical ultrasound. For *in vivo* application, MSC labeling by MBs is theorized to permit the retention of acoustic activity and cell viability once the stem cells have been accepted by a host tissue. Because the MBs degrade slowly, this approach may permit non-invasive serial *in vivo* tracking of MSC fate over a protracted period, and thus facilitate optimization of cell therapy strategies.

Experimental investigation of microbubble response to ultrasonic pulses used in therapeutic applications

Christophoros Mannaris[1], Kypros Stylianou[1], Nico de Jong[2] and Michalakis Averkiou[1]

1-Dept. of Mechanical and Manufacturing Engineering, University of Cyprus, Nicosia, Cyprus
2-Dept. of Biomedical Engineering, Thoraxcentre, Erasmus MC, Rotterdam, The Netherlands

Introduction

Research interest in the area of ultrasound contrast agents is shifting towards therapeutic applications such as targeted drug delivery, gene and DNA transfection [1], sonothrombolysis [2], and sonoporation [3]. To date however, the microbubble response to therapeutic-type excitations has not been studied in detail and it is not well understood. Often the conditions used in published works are simply a case of trial and error during which the microbubbles are subjected to pulses ranging from a few cycles [1] up to several thousand cycles [4].

In the present work, we present an in-vitro experimental method developed to examine the response of microbubbles to ultrasonic pulses of various amplitudes, pulse duration and pulse repetition frequency (PRF) in an attempt to find the optimal conditions to use in therapeutic applications. Two in-vitro setups are considered, a) with the microbubbles freely suspended in deionized water and b) with the microbubbles enclosed in a capillary.

Materials and methods

A schematic of the ultrasonic enclosure designed to accommodate two single element circular transducers (Panametrics-NDT, Waltham, Massachusetts, USA) is shown in figure 1. A focused 1.0 MHz transducer was used as the transmitter and another 2.25 MHz as the receiver. Care was taken so that the foci of the two transducers are placed in the same spot. An acoustic absorbing material lined the walls to minimize reflections and contamination of the scattered signal from microbubbles. In the setup with freely suspended microbubbles, a dilute concentration (36 bubbles/μL) of SonoVue (Bracco, Geneva, Switzerland) was used in order to achieve response from single microbubbles. Before each excitation, the solution was stirred and allowed to settle, enough for the bubbles to stop moving but not float. In the capillary setup, the microbubbles were allowed to flow in a 200 μm acoustically transparent cellulose capillary which was placed at the overlapping foci of the two transducers. This setup was designed to better imitate in-vivo conditions of microbubbles flowing in the microcirculation. Before each excitation, the flow was stopped for the bubbles to remain still inside the capillary. The pulse settings studied are: number of cycles (10-2000), MI (0.05-1.1) and PRF (0.05-1.0 KHz). For all

experiments, an iU-22 scanner (Phillips, Bothell, WA, USA) was used to verify the uniformity of the solution. An example of the microbubble-filled capillary moments after a therapy pulse is fired is shown in fig.2. The area where the bubbles were destroyed is marked with a circle.

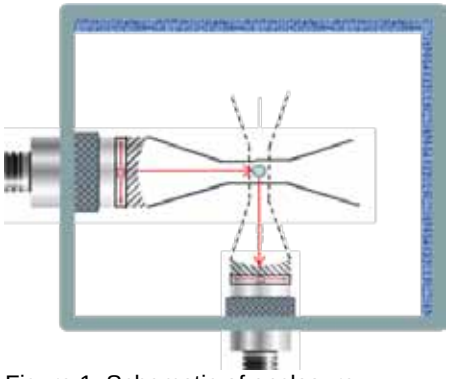

Figure 1: Schematic of enclosure

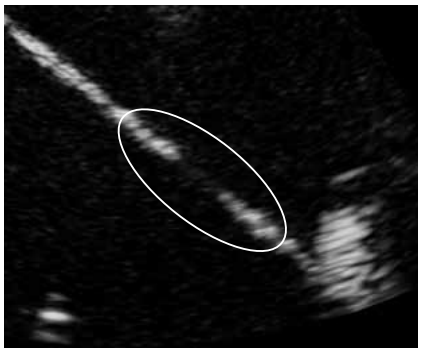

Figure 2: Microbubble disruption in capillary due to therapy pulse firing

Data analysis and results

The response of freely suspended microbubbles to a series of 1 MHz, 10-cycle tone bursts spaced 20 ms apart (PRF = 50 Hz) is shown in figure 3. MI 0.1, 0.2 and 0.4 are shown in fig.3 (a)-(c), respectively. The horizontal axis is time in milliseconds and the vertical axis is the scattered intensity in mV. At MI 0.1, the amplitude of response remains unaltered suggesting that the microbubble remained intact for the duration of the experiment. At MI 0.2, there's a gradual decrease in amplitude of the response, suggesting disruption of the microbubble and gradual diffusion of the gas. Finally at MI 0.4, there is no response from the 2nd burst (detected signal is a reflection from the walls) suggesting that the microbubble is destroyed by the 1st pulse and completely diffuses away within 10 ms.

The response of microbubbles to such short tone bursts is of course very well known and previously published. The response to much longer pulses similar to those used in therapy, however, is not yet clearly understood. Figure 4(a) shows the response to a series of 500-cycle bursts at MI 0.2. At this pressure, bubble destruction and gradual diffusion is expected. Instead the signal seems to increase with time. Microbubbles are probably moving from the perimeter to the center of the detection area. Similar results that suggest motion of the microbubbles were seen even at lower pressures. The bubble response to 500-cycle bursts of MI 0.1 and 2000-cycle bursts of MI 0.05 are shown in figs. 4 (b) and (c), respectively. At such low pressures, the scattered signal intensity was expected to stay constant throughout the experiment instead of fluctuating considerably as seen in the figures. Microbubbles that move in and out of the center of the detection area can explain the fluctuations in both these cases. The motion of microbubbles during these therapy-type excitations can be attributed to acoustic streaming, the motion of the fluid in the direction of propagation of the sound [5]. Streaming was verified with ultrasound imaging where video loops of moving microbubbles during the excitations have been

recorded. Since any motion of the microbubbles during an excitation affects the results, longer bursts using the freely suspended microbubbles setup were not investigated.

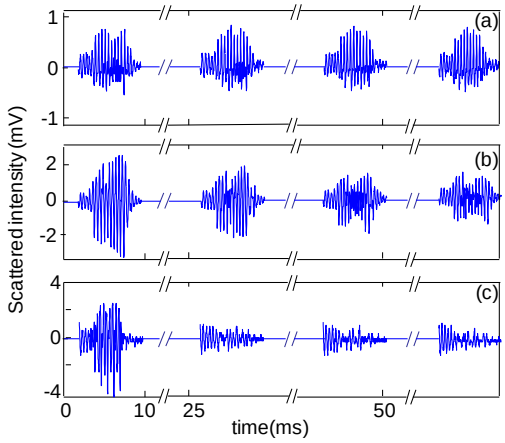

Figure 3: Scattered response for 1.0 MHz, 10 cycles, MI (a) 0.1, (b) 0.2, (c) 0.4

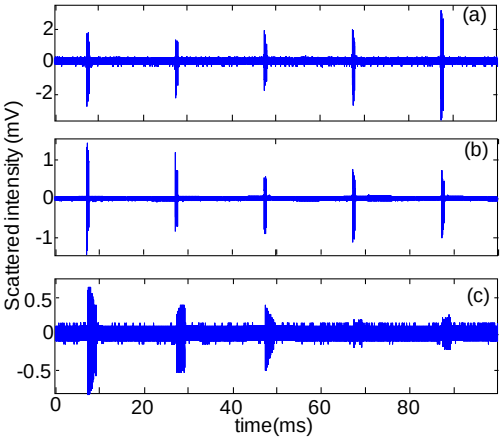

Figure 4: Streaming; (a) 500 cycles, MI 0.2, (b) 500 cycles, MI 0.1 and (c) 2000 cycles, MI 0.05

Streaming is successfully eliminated in the capillary setup and thus longer tone burst may be investigated. The capillary set-up better resembles in-vivo conditions where streaming does not occur in the microcirculation and microbubbles flowing in capillaries are not allowed to be "pushed" by the ultrasound. Figure 5 shows the response of microbubbles in the capillary to a series of 200-cycle tone bursts spaced 10 ms apart (PRF=100 Hz). MIs 0.1, 0.2 and 0.4 are shown in fig. 5 (a)-(c) respectively. In a similar fashion to the freely suspended bubbles, we observe that MI 0.1 is non-destructive (intensity remains constant with time), MI 0.2 is semi-destructive (intensity gradually decreases), and MI 0.4 is highly destructive (bubble disappears by the 2nd pulse). At MI 0.4 the bubble scattered signal disappears completely half-way through the 1st pulse (i.e. within 100 cycles or 100 μs). Two regions are selected within the 1st pulse, one at the beginning and one at the end. A Blackman-Harris window is applied to the selected regions and their frequency content is plotted. The time domain and frequency spectrum of the first region is shown in figs. 5(d) and (e), respectively whereas the spectrum of the 2nd region is shown in fig. 5(f). The absence of higher harmonics in fig. 5(f) verifies that the bubbles in the detection area have been destroyed.

Discussion The response of microbubbles to a large range of pulse settings has been studied in two different experimental setups: (a) with the microbubbles freely suspended in deionized water and b) with the microbubbles enclosed in a capillary. We have shown that acoustic streaming occurs in the freely suspended microbubbles setup (during long, high energy pulses) and induces motion of the microbubbles that affects the results. Experimental setups similar to the one described here where the

microbubbles are freely suspended in a medium (e.g. microbubbles in opti-cell) probably suffer from the similar problems.

Enclosing the microbubbles in a cellulose capillary eliminates acoustic streaming and allows a more accurate observation and measurement of the bubble response, while at the same time closely resembles the in-vivo scenario of microbubbles in the microcirculation. An MI less than 0.2 was found to be non-destructive while destruction begins at an MI 0.2. At MIs greater than 0.4, the microbubbles were destroyed and diffused within 100 cycles or 100 μs irrespective of the pulse length (number of cycles). Hence a question arises whether the use of longer ultrasound pulses at such high pressures is beneficial or not. The results shown in the present work refer to Sonovue. Experiments with polymer shelled and drug loaded microbubbles are underway.

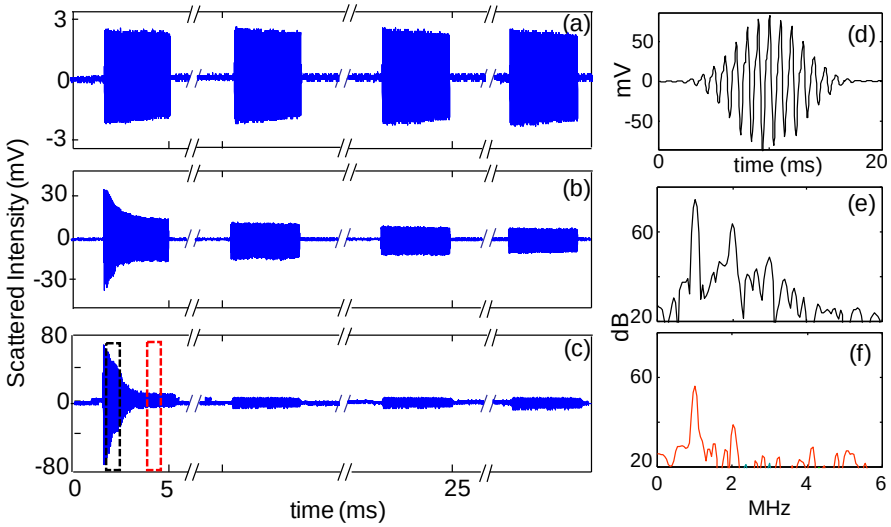

Figure 5: 200 cycles, PRF=100 Hz, MI = 0.1(a), 0.2(b), 0.4(c). (d)-(e) time domain and spectrum of 1st selected region of pulse at MI 0.4, (f) spectra of 2nd selected region

References

[1] P. A. Dijkmans, L. J. Juffermans, R. J. Musters, A. van Wamel, F. J. ten Cate, W. van Gilst, C. A. Visser, N. de Jong, and O. Kamp, "Microbubbles and ultrasound: from diagnosis to therapy," *Eur J Echocardiogr*, vol. 5, pp. 245-56, 2004.

[2] C. A. Molina, M. Ribo, M. Rubiera, J. Montaner, E. Santamarina, R. Delgado-Mederos, J. F. Arenillas, R. Huertas, F. Purroy, P. Delgado, and J. Alvarez-Sabin, "Microbubble administration accelerates clot lysis during continuous 2-MHz ultrasound monitoring in stroke patients treated with intravenous tissue plasminogen activator," *Stroke*, vol. 37, pp. 425-9, 2006.

[3] A. van Wamel, K. Kooiman, M. Harteveld, M. Emmer, F. J. ten Cate, M. Versluis, and N. de Jong, "Vibrating microbubbles poking individual cells: drug transfer into cells via sonoporation," *J Control Release*, vol. 112, pp. 149-55, 2006.

[4] A. Ghanem, C. Steingen, F. Brenig, F. Funcke, Z. Y. Bai, C. Hall, C. T. Chin, G. Nickenig, W. Bloch, and K. Tiemann, "Focused ultrasound-induced stimulation of microbubbles augments site-targeted engraftment of mesenchymal stem cells after acute myocardial infarction," *J Mol Cell Cardiol*, vol. 47, pp. 411-8, 2009.

[5] H. C. Starritt, F. A. Duck, and V. F. Humphrey, "An experimental investigation of streaming in pulsed diagnostic ultrasound beams," *Ultrasound Med Biol*, vol. 15, pp. 363-73, 1989.

SPECT/CT Imaging and Quantification of Focused Ultrasound Induced Extravasation

Sanches, Pedro[1]; Rossin, Raffaella[2]; Böhmer, Marcel[2]; Tieman, Klaus[3]; Grüll, Holger[1, 2]

[1]Biomedical NMR, Eindhoven University of Technology; [2]Biomolecular Engineering, Philips Research Eindhoven; [3]Department Cardiology and Angiology, Hospital University Muenster

Introduction: Focused ultrasound allows to locally trigger drug delivery with a high spatial control. Circulating ultrasound contrast agents (microbubbles) burst upon focused ultrasound exposure, which leads to transient openings in the endothelium and creates transient pores in cell membranes. These effects allow for extravasation of macromolecular drugs into surrounding tissues and/or uptake into cells that otherwise would be confined to the vascular system (Ferrara 2008). The temporal evolution and fate of the pores in the endothelial barrier is not well known but indications are obtained that the effect lasts for more than 1 hour (Hancock *et al.* 2009). In this study we used small animal Single Photon Emission Computed Tomography/Computed Tomography (SPECT/CT) to image and quantify the kinetics of extravasation of radiolabeled albumin in skeletal muscle in mice, after treatment with focused ultrasound and microbubbles.

Methods: Bovine serum albumin coupled to diethylene triamine pentaacetic acid groups (DTPA-BSA) was synthesized and radiolabeled with ^{111}In for use as an extravasation agent. Microbubbles were used at a concentration of $1x10^9$ microbubbles/mL in saline. The ultrasound setup consisted of a focused ultrasound probe (Therapy and Imaging Probe System, Philips) with a focus of 1x1x6mm which was used under ultrasound image guidance (HDI5000, Philips). All experiments were performed on female Swiss mice weighing 24 to 30g.

Immediately after microbubble intravenous bolus injection (50µL) the hind limb skeletal muscle in mice was exposed to focused ultrasound (1.2MHz, 2MPa, 10000cycles, Pulse Repetition Frequency 0.2Hz). Approximately 20 minutes after ultrasound treatment, 30 to 50MBq of ^{111}In-DTPA-BSA (200µg) were intravenously injected followed by SPECT/CT scans at different time points. A *post-mortem* biodistribution study was performed for every animal.

Results: 7 minutes post-injection (p.i.) of radiolabeled albumin, localized extravasation of albumin can be imaged with SPECT. Consecutive scans show an increase in signal in the treated area up to 60min p.i. (Figure 1). Biodistribution data show values of up to 3.2 %ID/g accumulation in treated areas and 0.2 %ID/g in control areas, leading to a ratio treated/non-treated muscle of approx. 16.

Conclusions: Our results demonstrate that non invasive imaging of ultrasound-induced extravasation in mice with SPECT/CT is a useful tool as it allows to image extravasation and to follow the kinetics of the process. Another important finding is that localized extravasation of albumin (~7nm) increases over a period of 1h after ultrasound treatment, as evidenced by SPECT imaging.

Results show that SPECT is a useful tool to follow and quantify ultrasound induced drug delivery *in vivo* in combination with radiolabeled drugs. This important tool will be used in future preclinical studies to probe the time and size characteristics of pores in the endothelial barrier and relate them to the respective ultrasound delivery characteristics.

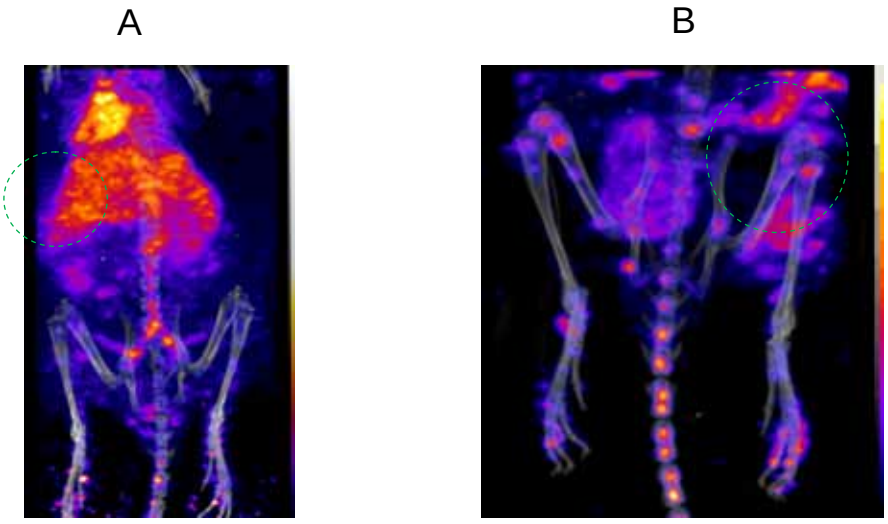

Figure 1. SPECT/CT images**.** A – dynamic scan 7min p.i. B – static scan 1h p.i. Green circle marks treated area in left limb. Notice signal difference to the same area in right limb

- Ferrara, KW, Driving delivery vehicles with ultrasound. Adv Drug Delivery Rev **2008**, 60 (10), 1097-1102
- Hancock, H. A.; Smith, L. H.; Cuesta, J.; Durrani, A. K.; Angstadt, M.; Palmeri, M. L.; Kimmel, E.; Frenkel, V., Investigations into pulsed high-intensity focused ultrasound-enhanced delivery: preliminary evidence for a novel mechanism. *Ultrasound Med Biol* **2009,** 35, (10), 1722-36.)

This study is part of the FP7 European Project Sonodrugs (ref. 213706).

The origin of “compression only” and enhanced subharmonic behaviour of phospholipid-coated ultrasound contrast agent microbubbles

Jeroen Sijl, Marlies Overvelde, Benjamin Dollet, Valeria Garbin, Timo Rozendal, Nico de Jong, Detlef Lohse and Michel Versluis

Unlike tissue, coated microbubbles are able to scatter sound subharmonically. Therefore, subharmonic behavior of coated microbubbles can be used to enhance the contrast in ultrasound contrast imaging. We present a study into the origin of the subharmonic and “compression only“ behavior of phospholipid coated microbubbles. The Brandaris ultrahigh-speed camera is exploited to investigate the effect of the amplitude and the frequency of the driving pressure on both the subharmonic and “compression only” behavior of individual differently sized BR14 (Bracco Research S.A., Geneva, Switzerland) coated microbubbles with initial radii between 2.2 and 4.8 micrometer. The experimental results show that the phospholipid shell of the microbubbles induce “compression only” behaviour and can enhance subharmonic behavior of coated bubbles as compared to uncoated bubbles. Subharmonic oscillations are observed to occur already for driving pressures as low as 5 kPa. This is in contradiction with the assumption that the damping induced by the phospholipid shell reduces this non-linear behavior. An explanation is presented for the enhanced subharmonic and “compression only” behavior of phospholipid coated bubbles. Through a weakly non-linear analysis of a general form of the numerical model describing the dynamics of coated bubbles it is shown that a shell elasticity that rapidly changes with bubble oscillation amplitude enhances both the subharmonic and “compression only”behavior. This rapid change in elasticity is hypothesized to result from the 3D-collapse of the phospholipid monolayer coating of the bubble, i.e. buckling of the phospholipid shell. The agreement that is found between the experimentally determined radial dynamics and the numerical model of Marmottant *et. al.*[1] that takes into account the buckling of the shell confirms this hypothesis. The comparison between the numerical model and the experimental results shown that both the subharmonic and “compression only” behavior of phospholipid coated microbubbles are strongly determined by the initial surface tension of the phospholipid coated microbubble. A bubble with an initial surface tension close to zero, i.e. a bubble of which the surface is initially completely saturated with phospholipids shows strong subharmonic and “compression only” behavior at low acoustic driving pressure amplitudes. In contrast, a bubble of which the surface is initially unsaturated with phospholipids shows no subharmonic behavior and less “compression only” behaviour.

1) *P. Marmottant, S. van der Meer, M. Emmer, M. Versluis, N. de Jong, S. Hilgenfeldt, and D. Lohse, "A model for large amplitude oscillations of coated bubbles accounting for buckling and rupture", J. Acoust. Soc. Am. 118, 3499 – 3505 (2005).*

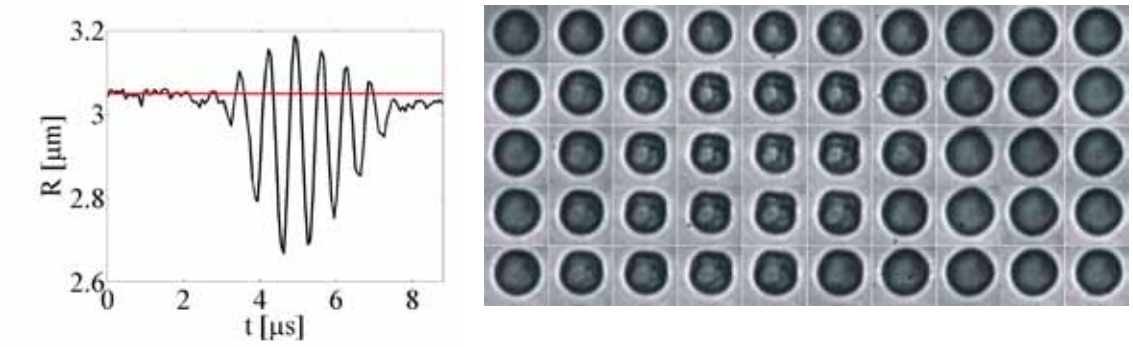

An example of the radial response of a phospholipid coated microbubble, recorded with the Brandaris ultrahigh-speed camera, showing "compression-only" behaviour. The left figure shows the radius time curve, and on the right we observe the corresponding optical images, showing buckling of the phospholipid shell.

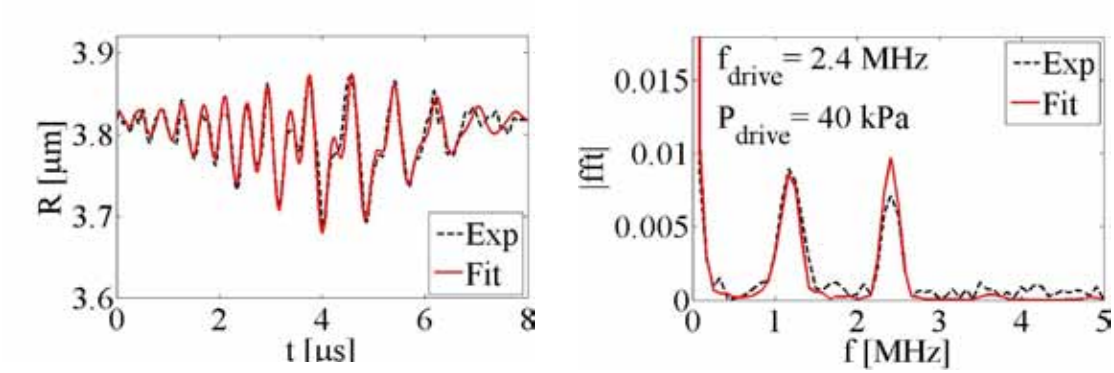

A radius time curve and the corresponding Fourier transform of a phospolipid coated microbubble as recorded with the Brandaris ultrahigh-speed camera showing subharmonic behaviour for a driving pressure with a frequency of 2.4 MHz and an amplitude as low as 40 kPa. A good agreement was found between the experimental curve (black) and the numerical model as proposed by Marmottant et al.[1] (red) only if the initial surface tension of the bubble was assumed to be close to zero $\sigma(R_0) = 0$ N/m, i.e the bubble surface is initially completely saturated with phospholipids and close to the buckling state.

Follow-up of Cryoablation in kidney cancer: CT versus CEUS

Hessel Wijkstra

AMC University Hospital, Amsterdam, the Netherlands

Kidney and renal pelvic cancers represent approximately 3% of all cancer cases, thus accounting for ~40,000 new cases and ~13,000 deaths in the United States per year. The most frequent type of tumor, occurring in about 80% of the cases, is renal-cell carcinoma, and ~60% of these tumors are found incidentally. A suspect lesion is often observed during ultrasound studies, and a contrast-enhanced CT (or MRI) scan is performed to confirm the diagnosis. Contrast-enhanced CT shows the perfusion pattern of the lesion, and this information is used to characterize the mass. CT is considered the primary imaging modality in the diagnosis of RCC.

The gold standard in the treatment of renal masses is still the radical nephrectomy, however, it is more and more replaced by a partial nephrectomy, especially for small renal masses. Radiofrequency ablation (RFA) and cryoablation are new minimally invasive therapeutic options for small masses (~diameter <4 cm). Because the tumor is not removed when using these ablative treatment methods, the viability of this tissue needs to be assessed. Histological evaluation would be the best option to assess the efficacy of the treatment. However, the diagnostic value of renal biopsies is too low. Follow-up of cryoablation with biopsies is even more unreliable, because of the expected small recurrences or residual tumors.

Ablation of the tumor results in the destruction of tissue and thus in vascular damage, resulting in necrosis of the tumor tissue. The mainstay of evaluating ablative treatments therefore focuses on evaluating the absence of perfusion. Contrast-enhanced CT is able to visualize these perfusion defects, and is currently the reference standard in the follow-up of ablative treatments.

For diagnosis one or more contrast CT's are performed. The general follow-up scheme of cryoablation consists of a contrast CT at 3,6,9,12,18,24 months and thereafter once a year. This implies that within 5 years most patients will undergo at least 10 contrast CT's. Because of the potential hazards involved with radiation exposure, especially for the younger patients, replacement of all or at least a majority of these contrast CT's by CEUS would, in potential, be very beneficial.

Contrast-enhanced ultrasonography (CEUS) can be used to examine the perfusion patterns of lesions, and therefore could also be used in diagnosis and follow-up of treatment, without radiation exposure.

Two main side effects of the contrast agents used with CT are allergic reactions and damage to the kidneys. CT contrast allergies are rare, but may be serious if they occur. Contrast may also be damaging to the kidneys, especially in patients with kidney problems. Ultrasound contrast agents do not have these side effects, and are thus are preferred above CT contrast.
We currently are comparing CEUS with contrast CT imaging (gold standard) in the diagnosis and follow-up of treatment of small renal masses. Whenever the patients undergo a contrast CT, they are also imaged with CEUS.

Over 100 patients, treated with cryoablation, have been included in this study, with a follow-up period up to three years.

In this presentation, the use of CEUS for the follow-up of cryoablation will be discussed. The conclusion is that we expect that at least the majority of contrast CT's can be replaced by CEUS, lowering the radiation exposure and possible side-effects of the CT contrast agents.

CAN CONTRAST ENHANCED ULTRASOUND OF THE SCROTUM BE USED AS A PROBLEM SOLVING TOOL?

Paul Sidhu

Ultrasound is the imaging modality of choice for the investigation of scrotal abnormalities, the addition of colour and spectral Doppler ultrasound an important adjuvant. Rarely does the examiner have to resort to magnetic resonance imaging to delineate the abnormality and obtain a diagnosis. With the advent of microbubble contrast agents a new pathway in the diagnostic workup of patients is available. The diagnostic challenges presented by some lesions of the scrotum will be reviewed. A demonstration of the effectiveness of microbubble contrast ultrasound at improving the diagnostic accuracy, reducing delays and preventing unnecessary operations will be discussed. Areas of vascularity and non-vascularity present important parameters in the diagnostic pathways, and contrast enhanced ultrasound provides a useful tool in this situation. By improving operator confidence, a correct diagnosis is achieved, further dispensing with the need for further imaging.

The future of prostate cancer diagnosis

Ferdinand Frauscher, MD

Uroradiology
Department of Radiology
Medical University Innsbruck, Austria

Introduction:

Ultrasound (US) is a widely used and well tolerated imaging modality for evaluation of the prostate. Recent technical advances of US applications have enabled new aspects in the analysis of the prostate. Structural analysis is applied for measurement of prostate volume, studying of echo texture, and the illustration of tissue stiffness or elasticity. Functional analysis contains the illustration of macrovascularity and microvascularity, which are indicators of tissue perfusion. The purpose is to provide an overview of the use of ultrasound imaging techniques and to discuss current trends and future directions.

Materials and Methods:

We compared contrast enhanced ultrasound targeted biopsy (CB) of the prostate with gray scale ultrasound guided systematic biopsy (SB). Two hundred thirty male screening volunteers were included. The detection rate was 30%, including 24% by CB and in 23% by SB. Cancer was detected by CB alone in 7% and by SB alone in 6% of the patients. The detection rate for CB cores (10% of cores) was significantly better than for SB cores (5% of cores). CB in a patient with cancer was 2.6-fold more likely to detect PCa than SB. CB detected as many cancers as SB with fewer than half the number of biopsy cores.

Furthermore we evaluated CB versus SB for the impact on Gleason score findings. The study included 690 men and Sonovue (Bracco, Italy) was used. PCa was identified in 221 of 690 subjects (32%) with a mean PSA of 4.6ng/ml. The Gleason score of all 180 cancers detected by CB targeted biopsy was 6 or higher (mean 6.8). The Gleason score of all 166 cancers detected by SB ranged between 4 and 6 (mean 5.4). CB detected significantly higher Gleason scores compared with SB. Though CB may allow identification of more aggressive cancers, which is important for defining prognosis and deciding treatment.

Preliminary data on the use of cadence-contrast pulse sequencing (CPS) technology, for detecting prostate cancer have shown, that cancer was detected in 35 of 44 patients (80%), with a mean PSA level of 3.8 ng/mL. Lesions suspicious on CPS showed cancer in 35 of 44 patients (80%) and

systematic biopsy detected cancer in 15 of 44 patients (34%). CPS-targeted cores were positive in 105 of 220 cores (47.7%) and in 41 of 440 systematic biopsy cores (9.3%) ($P < 0.001$). Therefore CPS enables excellent visualization of the microvasculature associated with prostate cancer, and can improve the detection of prostate cancer compared with systematic biopsy.

Conclusions

Currently 10 to 12 TRUS-guided prostate biopsies of the peripheral zone remain the gold standard of PCa detection. Contrast-enhanced targeted biopsy showed to significantly increase cancer and per core biopsy rate compared with SB. Furthermore contrast-enhanced targeted biopsy detected a significantly higher mean Gleason score. In the future targeted bubbles may further improve PCa detection and bubbles loaded with drugs will offer new therapeutic options. However, these methods, are still not used in standard clinical practice.

References:

1. Jemal A, Siegel R, Ward E, Hao Y, Xu J, Murray T, et al. Cancer statistics, 2008. CA Cancer J Clin 2008;58(2):71-96.
2. Pallwein L, Mitterberger M, Pelzer A, Bartsch G, Strasser H, Pinggera GM, et al. Ultrasound of prostate cancer: recent advances. Eur Radiol 2008;18(4):707-15.
3. Heidenreich A, Aus G, Bolla M, Joniau S, Matveev VB, Schmid HP, et al. EAU guidelines on prostate cancer. Eur Urol 2008;53(1):68-80.
4. Tang J, Li S, Li J, Luo Y, Xu J, Zhang Y, et al. Correlation between prostate cancer grade and vascularity on color doppler imaging: preliminary findings. J Clin Ultrasound 2003;31(2):61-8.
5. Frauscher F, Klauser A, Volgger H, Halpern EJ, Pallwein L, Steiner H, et al. Comparison of contrast enhanced color Doppler targeted biopsy with conventional systematic biopsy: impact on prostate cancer detection. J Urol 2002;167(4):1648-52.
6. Mitterberger M, Pinggera GM, Horninger W, Bartsch G, Strasser H, Schafer G, et al. Comparison of contrast enhanced color Doppler targeted biopsy to conventional systematic biopsy: impact on Gleason score. J Urol 2007;178(2):464-8; discussion 468.
7. Mitterberger M, Horninger W, Pelzer A, Strasser H, Bartsch G, Moser P, et al. A prospective randomized trial comparing contrast-enhanced targeted versus systematic ultrasound guided biopsies: impact on prostate cancer detection. Prostate 2007;67(14):1537-42.

Ultrasound contrast agent diffusion imaging for localization of prostate cancer

M. P. J. Kuenen[1], M. Mischi[1], H. Wijkstra[2], A. J. M. Hendrikx[3] and H. H. M. Korsten[1, 4]

1

Eindhoven University of Technology, Department of Electrical Engineering, The Netherlands
[2] Academic Medical Center, Department of Urology, Amsterdam, The Netherlands
[3] Catharina Hospital, Department of Urology, Eindhoven, The Netherlands
[4] Catharina Hospital, Department of Anesthesiology and Intensive Care, Eindhoven, The Netherlands

Introduction

Prostate cancer is the most common form of cancer in Western men [1, 2]. Accurate quantitative imaging methods may possibly provide an early detection and enable an efficient use of focal treatments. However, no such imaging method is yet available. As a consequence, the diagnosis is currently based on 6 to 12 geometrically distributed biopsies. This invasive procedure is often repeated several times to achieve sufficient reliability.

Cancer growth and aggressiveness are related to angiogenesis, i.e., to the formation of a dense network of microvessels [3]. Recent technical developments permit dynamic contrast-enhanced ultrasound imaging of the prostate circulation at a high resolution [4]. This involves the intravenous injection of a small ultrasound contrast agent bolus, followed by the ultrasound measurement of indicator dilution curves (IDCs), representing the bolus first pass through the prostate circulation [5, 6]. Although promising, quantification of IDC patterns is necessary for a clinical application.

Aimed at the quantification of angiogenesis, several methods have proposed the estimation of perfusion from IDC parameters, based on timing or intensity features [7, 8]. However, timing features depend on the entire bolus history, and don't represent the local hemodynamic characteristics at the measurement site; intensity features are affected by nonlinear attenuation [9]. Furthermore, the effects of angiogenesis on perfusion are complex, inconsistent and contradictory [10].

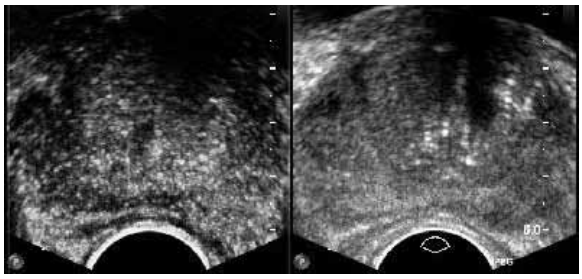

Figure 3 Contrast-enhanced ultrasound image of the prostate, showing both the contrast-enhanced (left) and fundamental (right) imaging modes.

In this study we propose an alternative method, which quantifies the local, intravascular diffusion of ultrasound contrast agents. We expect diffusion to correlate better than perfusion to changes in the microvascular architecture that are caused by angiogenesis.

Materials and methods

Data acquisition was performed at the AMC, Amsterdam. A 2.4 mL SonoVue® (Bracco, Milan, Italy) bolus was injected intravenously. Transrectal ultrasound power modulation imaging (frequency 3.5 MHz, mechanical index 0.06) was performed using an iU22 scanner (Philips Healthcare, Bothell, USA) equipped with a C8-4v transducer.

An IDC is measured at every pixel of the resulting B-mode video. The IDCs are modeled by the Local Density Random Walk model, which is a solution of the convective diffusion equation [11]. We have refined the IDC formalization, such that it permits the estimation of a diffusion-related parameter that can be interpreted locally, i.e., independently of the entire vascular path. In particular, this parameter, related to local diffusion, is reflected in the IDC skewness.

We present a fast fitting algorithm to estimate the IDC parameters at every video pixel, producing a parametric image (see Figure 2). The algorithm, which relies on the linear relation between measured acoustic intensity and contrast agent concentration, compensates for the dynamic-range compression applied by the scanner. Dedicated spatio-temporal filtering is applied to improve the fitting robustness.

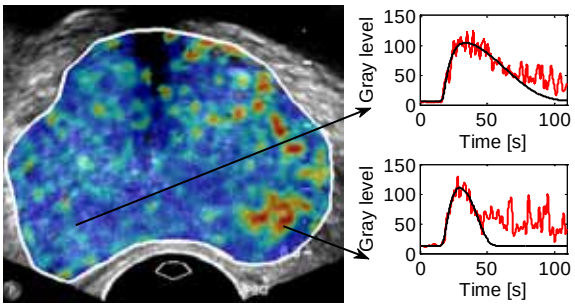

Figure 4 Diffusion parametric image with typical IDC patterns encountered in healthy (top right) and cancerous (bottom right) tissue.

A preliminary validation was conducted based on two patients. The diffusion parametric images were compared to histology data, obtained after radical prostatectomy at the AMC in Amsterdam.

Results

On a pixel basis, there was a good agreement between the diffusion parametric images and the histology assessment. Regions of interest of at least 1000 pixels were considered. Sensitivity and specificity were 78% and 92%, respectively. The ROC curve area was 0.91, which was superior to that obtained by testing all the other IDC parameters reported in the literature [7, 8].

Conclusions

Quantification of local diffusion of ultrasound contrast agents is a promising method for the localization of prostate cancer. A more extensive validation, e.g., by a comparison with other techniques and with a higher number of patients, is however necessary to assess the clinical reliability of the method.

References

[1] Jemal, A. et al, Cancer statistics, 2008, *CA Cancer J. Clin.*, 58(2), 71-96, 2008.
[2] Ferlay, J. et al, Estimates of the cancer incidence and mortality in Europe in 2006, *Ann. Oncol.*, 18, 581-592, 2007.
[3] Weidner, N. et al, Tumor angiogenesis correlates with metastasis in invasive prostate carcinoma. *Am. J. Pathology*, 143(2), 401-409, 1993.
[4] De Jong, N. et al, Detection procedures of ultrasound contrast agents, *Ultrasonics*, 38, 87-92, 2000.
[5] Wink, M. H. et al, Transrectal contrast enhanced ultrasound for diagnosis of prostate cancer, *World J. Urol.*, 25, 367-373, 2007.
[6] Pallwein, L. et al, Ultrasound of prostate cancer: recent advances, *Eur. Radiol.*, 18, 707-715, 2008.
[7] Eckersley, R. J. et al., Quantitative microbubble enhanced transrectal ultrasound as a tool for monitoring hormonal treatment of prostate carcinoma, *Prostate*, 51, 256-267, 2002.
[8] Elie, N. et al, Methodology for quantifying interactions between perfusion evaluated by DCE-US and hypoxia throughout tumor growth, *Ultrasound in Med. & Biol.*, 33(4), 549-560, 2007.
[9] Tang, M.-X. and R. J. Eckersley, Nonlinear propagation of ultrasound through microbubble contrast agents and implications for imaging, *IEEE Trans. Ultrason. Ferroelect. Freq. Contr.*, 53(12), 2406-2415, 2006.
[10] Delorme, S. and M. V. Knopp, Non-invasive vascular imaging: assessing tumour vascularity, *Eur. Radiol.*, 8, 517-527, 1998.
[11] Sheppard, C. W., *Basic principles of the tracer method*, New York: John Wiley and Sons, 1962.

REAL-TIME CONTRAST-ENHANCED ULTRASOUND PARAMETRIC IMAGING IN PROSTATE

Peter Frinking, Laurent Mercier, Nicolas Rognin, Marcel Arditi, François Tranquart and Michel Schneider

Bracco Research S.A. – Geneva / Switzerland

Introduction

Lesion detection and characterization for cancer diagnosis in e.g. liver, breast or prostate has become an important field of application in contrast-enhanced ultrasound imaging. In prostate, for example, systematic biopsy, currently still the "gold standard" for prostate cancer diagnosis, misses approximately 30% of cancers [1]. Even new biopsy strategies, such as increasing the number of cores taken during a biopsy examination, have low success rates [2]. With conventional (i.e. unenhanced) ultrasound imaging, the detection of prostate cancer, aimed at identifying hypoechoic areas in the peripheral zone, is unreliable [3]. However, studies of targeted biopsy approaches using contrast-enhanced ultrasound guidance have shown that the number of positive biopsy cores increases, and that the total number of cores normally taken with systematic biopsy approaches can be reduced [4]. Moreover, with the help of new perfusion quantification analysis methods, contrast-enhanced ultrasound may soon provide an alternative to systematic biopsy as the first choice for prostate cancer diagnosis. This could result in a major and welcome reduction in patient discomfort and morbidity, and could dramatically decrease associated costs.

In contrast-enhanced ultrasound imaging, lesion detection is typically based on differences in contrast enhancement (hypo- or hyper-enhancement) and perfusion kinetics compared to normal tissue [5][6]. Perfusion kinetics can be measured and quantified by recording so-called time-intensity curves (TIC), which represent the echo-power as a function of time and, consequently, relate to the time evolution of the local instantaneous contrast agent concentration after, for example, a bolus injection [7]. These TIC are normally analyzed after the examinations using dedicated off-line post-processing quantification software. By off-line analysis using best-fit optimization approaches, perfusion parameters, such as Rise Time (*RT*), Time-to-Peak (*TP*) enhancement, mean Transit Time (*mTT*), Peak Intensity/Enhancement (*PI*), Wash-in Rate (*WiR*), Wash-out Rate (*WoR*), etc., are extracted from sophisticated mathematical models describing the bolus kinetics of the contrast agent [8]. These perfusion parameters are typically presented as single values obtained from analyzing a pre-defined region-of-interest (ROI), or they can be presented as static parametric images showing the spatial variation of values of any parameter of interest, on a pixel-by-pixel basis [9].

For lesion characterization, benign lesions can be differentiated from malignant lesions based on differences in their vascular properties, such as microvascular density and/or structure. Thus, lesions can be characterized by imaging and analyzing the finest details of the microvascular network, preferably on full resolution images. Capturing the complete microvascular structure of a lesion under investigation is often challenging in contrast-enhanced ultrasound imaging because the instantaneous local agent concentration can be extremely low, even to the extent that single microbubbles are imaged flowing in microvessels. This hinders the rendering of the complete microvascular structure and, therefore, limits correct lesion characterization. The microvascular structure can, however, be imaged with contrast-enhanced ultrasound using so-called maximum-hold or maximum intensity projection (MIP) imaging approaches (such as MVI™, MFI™, CPS-capture™), especially in situations of low instantaneous local contrast agent concentrations. In MIP imaging, the absolute maximum echo value is preserved over time in each pixel. In this way, trajectories of individual bubbles flowing through microvessels are 'projected', and the finest details of the microvascular network can thus be imaged. However, at times beyond the initial 'arterial' wash-in phase, MIP images generally have become 'diffuse' due to perfusion of normal parenchyma tissue, and image information specific to the microvascular structure of a lesion has a tendency to fade. This limits the usefulness of MIP imaging for lesion characterization considerably. Another limitation of MIP imaging may be its high sensitivity to motion resulting in blooming artifacts.

Real-time parametric imaging

In this work, a new method was developed which allows for improved contrast perfusion imaging, by displaying parametric images of contrast-enhanced ultrasound sequences in real-time. The method is based on a robust smoothing algorithm, combining a maximum- and minimum-hold filter, applied on image data in real-time. The video data are linearized also in real-time (i.e. producing echo-power signals proportional to local contrast agent concentration) to revert the effects of non-linear log-compression and color rendering. In this way, images of microvascular structures are displayed in real-time during the wash-in phase after a bolus injection of a contrast agent, whereas distinct perfusion kinetics related to the wash-in phase (and/or wash-out phase) are accurately preserved and can be exploited in a rigorous way for dynamically displaying parametric images (i.e. the parametric images are created also in real-time). Because of the robustness of the algorithm, the new method can be applied on full resolution data with a low signal-to-noise ratio without the need for spatial filtering. Consequently, full resolution parametric images can be created without loss of information. Thus, differences in contrast agent perfusion between normal tissue, benign lesions and malignant lesions can be optimally exploited for improved lesion detection.

The method has been optimized for contrast-enhanced ultrasound examinations of the prostate and is implemented in a software program called *SonoProstate*^{Live}. Because of the symmetry of the prostate gland and its zonal anatomy, lesion detection is typically based on comparing contrast perfusion kinetics in contra-lateral regions. Moreover, contrast-enhanced image sequences of prostate examinations are convenient for real-time processing purposes since the images are relatively stable and motion artefacts are practically non-existent. In this work, lesion detection and characterization was restricted to the peripheral zone (PZ) since 80% of prostate cancer is located in the PZ [10]. Figure 1 illustrates an example of the new method applied on an image sequence recorded during a prostate examination after a 2.4 mL bolus injection of SonoVue®.

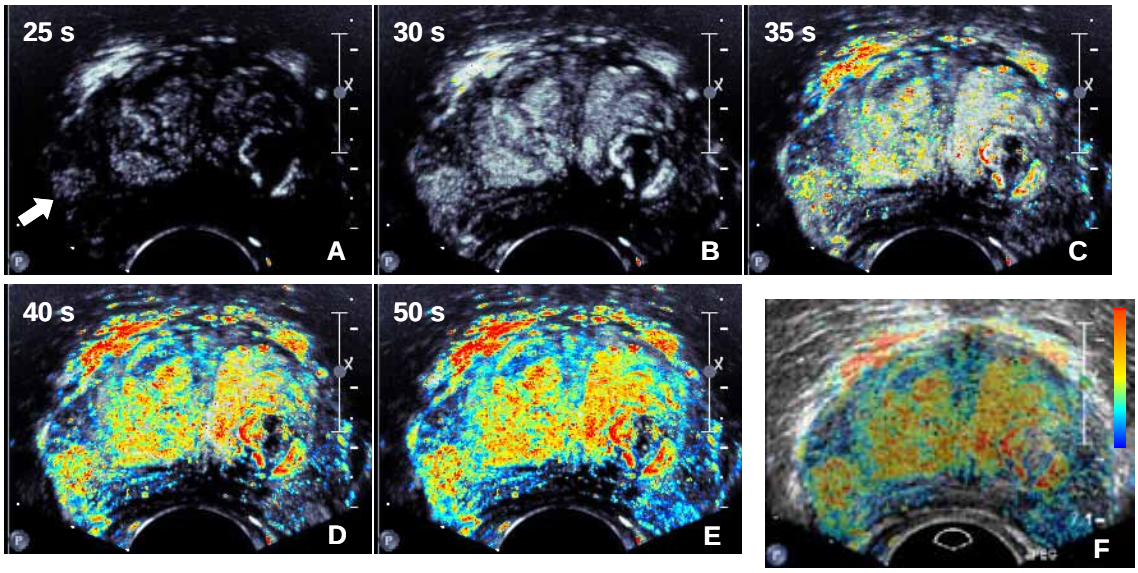

Figure 1. Prostate images obtained during real-time *WiR* parametric image processing at different time instants: at 25 s (A), 30 s (B), 35 s (C), 40 s (D) and 50 s (E) after a bolus injection of SonoVue®. The final *WiR* parametric image (E) is overlaid with 50% transparency on the B-mode image in F.

Figures 1A to 1E show the results at different time instants during real-time processing. During the early part of the wash-in phase 25 s after injection (Figure 1A), the contrast agent appears in the highly vascularized central zone (i.e. middle part) of the prostate, showing the typical symmetric enhancement of this part of the prostate. The MIP character of the method at this stage of processing enhances relatively big vessels of the vascular network already at this early part of contrast wash-in (see for example the bright ring on the right side in Figure 1A). Also, an asymmetric enhancement pattern in the right peripheral zone of the prostate (i.e. on the lower-left side in the MIP image in Figure 1A indicated by the arrow), which is absent in the contra-lateral part of the prostate, appears and suggests the presence of a suspicious region in this part of the prostate. During late wash-in of the agent at 30 s after injection (Figure 1B), the suspicious region is well delineated, enhancing branches of its vascular network, which is a clear indication of a malignancy. After the wash-out has started in the lesion and

normal surrounding tissue is perfused at 35 s after injection (Figure 1C), the method switches to parametric imaging and starts to create parametric maps in real-time.

Figures 1D and 1E show examples of full-resolution parametric images (i.e. pixel-by-pixel with no spatial filtering applied) of *WiR* at 40 and 50 s after injection, respectively. For each pixel in the image, the *WiR* values are normalized to a reference value calculated globally, and are subsequently color coded according to a predefined palette with red colors corresponding to large values and blue colors corresponding to low values of the *WiR*. The suspicious region in the right PZ of the prostate can be clearly identified against normal regions in the contralateral zone, by the relatively high density of high *WiR* values, and remains conspicuous even during the (late) wash-out phase. Moreover, the high resolution parametric images reveal details of the microvascular system, allowing improved detection and may facilitate characterization. Functional information may be combined with anatomical information by overlaying the final *WiR* parametric image of Figure 1E on the B-mode image. Figure 1F shows the final results, applying a 50% transparency for the *WiR* parametric image. In this way, it can be easily recognized if a suspicious lesion is completely contained within the prostate gland or if it is extending outside the gland. This kind of information may be important as it will condition the choice of possible therapeutic strategies to follow. Note that also in the transition zone (TZ), regions with a high density of high *WiR* values are observed, which is mainly due to the hyper vascular character of TZ tissue. However, it is anticipated that for detecting prostate cancer (PCa) in PZ this will not be a problem in practice, since in most cases PZ can be easily separated from TZ due to the zonal anatomy of the prostate.

The method was tested in a clinical context during contrast-enhanced ultrasound examinations of four patients scheduled for radical prostatectomy. *SonoProstate*^{Live} was installed on a notebook computer, operating under MS-Windows XP, which was connected to the video output of an ultrasound scanner through a digital video frame grabber. This allowed to process the contrast sequences in real-time during the examination. The resulting *WiR* parametric images were analyzed subjectively, and suspicious regions were identified. Their locations were compared to data available from biopsy histopathology reports, and in all four cases, the final *WiR* parametric images allowed correct identification of PCa. Moreover, the method was validated in a qualitative way by retrospective off-line analyses on image sequences of previously recorded contrast-enhanced ultrasound examinations. Possible locations of PCa identified in the *WiR* parametric images generated by *SonoProstate*^{Live} were compared to histopathology data obtained after either biopsy or radical prostatectomy. The locations of PCa given by *SonoProstate*^{Live} corresponded in all cases with the histopathology data.

Figure 2 shows an example of the qualitative validation with the overlaid *WiR* parametric image of Figure 1F on the left-hand side and the corresponding histology section on the right-hand side. The suspicious region identified by a relatively high density of high *WiR* values in the right PZ of the parametric image (red arrow), correctly corresponded with PCa as outlined by the pathologist in blue in the histology section. An adenoma was also present in the left TZ of the same prostate, as is indicated by the green arrow in the histology section. The same location in the *WiR* parametric image (green arrow) corresponded to a region with a non perfused internal part (i.e. with *WiR* values close to zero) and a hyper vascular peripheral part with a high density of high *WiR* values. This might be a typical characteristic of adenoma in prostate and could be used for lesion characterization, but this is subject for future studies.

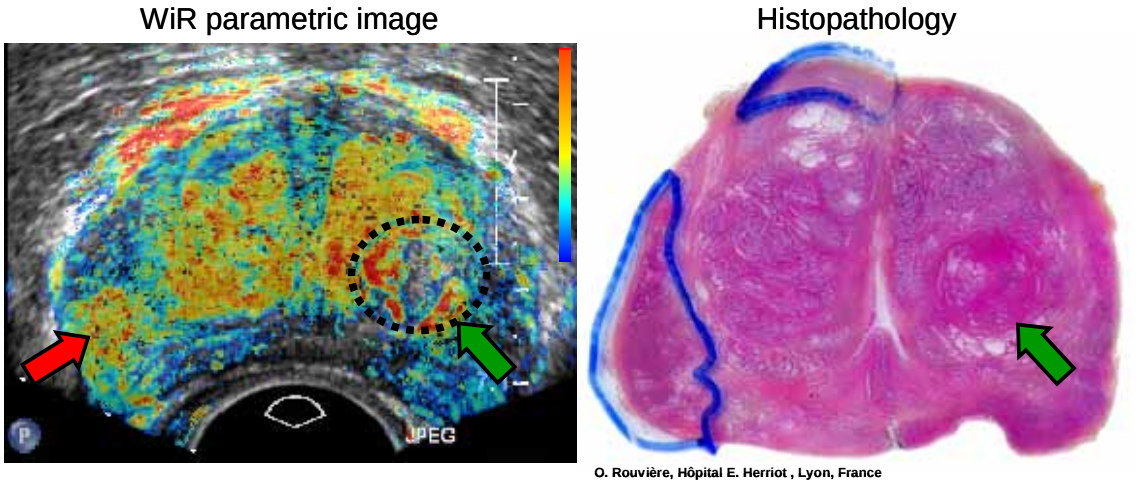

Figure 2. *WiR* parametric image (left) and corresponding histology coupe (right). A suspicious region identified in the *WiR* parametric image in the right PZ (red arrow) corresponds with PCa outlined by the pathologist in blue in the histology section. Adenoma was also detected in the left TZ of the same prostate (green arrow).

Statistical analysis.

Parametric images of *WiR* may facilitate the identification of possible locations of a pathological condition. Indeed, the example illustrated in Figure 2 showed that a region with a relatively high density of high *WiR* values in the right PZ corresponded to the location of PCa, whereas normal tissue corresponded to regions of low *WiR* values. Therefore, distributions of *WiR* values were statistically analyzed based on their histograms calculated in ROI placed in the parametric images (a histogram of *WiR* values calculated in a ROI of a parametric image reflects perfusion information at the pixel level). Figure 3 illustrates the principle on the *WiR* parametric image of Figure 1. A ROI was drawn in the parametric image around the right PZ with PCa, and a histogram of all *WiR* values within this ROI was calculated. The graph on the right-hand side of Figure 3 shows the resulting histogram (blue bars), where *WiR* values are plotted on the x-axis and the corresponding normalized counts are plotted on the y-axis. The counts were normalized to the total number of counts in the ROI to make the distribution independent of the ROI size.

Next, the original histogram was smoothed (red curve shown on the right-hand side in Figure 3) with a lognormal probability density function of the form:

$$F(x) = \frac{e^{-\frac{[\ln(x)-m]^2}{2s^2}}}{x\, s\sqrt{2p}}$$

where m and s are the mean and standard deviation of the natural logarithm of x, respectively (x corresponds to the *WiR* values). Values for m and s are determined by a best-fit analysis between $F(x)$ and the original histogram. Smoothing the original histograms allows improved comparison between histograms obtained from different regions in the prostate. For example, Figure 4 on the left shows in red the smoothed histogram of Figure 3 calculated in the right PZ with PCa, and in green the one calculated in the contra-lateral region representing normal tissue, i.e. in the left PZ. The histogram curve corresponding to the right PZ with PCa is very different in shape compared to the one from normal tissue in the left PZ; its peak value is lower, its peak position is shifted to the right, i.e. to higher *WiR* values, and its peak is wider, i.e. reflecting a larger variation of *WiR* values.

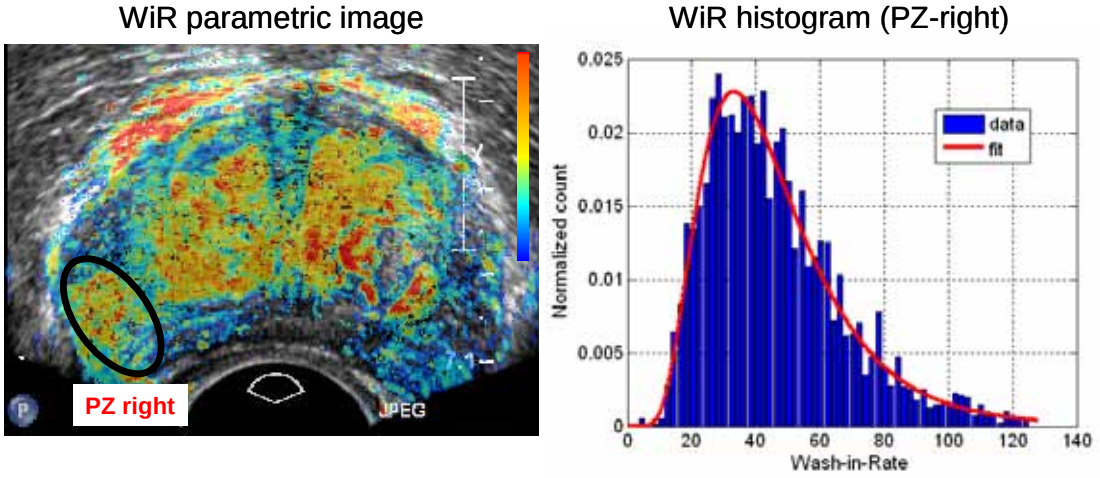

Figure 3. *WiR* parametric image (left) and corresponding histogram of *WiR* calculated in the right PZ shown in the parametric image (right). The original histogram (blue bar plot) is smoothed with a lognormal distribution function (red curve) obtained from a best-fit optimization procedure.

Shape differences between the histogram curves, corresponding to different lesions or types of tissue, may be exploited by extracting parameters from the lognormal distribution function, obtained after the best-fit optimization with the *WiR* histograms. Examples of such parameters are: the *Mean* (center of gravity of the histogram curve), *Mode* (value at the peak, i.e. the most frequently occurring value in the histogram), *Median* (middle value, i.e. the value such that an equal number of samples are less than and greater than said value), *Sigma* (standard deviation, i.e. the variability or dispersion around the *Mean* of the histogram curve) and *Skewness* (asymmetry of the histogram curve). These parameters can be calculated from the best-fit parameters m and s by:

$$Mean = e^{m+\frac{s^2}{2}},\ Mode = e^{m-s^2},\ Median = e^{m},\ Sigma = \sqrt{e^{s^2+2m}(e^{s^2}-1)} \text{ and } Skewness = \sqrt{e^{s^2}-1}\,(2+e^{s^2})$$

Here, we used a combination of the *Mode* and *Sigma* parameters to compare histogram curves corresponding to different lesions or types of tissue located in the PZ. For both histogram curves shown on the left-hand side of Figure 4, the *Mode* and *Sigma* parameters were calculated. Next, a 2-dimensional (2D) map of *Mode* and *Sigma* was generated in which the *Mode* was plotted on the x-axis and *Sigma* on the y-axis, and the results are shown on the right-hand side in Figure 4; the data point corresponding to normal tissue in PZ is plotted in the lower-left region of the 2D map, whereas the one corresponding to PCa in PZ is plotted in an upper right region relative to normal tissue. This example suggests that a 2D representation of shape parameters obtained from histogram curves of a *WiR* parametric image may be used to differentiate between PZ tissue with and without cancer.

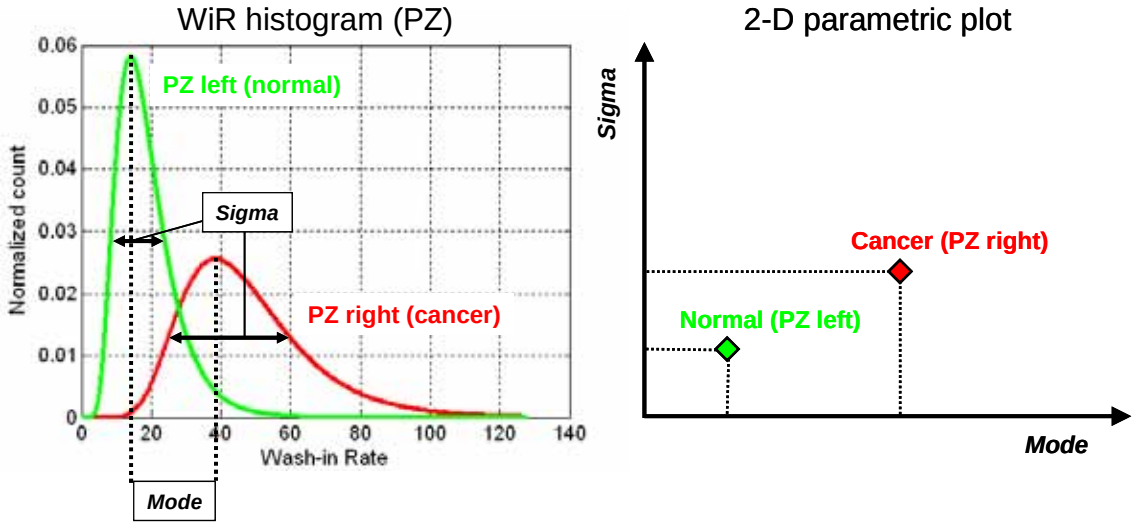

Figure 4. Fitted lognormal histogram curves (left) calculated in right PZ with PCa (red curve) and left PZ containing only normal tissue (green curve). Corresponding *Mode* and *Sigma* were calculated from the best-fit parameters *m* and *s*, and were plotted in a 2D map (right). Data points relating to normal tissue or PCa in PZ are plotted in very distinct regions in the 2D parametric plot.

To validate this approach, 23 DICOM image sequences of different patients were studied retrospectively off-line. The image sequences were acquired during contrast-enhanced ultrasound examinations with different ultrasound systems (18 with the Philips iU22, 4 with the Siemens Sequoia, and 1 with the Toshiba Aplio) by 5 different users. Histogram curves were calculated in 62 ROI located in PZ containing different lesions or types of tissue. For each histogram curve, the *Mode* and *Sigma* parameters were calculated and the 2D map of *Mode* and *Sigma* was generated. Histopathology data, obtained after biopsy examinations or radical prostatectomy, was available for 26 ROI in 8 patients and confirmed 14 cases of PCa, 2 cases of Prostatitis and 10 cases of normal tissue; no data was available for the remaining 36 ROI. Figure 5 shows the 2D map of *Mode* and *Sigma* calculated in all 62 ROI. Data points with known histopathology were colorized according to the type of lesion or tissue, *viz.*

green for normal tissue, red for PCa and orange for Prostatitis in the PZ. Data from PCa and normal tissue in PZ are located in distinct regions in the 2D map, as was described above; normal tissue data appears to be relatively uniform distributed in the lower-left region, whereas PCa data is more dispersed and located in an upper-right region relative to normal tissue data. The dispersion observed for PCa data may be explained by a high heterogeneity in tumor development, as would be expected for different patients. Moreover, based on the results shown in Figure 5, it may be possible to differentiate Prostatitis (benign tissue) from PCa in PZ, but this should be confirmed by including more data.

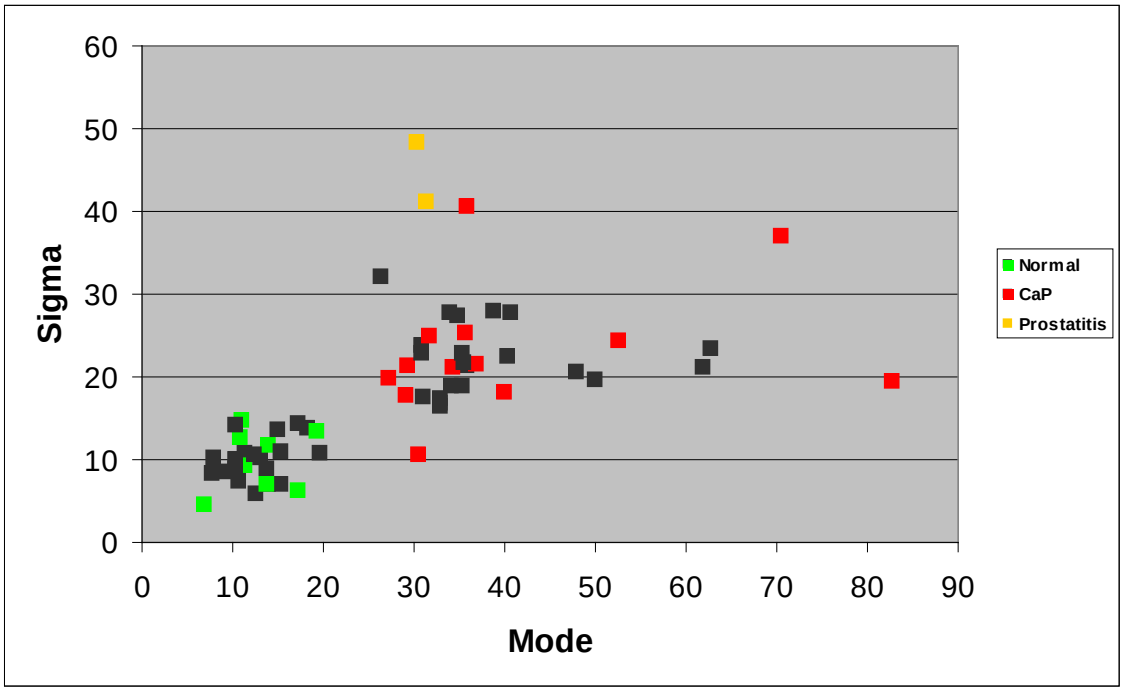

Figure 5. 2D map of *Mode* and *Sigma* calculated in 62 ROI. Data points with known histopathology were colorized according to the type of lesion or tissue (see color legend).

The results shown in Figure 5 confirm the suggestion made above that the distinct regions in the 2D map of *Mode* and *Sigma* correspond to the different lesions or tissue located in the PZ, and thus that this method may be used for improved lesion characterization in PZ of the prostate. It is furthermore interesting to note that, especially for normal tissue, all results are consistent even though the data were acquired with different ultrasound systems and by different users, each with their own preferred settings. This suggests that the method is very robust and could reduce operator-dependent variability.

Conclusion

In summary, real-time *WiR* parametric imaging, as implemented in *SonoProstate*^{Live}, is a new imaging modality which may allow improved lesion detection in PZ during contrast-enhanced ultrasound examinations of the prostate. Parametric images of *WiR* are generated during the examinations, mapping the spatial distributions of *WiR* values in the prostate as soon as 50 s after agent injection, and could be used for targeted biopsy guidance. Moreover, perfusion kinetics information is available to the

examiner even after the wash-out phase of the agent, whereas in normal contrast examinations the effective observation time for lesion detection is limited to 20 to 30 s only. Since multiple foci occur in more than 85% of the cases of PCa [11], *SonoProstate*^{Live} might increase chances of detecting small lesions which would have been missed during a conventional contrast examination.

The results from *SonoProstate*^{Live} can be further analyzed for characterization purposes. A 2D map of *Mode* and *Sigma* of the statistical distribution of *WiR* in a ROI could facilitate lesion characterization in PZ of the prostate by contrast-enhanced ultrasound. Consequently, it could lower false-positive findings in prostate cancer detection and thus would decrease overdiagnosis and overtreatment of patients with prostate cancer. However, the preliminary results of this work need to be confirmed by a prospective clinical validation study. Another interesting topic would be to see if *SonoProstate*^{Live} in combination with the 2D map of *Mode* and *Sigma* could aid in determining the effect of a therapeutic treatment (e.g. HIFU, brachy- or cryo-therapy), by assessing tumor response to treatment, and could identify non-responders at an early stage during therapy. Finally, the possibility of detecting cancer in highly vascular regions, such as in the TZ, should also be investigated.

Acknowledgment

Image sequences were kindly provided by Dr. H. Wijkstra (AMC, Amsterdam, The Netherlands), Prof. O. Rouvière (Hôpital E. Herriot, Lyon, France), Dr. F. Frauscher (University Hospital Innsbruck, Austria), Prof. T Fischer (Charité, University of Berlin, Germany) and Dr. Li Feng-Hua (Renji Hospital, Shanghai, China). Dr. Wijkstra is also acknowledged for his valuable input and for allowing the opportunity for the *live* clinical test.

References

[1] M. Norberg *et al.*, "The sextant protocol for ultrasound-guided core biopsies of the prostate underestimates the presence of cancer," Urology, vol. 50, pp. 562-566, 1997.

[2] J.S. Jones *et al.*, "Saturation technique does not improve cancer detection as an initial prostate biopsy strategy," J. Urol., vol. 175(2), pp.485-488, 2006.

[3] M. Moradi *et al.*, "Computer-aided diagnoses of prostate cancert with emphasis on ultrasound-based approaches: A review," Ultras. Med. Biol., vol. 33(7), pp. 1010-1028, 2007.

[4] M. Mitterberger *et al.*, "A prospective randomized trial comparing contrast-mhanced targeted versus systematic ultrasound guided biopsies: Impact on prostate cancer detection," The Prostate, vol. 67, pp. 1537-1542, 2007.

[5] F. Frauscher *et al.*, "Ultraschallkontrastmittel un prostatakarzinom," Radiologe, vol. 45, pp. 544-551, 2005.

[6] A.R. Padhani *et al.*, "Angiogenesis imaging in the management of prostate cancer," Nature Clin. Pract. Urology, vol. 2(12), pp.596-607, 2005.

[7] N. Elie *et al.*, "Methodology for quantifying interactions between perfusion evaluated by DCE-US and hypoxia throughout tumor growth," Ultras. Med. Biol., vol. 33(4), pp. 549-560, 2007.

[8] M. Averkiou *et al.*, "Quantification of tumor microvascularity with respiratory gated contrast enhanced ultrasound for monitoring therapy," Ultras. Med. Biol., In Press.

[9] X. Gu *et al.*, "Parametric perfusion imaging based on low-cost ultrasound platform," Ultras. Med. Biol., In Press.

[10] J.E. McNeal *et al.*, "Zonal distribution of prostate adenocarcinoma. Correlation with histologic pattern and direction of spread," Am. J. Surg. Path., vol. 12(12), pp. 897-906, 1988.

[11] D.P. Byar and F.K. Mostofi, "Carcinoma of the prostate: prognostic evaluation of certain pathological features in 208 radical prostatectomies. Examined by a the step-section technique," Cancer, vol. 30(1), pp. 5-13, 1972.

SOCIAL EVENT

Sponsored by GE Healthcare

Thursday JANUARY 21

Oceanium, Blijdorp Zoo
Blijdorplaan 8, Rotterdam
Dinner buffet: 7.30- 10.15pm

Coaches will be leaving from Hilton at 6.30pm and will be back there around 10.30pm.

Development of a cannulated vessel model for simultaneous ultrasound exposure and microscope imaging

Anna Tokarczyk, Ian Rivens, Gail ter Haar

Joint Department of Physics, The Institute of Cancer Research: Royal Marsden NHS Foundation Trust, Sutton, Surrey, SM2 5PT, UK

Ultrasound microbubble contrast agents (UCAs) are now commonly used in diagnostic ultrasound, and their use as therapeutic agents for cancer treatments is under active consideration. The intention of this study is to investigate the effects of ultrasound (US) exposure of UCAs on the blood vessels through which they flow, in order to assess potential hazard, and also to investigate beneficial therapeutic effect.

An experimental model which uses an isolated, cannulated blood vessel (~400 μm diameter) has been developed. This allows microscopic visualisation of vessel behaviour and damage during therapeutic ultrasound exposures in the presence of contrast agent, and assessment of changes in endothelial and smooth muscle cells.

Continuous 5 s exposures of 1.7 MHz High Intensity Focused Ultrasound have been used. Vessel wall damage and leakage of intravascular buffer have been observed, predominantly in the presence of Sonovue and at a peak negative pressure of 1.36 MPa.

The observed lack of vascular constriction and expansion in response to Phenylephrine and Acetylcholine indicates smooth muscle and endothelial cell damage. This has been confirmed by haematoxylin and eosin staining which revealed the changes in a blood vessel wall structure.

This vessel model will also be used to investigate the bio-effects induced by the exposure of vessels to diagnostic US exposures in the presence of contrast agents.

Assessment of coronary flow reserve, myocardial perfusion and function in two cases of Takotsubo cardiomyopathy. Insights into pathophysiological mechanisms

Francesco Bartolomucci MD, Ph.D, *Giovanni Deluca MD, *Riccardo Ursi MD,

Domenico Paulillo MD, §Alessandro Distante MD.

Department of Cardiology ASL BAT, § Departemnt of Cardiology – University of Pisa

Transient apical ballooning syndrome is a cardiac condition characterized by chest pain, transient ECG and wall motion abnormalities, associated with minimal release of biochemical indexes of myocardial necrosis, and with no evidence of obstructive coronary artery disease. This syndrome that was first described by Sato and colleagues and named by these authors "Takotsubo Cardiomyopathy. We report three case of Takotsubo cardiomyopathy that recently came to or observation and underwent a series of investigations, aimed at clarifying the potential mechanisms responsible for its occurrence.

A 2 old women with a history of hypertension presented to the emergency room of our hospital complaining of acute-onset, constrictive retrosternal chest pain, that lasted approximately 30 minutes. The day before symptoms' onset, the patients have suffered severe emotional stress. The ECG showed (Fig.1), typical ischemic-like, 3mm ST segment elevation across the chest leads; the echocardiogram documented normal cavity dimensions, severe LV systolic dysfunction (EF 35%) with and apical and mid-ventricular akinesis and hyperkinesis of the basal segments. The patients were as immediately brought to the catheterisation laboratory to undergo selective coronary arteriography that ruled out significant coronary artery disease. Left ventriculography confirmed impairment of systolic function with typical apical ballooning.(fig.1) Troponin levels peaked approximately 10 hours after symptoms' onset to a value of 2.6 mg/L and completely normalized within 36 hours.

Twenty-four hours after admission, the patients underwent assessment of left anterior descending (LAD) coronary flow reserve (CFR) by transthoracic color-doppler echocardiography. CFR was measured at the distal end of the LAD, during intravenous adenosine infusion (0.14mg/Kg/min over 2 min), and found to be mildly depressed (x 2.1 resting flow velocity).

Four hours after completion of the LAD flow velocity study, regional myocardial perfusion was assessed, in real-time, by contrast echocardiography by i.v. injection of Sono-View, low mechanical index microbubbles. (fig.2) Perfusion was essentially preserved in most dysfunctional segments, with the exception of a limited subendocardial portion of the left ventricular apex in a case and in the other case there is a delay replenishment of the left ventricular apex. During the same session, the patients underwent a viability study by low-dose dobutamine echocardiography (LDDE), with a starting dose of

5mcg/Kg/min for 5 minutes, followed by a 15mcg/Kg/min dose for 10 more minutes. No apparent improvement in regional systolic wall motion was observed.

During hospitalisation, the patients remained asymptomatic, with no clinical sign of heart failure. The echocardiogram showed normal global and regional LV function. Hyperaemic response to adenosine was also substantially improved (33% improvement) (fig. 3), relative to the initial study. Finally, contrast echocardiography demonstrated complete normalisation of myocardial perfusion in the affected area.

Our observations and those reported in the literature, support the idea that the fundamental process underlying the development of this condition is represented by neurogenic myocardial stunning, caused by catecholamine-mediated direct myocardial injury. Although microvascular function and myocardial perfusion can be somewhat impaired in some case, these alterations are probably epiphenomena of the latter mechanism, and likely to play a minor causative role, rather than being primary pathophysiological determinants of Takotsubo cardiomyopathy.

Address for Correspondence

Francesco Bartolomucci MD, Ph.D, FESC
U.O.C. di Cardiologia e UTIC, Ospedale "L. Bonomo"
Viale Istria 1
70031 Andria
tel. + 39.0883.541759
Fax + 39.0883.299225
E-mail:francescobartolomucci@virgilio.it

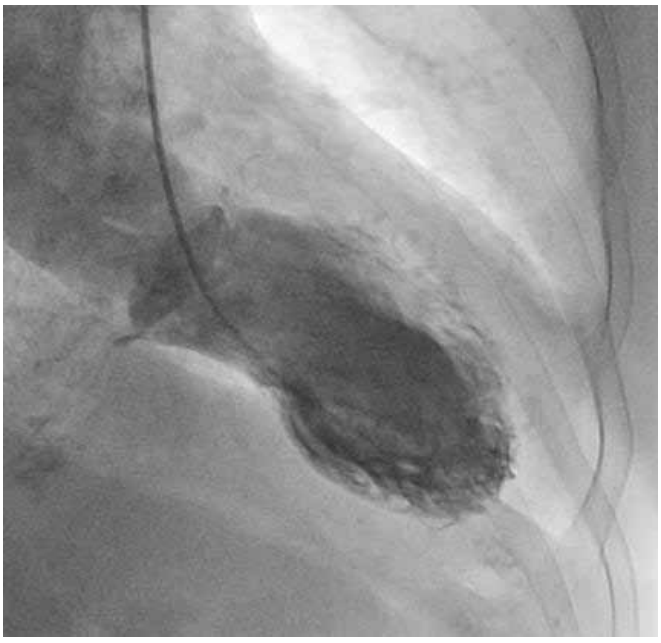

Fig.1. Left ventricular angiography (end-systolic frame) obtained on admission

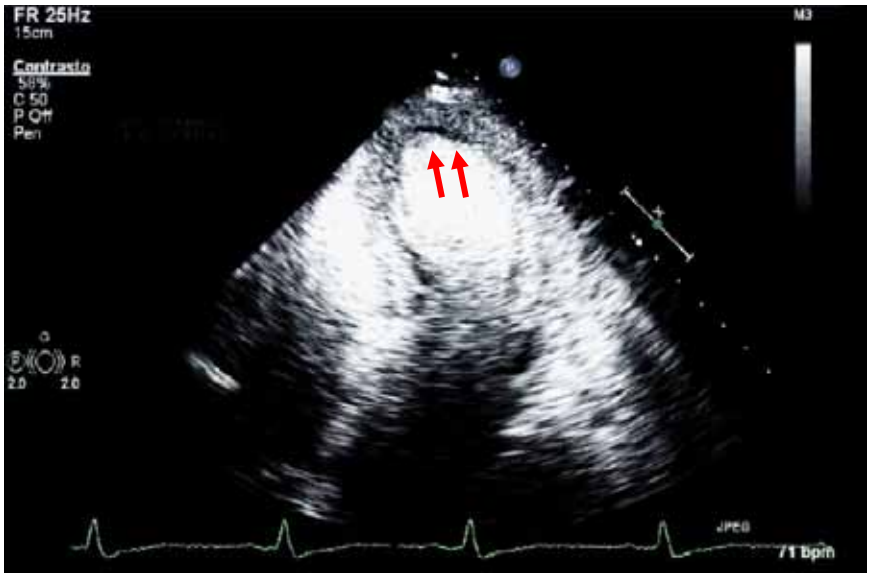

Fig.2 Real-time evaluation of myocardial perfusion by contrast echocardiography. Mild subendocardial underperfusion of the left ventricular apex is observed (red arrows). Myocardial perfusion completely normalized at follow-up (see text).

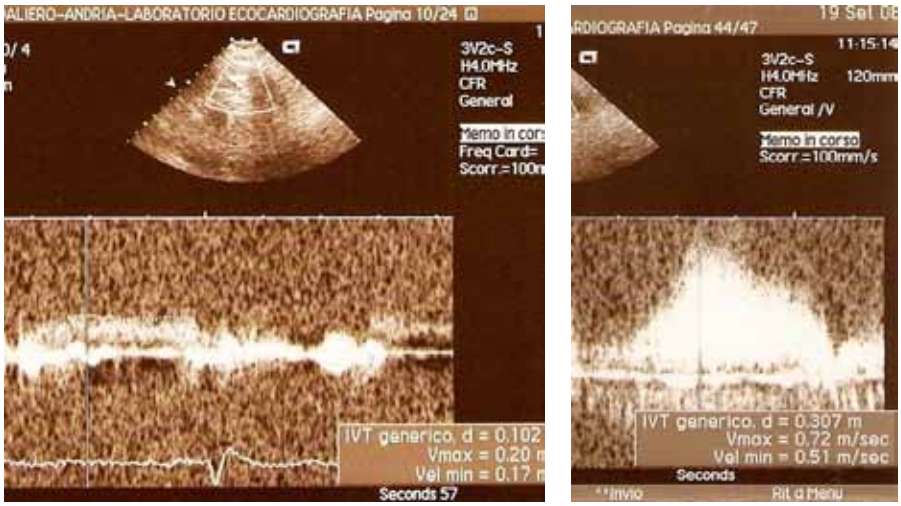

Fig. 3 Non invasive assessment of LAD coronary blood flow velocity and flow reserve one month after admission. Coronary flow reserve has completely normalized (x 3 resting flow). See text

Blood volume and ejection fraction measurements using CEUS

Drs. I.H.F. Herold[1], Ir. M.P.J. Kuenen[2], Dr. Ir. M.Mischi[2], Prof. Dr. H.H.M. Korsten[1,2]

1. *Catharina Hospital Eindhoven, Department of Anesthesiology and Intensive Care*
2. *Eindhoven University of Technology, Department of Electrical Engineering*

Maintenance of adequate circulating blood volume is essential to preserve sufficient cardiac output (CO) and organ perfusion. A safe and minimally invasive technique to quantify the circulating blood volume during surgery and Intensive-Care is therefore required. Mischi et al. showed that blood volumes can be assessed using Contrast Enhanced Ultrasound (CEUS) [1-3]. This assessment involves the estimation of the CO and the differences in Mean Transit Time (MTT) of Ultrasound Contrast Agent (UCA) Indicator Dilution Curves (IDCs) measured in different regions of interest (ROI) in the cardiac chambers. These measurements provide an accurate and minimally invasive estimation of the main blood volumes. The Pulmonary Blood Volume is analyzed by two first-pass IDCs measured in the right ventricle and left atrium ROI. The Total Circulating Blood Volume is analyzed by a first- and second-pass IDC in the same ROI, and the Systemic Circulating Blood Volume is analyzed by a first-pass IDC in the left ventricle ROI and a second-pass IDC in the right atrium ROI.

The golden standard for CO measurements is cold thermodilution, based on the injection of a cold saline bolus. A simultaneous measurement of both CO and UCA-IDCs can be performed by the intravenous injection of a cold (4°C) bolus of an UCA dispersion in saline. In our study, SonoVue® (Bracco, Italy) UCA was adopted.

The quantitative analysis of UCA IDCs involves the establishment of the relationship between UCA concentration and acoustic backscatter. This procedure is referred to as calibration. Given the contradictory results that are reported on the reflective properties of cold bubbles in the literature [6], we repeated a calibration study prior to our measurements in patients. The acoustic response of cold SonoVue® was determined using an iE 33 ultrasound scanner (Philips Healthcare, the Netherlands) equipped with a transesophageal X7-2t 3D transducer. A transesophageal transducer was chosen because of its increasing utilization in surgery and intensive-care as well as its position, very close to the left atrium. The choice for a 3D transducer was made to permit validation by full-volume (3D) measurements of the algorithm proposed by Mischi et al. [3-5] for IDC-based ejection fraction measurements.

Similarly to the measurements at room temperature (RT), also in the lower concentration range, up to 1,5 mg/L (Fig. 1), the acoustic backscatter of cold SonoVue® is linearly related to the UCA concentration. Moreover, the acoustic backscatter of SonoVue® at 4°C is surprisingly similar to that at RT in the lower range (fig.1). The life time of bubbles at 4°C is 30% longer than at RT, facilitating the detection of the UCA recirculation and, therefore, the assessment of Total and Systemic Circulating Blood Volumes.

The dose for the intravenous injection in patients can be estimated on the base of the calibration results in order to keep the measurement in the linear calibration range. However, a larger dose must sometimes be injected to improve the detection of recirculation IDCs, resulting in first-pass IDCs that are distorted by ultrasound attenuation. A dedicated algorithm has therefore been developed to correct for the IDC distortion based on the calibration results and proper dilution modeling.

We believe that this novel, minimally invasive, non-nuclear method for measuring Pulmonary Blood Volume as well as Total and Systemic Circulating Blood Volumes may be an asset in clinical research and practice.

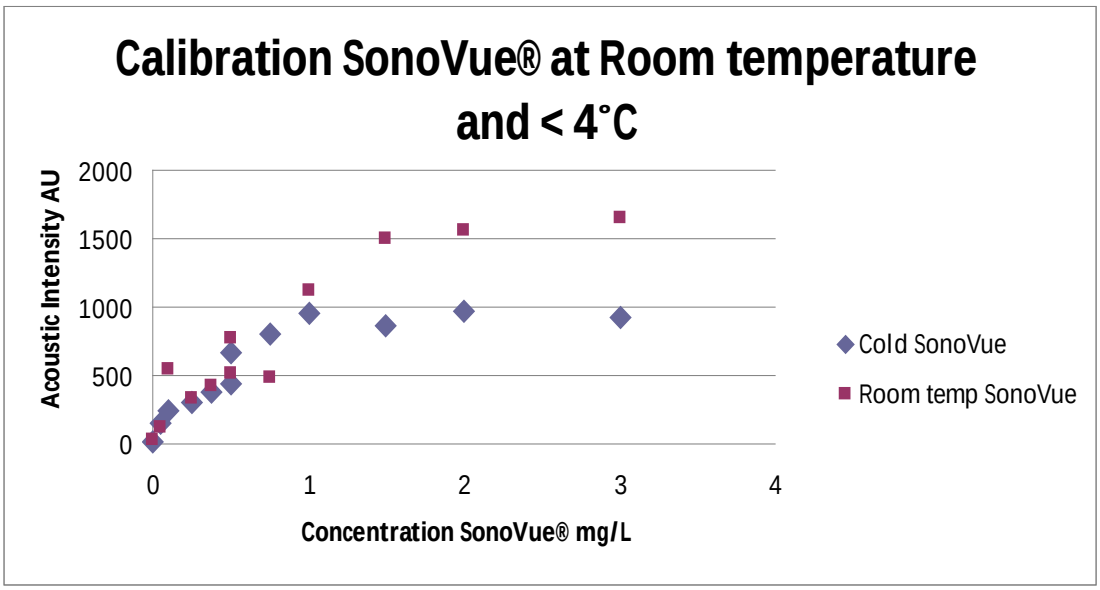

Figure 1

References

1. M. Mischi, A.A.C.M. Kalker, H.H.M. Korsten, "Contrast Echocardiography for Pulmonary Blood Volume Quantification," IEEE Transactions on Ultrasonics, Ferroelectrics, and Frequency Control, vol. 51, no. 9 , pp. 1137-1147, Sep. 2004.
2. H.H.M. Korsten, M. Mischi, R.J.E. Grouls, A. Jansen, J.-M. van Dantzig, and K. Peels, "Quantification in Echocardiography," Seminars in Cardiothoracic and Vascular Anesthesia, vol. 10, no. 1, pp. 57-62, 2006.
3. M. Mischi, A.H.M. Jansen, and H.H.M. Korsten, "Identification of cardiovascular dilution systems by contrast ultrasound," Ultrasound in Med. & Biol., vol. 33, no. 3, pp. 439-451, 2007.
4. M. Mischi, A.H.M. Jansen, A.A.C.M. Kalker, H.H.M. Korsten, "Identification of Ultrasound-Contrast-Agent Dilution Systems for Ejection Fraction Measurements," IEEE Transactions on Ultrasonics, Ferroelectrics, and Frequency Control, vol. 52, no. 3, pp. 410-420, 2005.
5. A.H.M. Jansen, M. Mischi, F. Bracke, J.-M. van Dantzig, K. Peels, N. van Hemel, H.H.M. Korsten, "Novel Ultrasound-Contrast-Agent Dilution Method for Assessment of Ventricular Ejection Fraction," European Journal of Echocardiography, vol. 9, no. 4, pp. 489-493, 2008.
6. V. Mor-Avi, K.A. Robinson, S.G. Schroff, R.M. Lang, "Effects of temperature on Albunex and FS069 echocardiographic contrast agents: in vitro investigation usting ultrasonic irradiation," Echocardiography, vol 14, no , pp39-49, 1997

Ultrasound and microbubble mediated gene therapy: effectiveness of siRNA versus plasmid DNA delivery

Bernadet.D.M. Meijering[1,2], Robert H. Henning[1], Lynda Juffermans[3], Leo.E.Deelman[1].

[1] Department of Clinical Pharmacology, Groningen Institute for Drug Exploration (GUIDE), University Medical Center Groningen, University of Groningen, Groningen, Netherlands.
[2] Interuniversity Cardiology Institute of The Netherlands, Utrecht, Netherlands, [3] Department of Physiology, VU University Medical Center, Amsterdam, Netherlands.

Background: Ultrasound and microbubbles targeted delivery (UMTD) may become a therapeutic tool in the treatment of vascular disease. Recently, we demonstrated that in UMTD, small molecules enter the cell through transient pores while the entry of larger molecules is dependent on endocytosis. We therefore now hypothesize that UMTD of siRNA is more efficient in changing gene expression than UMTD of plasmids.

Methods: the efficiencies of UMTD of SiRNA and plasmid DNA in changing the expression of the moderately expressed gene GAPDH was compared in cultured primary endothelial cells.

Results: UMTD of siRNA transfected 97.9±1.5% of all endothelial cells, with labeled siRNA both in the nucleus and cytoplasm immediately and decreased GAPDH protein levels by 70%. In contrast, following UMTD of GAPDH plasmid DNA, only 2.0 ± 0.7 % of cells expressed the transgene, which failed to increase overall GAPDH protein levels. Importantly, labeled plasmid DNA was delivered to 43.0 ± 4.2% of all cells and was detected in endosomes positive for clathrin and caveolin immediately and 24 hours after UMTD.

Conclusion: UMTD of siRNA is more effective than UMDT of plasmid in modifying protein levels of the moderately expressed gene GAPDH in cultured endothelial cells.

Virus loaded microbubbles as a tool for targeted gene delivery

***Bart Geers*[1], *Ine Lentacker*[1], *Angelika Alonso*[3], *Stephen Meairs*[3], *Joseph Demeester*[1], *Stefaan C. De Smedt*[1], *Niek N. Sanders*[2]**

[1]*Laboratory of General Biochemistry and Physical Pharmacy; Faculty of Pharmaceutical sciences; Ghent University; Harelbekestraat 72 9000 Gent, Belgium*
[2]*Laboratory of Veterinary Gene therapy; Faculty of Veterinary sciences; Ghent University; Heidestraat 19 9820 Merelbeke, Belgium*
[3] *Univ. Klinikum Mannheim, Department of Neurology, Heidelberg University, D-68167 Mannheim, Germany*

Objectives: Adeno-associated virus is a promising gene therapy vector because of its high transfection efficiency. However, the use of AAVs in humans is limited by their high toxicity and their risk of infecting non-target cells. To obtain a safe viral vector, the immunogenic capsid of the AAV should be shielded from the immune system and the vector should be targeted to specific tissues. The objective of this study is to couple PEGylated AAVs with avidin-biotin chemistry to lipid microbubbles in order to obtain an ultrasound targeted release and transfection. This study will evaluate whether lipid microbubbles release PEG-biotinylated AAVs upon ultrasound exposure and evaluate the transfection efficiency of AAV loaded microbubbles *in vitro*. Hence AAV-loaded microbubbles may provide a solution for ultrasound targeted viral gene delivery.

Methods: PEGylation of EGFP expressing AAV2 was done using NHS-PEG-Biotin (Iris Biotech GmbH, Marktredwitz, Germany). Lipid microbubbles containing 85 mol% DPPC and 15 mol% of DSPE-PEG-Biotin were prepared. *In vitro* experiments were performed on BLM melanoma cells in Opticell plates and EGFP expression was measured with an FC500 Flow Cytometer. Ultrasound experiments were performed using a Sonitron sonoporator with an ultrasound frequency of 1MHz, 2W/cm^2 intensity and a 10% duty cycle.

Results: : Zeta-potential measurements confirmed AAV pegylation using NHS chemistry. Flow cytometry revealed that PEGylation of the AAV surface lowers their biological activity. We could prove microbubble coupling of AAVs through NHS-PEG-Biotin chemistry, by confocal microscopy. Flow cytometry analysis showed that melanoma cells can be infected by AAV loaded microbubbles and ultrasound, provided that the AAVs are not too strongly PEGylated. Confocal microscopy uptake studies however, showed an increased uptake after ultrasound treatment, possibly due to sonoporation

after bubble implosion. Although enhanced uptake was observed, an increased transfection rate is not seen, possibly due to the fact sonoporation evades receptor mediated endocytosis.

Conclusion: This study shows that loading of softly-PEGylated AAV vectors to microbubbles by avidin-biotin linkers is possible and ultrasound targeted delivery is possible using these constructs. Targeted delivery of fully-PEGylated AAVs however is shown to be impossible, although more adenoviruses are taken up ultrasound exposure. We believe that this uptake is due to sonoporation, a mechanism which is believed to evade receptor mediated uptake. Adenoviral vectors are mostly dependent of this mechanism, hereby limiting the functionality of ultrasound targeted drug delivery of viral vectors.

Enhancement of doxorubicin effect on cancer cell mortality with ultrasound and microbubbles

J. Piron, A. Novell, K. Kaddur, A. Bouakaz

INSERM U930-CNRS ERL 3106, 37044 Tours cedex 1; Université François Rabelais, 37032 Tours, France.

Potential use of clinical ultrasound (US) in enhancing the anti-cancer drugs effects in the treatment of cancers has been recently reported. Moreover US in combination with microbubbles have proven its efficiency in improving molecule uptake into cells through sonoporation mechanism. In this work, we want to verify that low intensity US and microbubbles could enhance anticancer-drug effect.

We evaluate the benefit of sonoporation in enhancing cell mortality using anti-cancer drug doxorubicin with U87MG cells (human glioma cells) and MDA-MB231 cells (human breast adenocarcinoma). Experiments were conducted in five groups: non treated, doxorubicin treated, US-microbubble treated, doxorubicin + US, and doxorubicin + US-microbubble. Cells were exposed to 5µM doxorubicin and sonicated at 1 MHz (with 40% duty cycle for 30s and acoustic pressures from 0.4 to 0.8 MPa). Twenty-four and 48h after treatment, cell mortality was evaluated by Trypan blue dye exclusion test. Four experimental microbubble types were investigated: BR14, Sonovue, Vevo Micromarker® and Polylactide Shelled microbubbles.

The results showed that for all microbubble types, a significant enhancement in doxorubicin effect was achieved when it was co-administred with microbubbles in comparison to the drug alone. U87MG cell viability in doxorubicin + US group was comparable to doxorubicin alone (57.4 ± 3.4 % versus 56.8 ± 3.7 % at 48h). When Vevo Micromarker® bubbles were co-administrated with doxorubicin, cell viability percentage was only 21.0 ± 2.0 % at 48h respectively. Using Sonovue, Polylactide Shelled and BR14 microbubbles, cell viabilities at 48h were respectively 39.6 ± 8.3 %, 40.6 ± 6.4 % and 32.7 ± 4.1 %.

Thus, at 48h, ratios of doxorubicin + US-microbubble condition and doxorubicin alone are 1.08 and 1.31 for Sonovue and Polylactide Shelled microbubbles respectively. The highest ratios were obtained with Vevo Micromarker® and BR14 microbubbles: 1.83 and 1.85 respectively.

With MDA-MB231 cells, the highest effect was obtained at 800 kPa Vevo Micromarker® bubbles. Five more cells were died by doxorubicin treatment in presence of US and Vevo Micromarker® bubbles. For others microbubble types, ratios were similar as those observed with U87MG cells.

In order to provide insights into the differences in efficiency between the different microbubble types, attenuation measurements were carried out before and after sonoporation. These acoustic behaviour characterisation showed that at t=0, Vevo Micromarker® bubbles exhibit the lowest attenuation, and that although a large part of the microbubbles are destroyed during the 30 seconds of insonation, only Vevo Micromarker® bubbles were completely destroyed.

Our results demonstrate that low intensity US and microbubbles could enhance anti-cancer drug effect, suggesting that this combination might be a useful tool for the cancers therapy.

Targeted delivery of cell-based therapy for vascular repair using acoustic radiation force

Catalin Toma, MD; Andrew Fisher, Jianjun Wang, PhD; Xucai Chen, PhD, Michelle, Grata, BS, Huili Fu, PhD, William R. Wagner, PhD; Flordeliza S. Villanueva, MD.

Center for Ultrasound Molecular Imaging and Therapeutics, University of Pittsburgh and McGowan Institute for Regenerative Medicine, Pittsburgh, PA

Background: Restoration of a functional endothelial barrier is a major requirement to preventing late stent thrombosis; furthermore, intact endothelium protects against progression of atherosclerotic plaque. To enhance endothelial repair in such settings, we are proposing a novel method for delivering cell therapy to the vascular wall using ultrasound-generated acoustic radiation force (RF).

Methods: Fluorescently labeled mesenchymal stem cells (MSCs, zeta potential -23.2 mV) were exposed in suspension to cationic lipid microbubbles (MB, zeta +55.2 mV) or negatively charged control MB (zeta -10 mV), allowing for electrostatic MB:cell coating. MB:cell association was quantified by flow cytometry based on the increased light scatter of the cell: microbubble complexes and verified by microscopy. The concept was tested first *in vitro* in a PVC tube under flow conditions (0.5Pa shear stress), with ultrasound (5 MHz, 1.2 MPa, 20% duty cycle) applied perpendicular to the direction of flow. *In vivo* testing was then performed in rabbits following balloon injury to the abdominal aorta, using an intravascular probe (1.7 MHz) to deliver RF to cell:MB complexes ($3x10^5$ fluorescently labeled rabbit MSCs) injected upstream of the injured segment.

Results: When RF was applied on MSCs passing through the PVC vessel phantom, arrest of 30±4 of cells was observed when cationic MB were used (n=6), while no cell marginalization was present when cells pre-mixed with negatively charged control MB were perfused. The effect was maximal when the ratio of MSC:MB mixed together in suspension was 1:40, resulting in 88±5% of MSCs covered by MB, with an average of 7±1 MB/cell (n=6). Acute *in vivo* histological results obtained at 20 minutes following cell delivery identified 784±303 MSCs on the endoluminal surface of the RF-treated rabbit aortic segment, while only 4±1 cells were found in the control area without RF (n=4, $p<0.05$).

Conclusions: Acoustic RF can be used to control and direct targeted endoluminal cellular paving in a denuded arterial segment.

Tracking of the Left Ventricular Borders in Contrast-Enhanced Ultrasound Images

K.Y.E. Leung, M.D. Danilouchkine, M. van Stralen, N. de Jong, A.F.W. van der Steen, and J.G. Bosch

Biomedical Engineering, Thoraxcenter, Erasmus MC, The Netherlands

Contrast agents are often used to enhance the visualization of the myocardium. For three-dimensional (3D) imaging, studies have shown that contrast indeed allows better visual assessment of left ventricular (LV) wall motion than noncontrast imaging[1]. To obtain a more quantitative measure of cardiac motion, delineation of the LV border in contrast images is necessary. This delineation should preferably be automated, to avoid tedious and subjective manual analysis.

In this study, we propose an automated method for 3D tracking of the endocardial borders. Standard methods which suffice in noncontrast images may fail in contrast images, due to intricate swirling patterns of the contrast. In particular, prior knowledge of the typical cardiac motion may be beneficial for guiding the tracking. Here, we propose the use of statistical models to capture patient variability in cardiac motion. The models represent the cardiac motion as frame-by-frame spatial transforms (rotation, translation, scaling and shear) throughout the cardiac cycle, which are learned from manually drawn borders in many patient image sequences. After generating these models, they are used to guide an optical-flow method to track the end-diastolic LV borders throughout the cardiac cycle in a new image sequence. Using the optical-flow equation, the motion between two image frames can be estimated by taking into account the spatiotemporal gradients in image intensities[2]. The models are integrated into the optical-flow equation to allow prior knowledge on cardiac motion to guide the tracking. We compared this “motion-guided” tracking with the “basic” optical-flow method without integrated models.

Evaluation is performed on 28 3D contrast-enhanced echocardiograms. An example of the tracking performance is shown in Fig. 1. The motion-guided method gives better tracking results (volume error: -1.5±10.1ml, ejection fraction error: 1.3±11.7%) than the basic method (volume error: 11.7±12.4ml, ejection fraction error: 14.7±10.8%). In conclusion, tracking in contrast images is highly promising using the proposed motion-guided method. By incorporated statistical prior knowledge, more consistent tracking results can be achieved. This is an important step toward automated quantification of cardiac function in contrast images.

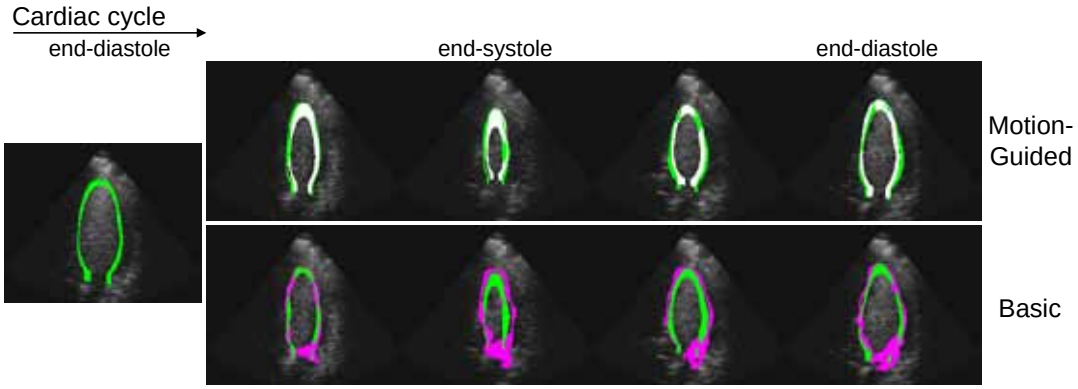

Fig. 1. Example of 3D tracking of the LV borders. Four-chamber cross-section is shown here. Green denotes the manually delineated ground truth, white the proposed "motion-guided" tracking, and magenta the basic tracking. Notice the irregular borders found by the basic tracking, due to complicated swirling patterns of the contrast.

1. Nemes A, Geleijnse ML, Krenning BJ, Soliman OII, Anwar AM, Vletter WB, Ten Cate FJ. Usefulness of ultrasound contrast agent to improve image quality during real-time three-dimensional stress echocardiography. Am J Cardiol 2007; 99:275-278.
2. Lucas BD, Kanade T. An iterative image registration technique with an application to stereo vision. Proc DARPA Image Understanding Workshop 1981:121-130.

Microbubbles for Acousto-Optic Imaging Signal Enhancement

Jack Honeysett[1], Terence Leung[1], Eleanor Stride[2]

[1]Department of Medical Physics and Bioengineering, University College London, London, UK
[2]Department of Mechanical Engineering, University College London, London, UK

Acousto-optic (AO) imaging is an attractive technique for biomedical applications on account of its high spatial resolution. In tissue however, the AO signal is often very weak due to strong optical scattering and this currently restricts the use of AO imaging to small tissue depths. Various schemes have been proposed to overcome this including the use of intense acoustic bursts, parallel detection using CCD cameras, and powerful long pulse laser illumination. The aim of this study is to investigate the potential for using microbubble ultrasound contrast agents to amplify the AO signals. The microbubble oscillations modify the AO signal in a number of ways. Firstly, they generate varying optical scattering due to changes in its surface area and internal refractive index. Secondly, they alter the pressure field around the bubble which in turn generates refractive index changes in the surrounding medium. In this work Monte Carlo (MC) simulations implemented on a graphical processing unit (Nvidia) are used to investigate how these factors affect the optical phase of a photon as it propagates through a turbid medium containing microbubbles. The scattering angle resulting from the collision between a photon and a microbubble is determined by a Mie scattering based phase function. The results show that the magnitude of the modulation depth of the AO signal is a function of the microbubble optical and acoustic characteristics, their concentration in the medium, the ultrasound frequency, the ultrasound intensity, as well as the optical absorption and scattering characteristics of the medium. The implications of these findings and experimental results for practical implementation will be discussed.

Development of quantitative contrast ultrasound imaging using the ovine ovarian model

Thomas DH[1], Lampaskis M[2], Silva N[1], Strouthos C[2], Averkiou M[2], McNeilly AM[3], Sboros V[1].

[1]Department of Medical Physics and Medical Engineering, University of Edinburgh, Edinburgh, UK.
[2] Department of Mechanical and Manufacturing Engineering, University of Cyprus, Nicosia, Cyprus.
[3]MRC Human reproductive Sciences Unit, University of Edinburgh.

The ovary is a unique organ with cyclical changes in its microvasculature, good endocrinological understanding and control, and has been used as a tumour model. It can thus be used as a model for developing tools for the accurate imaging of microvascular changes, with relevance to a wide range of microvascular disorders. The ability of parameters derived from time-intensity curves to provide quantitative microvasculature measurements is examined here using the ovine corpus luteum (CL), a highly vascular temporary endocrine structure within the ovary which is involved in production of progesterone. Five ewes across various days of the cycle were investigated using contrast-enhanced ultrasound with Sonovue®, in a pilot that assesses the usefulness of this model.

Each animal was opened under general anaesthesia, and the ovary was clamped in a fixed position ensuring unaltered function and surrounded by ultrasound gel to allow an unhindered image of the CL to be obtained with the L9-3 (Philips iU22) linear array probe. Contrast images were obtained using the nonlinear pulsing scheme power modulation. Bolus and flash-infusion protocols were followed and the captured uncompressed image data were analysed using first QLab v7.1 (Philips) image analysis software and then using Matlab 2009a (Mathworks) for statistical interpretation. Parameters derived from the time-intensity curves were calculated using the lognormal probability and the log normal cumulative distributions for the bolus and infusion protocols respectively. Two different bolus doses were used (1.2ml and 2.2ml) in order to asses the dose dependence of the time intensity parameters, with each injection repeated 5 times (in each animal) to measure the reproducibility. The infusions included 4.4ml of Sonovue® diluted in 10ml of saline at a rate of 4ml per min.

Mean values of standard error of 8% and 9% in the mean transit time (MTT) and wash in time (WIT) were measured in the bolus injections in each sheep, showing high levels of reproducibility with no significant dependence on the contrast dose. The peak intensity (I_{peak}) values showed a strong dependence on dose, both in amplitude and reproducibility; mean standard errors of 29% in the 1.2ml injections versus 26% in the 2.2ml injections across the five sheep. Similar results were observed in the area under the curve (AUC), with mean standard errors of 30% in the 1.2ml injections compared to

17% in the 2.2ml injections. A destruction-replenishment protocol (six high amplitude frames of 0.5MI, repeated every 30seconds) showed increased variation in MTT and WIT in the contrast replenishment curves, with standard errors of 29% and 42%. Variation of I_{peak} is similar to the 2.2ml bolus injections, with mean standard error of 19%.

The highly reproducible kinetic measurements with less than 10% variation in non-intensity related parameters (WIT, MTT) show that the ovarian angiogenic function lends itself for in depth quantitative non-invasive studies. Interestingly, amplitude related parameters (I_{peak}, AUC) provided encouraging results in this first attempt for quantification. Considering that a range of image settings, may affect these more than WIT and MTT, these results encourage further future work with reference tracer kinetics measurements from an independent vessel that may refine the measurement. In conclusion, the ovine CL model may develop into a 'golden standard' for contrast ultrasound imaging of microvascular measurements. The next steps include to fully exploit this model for the development of quantification of small microvascular changes, which has implications, apart from the female reproductive system, for a wide range of diseases such as ischemia, inflammation, cancer and their treatment monitoring.

Effect of Temperature on the Acoustic Characteristics and Stability of Ultrasound Contrast Agents

Helen Mulvana[1], Eleanor Stride[2], Mengxing Tang[3], Robert J Eckersley[1]

[1] Imaging Sciences Department, Imperial College London, UK; [2] Mechanical Engineering Department, University College London, UK; [3] Bioengineering Department, Imperial College London, UK.

Introduction

Accurate characterisation of ultrasound contrast agents is important to support their use in quantitative imaging and therapeutic applications. Laboratory investigations are frequently undertaken in a water bath at room temperature, and the validity of these measurements with respect to microbubble behaviour *in vivo* (37°C) is implicitly assumed.

In previous work (Mulvana et al., in press), we established that the bulk acoustic properties of a suspension of the ultrasound contrast agent SonoVue (Bracco Research, Geneva) were influenced by temperature. Increasing the suspending liquid temperature from 20 to 40°C led to an increase in attenuation from 1.5 – 2.9 dB (P = 0.004) and a 2 dB (P = 0.05) increase in the amplitude of the scattered signal from 2.3 – 2.9 kPa at an insonation pressure of 100 kPa. It was hypothesised that this increase was due primarily to temperature mediated gas expansion and its resulting influence on the size distribution of the bubble suspension. In addition, optical and acoustic experiments indicated that bubbles at body temperature were less stable than those at 20°C.

This work further explores these observations through the high speed imaging of single bubbles.

Methods

A high speed camera (Cordin 550, Cordin, Salt Lake City, USA) was used to assess the influence of increasing temperature from 20°C (*RT*) to 37°C *(BT)* on the dynamic behaviour of single SonoVue bubbles excited at low (~50 kPa) and moderate (~100 kPa) acoustic pressures. Additionally, a series of single bubbles were repeatedly excited at moderate acoustic pressures and their diameters prior to and following each excitation were compared to assess bubble stability.

A dilute suspension of SonoVue was injected into a 200 μm diameter cellulose capillary tube held within a tank of temperature controlled, filtered, de-ionised, gas-saturated, isotonic saline solution. Single isolated bubbles were excited with a 12 cycle, 0.5 MHz, Gaussian windowed pulse using a 0.5 MHz single element focused transducer (f = 40 mm). During repeat insonation a 10 pulse burst with a

pulse repetition frequency of 100 Hz was used. The high speed camera was run at 2.5 MHz and a series of 58 images obtained for each insonation. A fibre-optic hydrophone (Precision Acoustics, Dorset, UK) used with a tapered sensor at 90° alignment was used to characterise the acoustic field. Images were post-processed in Matlab to obtain time vs. diameter plots for each bubble.

Results

At the lower pressure (Fig. 1a), maximum bubble excursion was not influenced by temperature, indicating that under such conditions bubble behaviour is mainly determined by initial diameter. At higher pressure (Fig. 1b), a slight increase was recorded in the maximum excursion at *BT* compared to *RT*, as well as a slight change in the resonant frequency. Inspection of the images from which this data was generated shows that, at the higher pressure, bubbles oscillate in a dramatically more non-linear manner at *BT* than similarly sized bubbles at *RT*. This is particularly evident at resonance, with the result that jetting, shell fragmentation and gas expulsion are more likely to occur at *BT*. Due to these violent effects, purely spherical expansion of resonant bubbles no longer occurs, and the shell no longer encapsulates the gas core, hastening bubble dissolution.

Repeat insonation of single bubbles supported these findings. At *RT* a gradual decrease in resting diameter was seen with each subsequent excitation, as expected due to diffusion (Borden and Longo 2002). In contrast at *BT*, bubbles were frequently (33%) destroyed following the first insonation burst. Of the bubbles which did survive, a fivefold greater decrease in mean bubble diameter was seen as compared to *RT*, and no bubbles survived the second insonation burst.

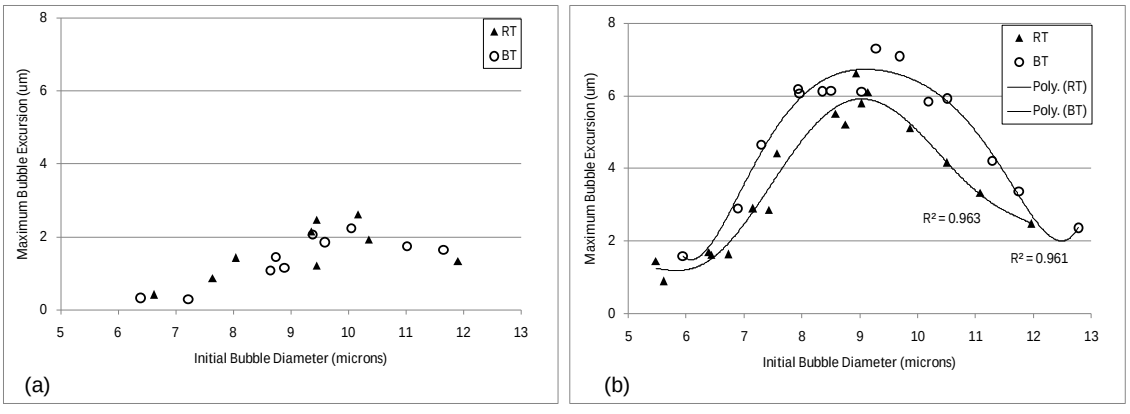

Figure 1 Maximum bubble excursion plotted against initial bubble diameter at room (20°C) and body (37°C) temperatures during (a) low MI excitation (~40 kPa) and (b) high MI (~100 kPa) excitation.

High speed observation of single bubbles provides evidence and justification for our hypothesis, generated as a result of bulk bubble investigation, i.e., that acoustic behaviour is dominated by bubble

diameter changes due to increasing temperature. In addition to this, increasing the temperature to approach the phase transition temperature of the phospholipid shell material, compromises the ability of the shell to contain the gas within the bubble, resulting in decreased stability of both static and acoustically driven bubbles. This effect is more noticeable at higher driving pressures, where the shell is not able to support the large amplitude non-linear oscillations which result.

Conclusions

High speed optical imaging has improved our understanding of the differences in behaviour between bubbles at *RT* and *BT*. In conclusion, investigation of USCAs should always be conducted at body temperature if results are to be related realistically to *in vivo* applications.

The authors would like to thank Dr John Civale and Anna Tokarczyk (Institute of Cancer Research, Sutton, UK) for their assistance with the hydrophone measurements.

This work was supported by an EPSRC grant (EP/F066740/1).

References

§ Borden MA, Longo ML, Dissolution behavior of lipid monolayer-coated, air-filled microbubbles: Effect of lipid hydrophobic chain length. Langmuir 2002;18:9225-33.

§ Mulvana HE, Stride E, Hajnal J, Eckersley R. Temperature dependent behaviour of ultrasound contrast agents. Accepted for publication in Ultras. In Med. And Biol.

OPTIMAL USE OF SILICA NANOPARTICLES FOR ENHANCED ULTRASOUND IMAGING AND AUTOMATIC TISSUE TYPING

Francesco Conversano[1], Andrea Ragusa[2], Antonio Greco[1], Sergio Casciaro[1]

Institute of Clinical Physiology, National Council of Research, Lecce, Italy
National Nanotechnology Laboratory of CNR-INFM, Distretto Tecnologico ISUFI, Lecce, Italy

Nowadays, all contrast agents that are approved for clinical ultrasound imaging applications consist of encapsulated gas microbubbles of a few micrometers[1], able to produce strong signal backscatter when insonified at frequencies belonging to the "diagnostic" range (typically 1-10 MHz). Since microbubbles cannot leave the vascular space, they cannot reach cells located beyond the capillary vasculature, such as many cancer cells. Actually, tumour angiogenesis vessels have the tendency to be "leaky"[2] and to exhibit the so-called EPR (enhanced permeability and retention) effect, which results in exaggerated extravasation and retention of particles that are smaller than the pore size of tumour endothelium (typically between 380 and 780 nm)[3,4].

For these reasons, intensive investigations have been undertaken to develop nano-sized cancer targeting agents for ultrasound molecular imaging[5-9]. The most significant experiments involving nanoparticles (NPs) as ultrasound contrast agents were carried out on nanobubbles[6], perfluorocarbon nanodroplets[7] and echogenic liposomes[8]. The use of solid NPs provides higher signal enhancement as well as longer stability than liquid and gaseous particles of the same size. Nevertheless, ultrasound investigations of solid NPs have been until now limited to very high frequencies (30-40 MHz)[5,9], whose clinical usefulness is restricted to few highly specific applications.

In this work we demonstrated the feasibility of using silica NPs as ultrasound contrast agents at common diagnostic frequencies, by investigating the enhancement produced by varying particle concentration and diameter in a range of clinical interest for tumour targeting and subsequent automatic detection through radiofrequency (RF) signal analysis.

Silica was chosen as the elective material for this investigation because of its biocompatibility[10-12], ease of bioactive molecule encapsulation[11], simplicity of nanoparticle formation[12], and successful use as drug delivery vector[11,13]. Silica NPs were synthesized in spherical shape with three different diameter values (150 nm, 300 nm, 600 nm), considering that "ideal" NPs should be suitably stable in the bloodstream without being detected and immediately removed by the reticuloendothelial system (RES). In fact, NP size has to be bigger than 50 nm (size of intercellular openings in normal vessel walls) to avoid non-specific distribution in the body, and not much bigger than 300 nm to escape as much as

possible the RES trapping effects[11] as well as to remain under the smallest reported value of tumour endothelium pores (380 nm)[3,4] for complying with targeting constraints.

Diagnostic power of the synthesized NPs was evaluated by studying ultrasound backscatter behaviour when dispersed in agarose gel samples contained into Petri dishes: pure agarose gel was essentially transparent to ultrasound, while silica NPs generated visible backscatter, already at low concentrations. For each considered NP size, in fact, we tested samples containing variable volume concentrations of dispersed silica NPs (up to 3%). Each prepared sample was imaged employing a digital ecograph (Megas GPX, Esaote Spa, Florence, Italy), equipped with a linear transducer (LA523, Esaote Spa) operating at 7.5 MHz and linked via optic fibre to a prototype platform for acquisition of unprocessed RF data (FEMMINA, ELEN Spa, Florence, Italy). The ultrasound probe was mounted on the motorized piston of an infusion pump (KDS 100, KD Scientific Inc., Holliston, MA, USA) and automatically scanned along the sample. The sample was immersed in distilled water and the transducer, in turn partially immersed in the water, was positioned perpendicular to the Petri dish bottom at such a distance that the transducer focus (set to 2 cm) was located half-way through gel depth. Each sample was scanned for 1 cm in its central part at a speed of 1 mm/min and 600 frames of RF data were each time acquired (frame-rate = 1 fps). Echograph parameters were the same for all the acquisitions: power = 50%, gain = 0 dB, linear TGC. Then, for each acquired frame, a rectangular region of interest (ROI) composed of 100 echographic tracks with 90 points/track was positioned in the central zone of the imaged gel section, so that the corresponding backscatter values were not influenced by any boundary effect. The mean backscatter amplitude of each frame was calculated as the average of the grey level values of the 9,000 pixels belonging to the ROI. The ultrasound backscatter amplitude associated to each sample was the average of the 600 values resulting from the corresponding frame sequence.

Obtained results show that, for each considered NP size, the average grey level in the ROI increases with NP concentration with a “logarithmic-like” trend, i.e. each grey level curve raises with progressively decreasing slopes, up the reaching of a kind of “plateau”, then any further increment in NP concentration does not produce any appreciable additional contrast enhancement. Therefore, we can state that the maximum achievable enhancement is always less than 8 times the control brightness, with a suitable value (between 4 and 6 times the control brightness) that can be reached by employing silica NPs within the following ranges of volume concentration: 0.8-2.3% for 150-nm NPs; 0.2-0.4% for 300-nm NPs; 0.4-0.8% for 600-nm NPs.

It is interesting to note that the lowest required NP concentration to obtain the same contrast enhancement does not correspond to the biggest NP diameter (600 nm), but to 300-nm NPs. This is due to the combined effect of number and diameter of NPs on the final image enhancement at the employed ultrasound frequency. In fact, by analysing the contrast enhancement as a function of NP size for a fixed volume concentration, image brightness always reaches its peak in correspondence of 300 nm.

This indicates that 150-nm NPs, although they are 8-fold as numerous as 300-nm NPs, are too small to produce an effective ultrasound backscattering, while 600-nm have a reduced global scattering efficacy being 8-fold less numerous with respect to 300-nm NPs, despite the increased diameter. Therefore, 300-nm silica NPs present the most suitable combination of number concentration and diameter value to act as powerful US scatterers with a low volume dose and at conventional diagnostic frequencies.

As a further goal of the present study, information available in the raw RF signal has been exploited to automatically discriminate tissue target by means of silica NPs. A software for wavelet decomposition and spectral analysis (RULES, ELEN SpA, Florence, Italy) has been employed to develop a tailored colour map then applied to raw RF signals acquired through FEMMINA[14]. This technique was applied on a different group of NP-containing agarose gel samples, synthesized just for this specific purpose and consisting of Petri dishes filled with a layer of agarose gel containing silica NPs placed between two different layers of pure agarose gel. One of these samples was prepared for each of the considered NP sizes and all of them underwent the same echographic scansion previously described.

RF acquired data were off-line processed with RULES, in order to find a specific algorithm configuration to selectively discriminate the NP-containing layer from the surrounding layers of pure agarose gel. In particular, a different configuration was found for each tested NP size, employing each time a different sub-group of the 25 parameters available in RULES, each parameter with its proper settings. The final output of this algorithm was the superimposition on the initial B-mode image of a specific colour map, capable of identifying the searched NPs in each of the acquired image frames.

Precision and accuracy of the adopted methodology was quantified through evaluation of sensibility, specificity and Dice similarity coefficient (DSC)[15], that were respectively: 16%, 98% and 20% for 150-nm NPs; 74%, 99% and 80% for 300-nm NPs; 63%, 98% and 69% for 600-nm NPs. Therefore, also for quantitative tissue typing applications, 300-nm silica NPs showed an impressive discrimination power in targeted tissues, significantly higher than the corresponding for smaller and bigger particles of the same material.

In conclusion, this study demonstrated the feasibility of ultrasound molecular imaging by means of silica NPs as contrast agents in the range of conventional diagnostic frequencies. The optimal size for medical applications resulted of 300 nm with a volume concentration of 0.4%. Furthermore, these contrast agents have been shown to provide a characteristic “signature” in the RF ultrasound signal, so offering a unique diagnostic opportunity to automatically discriminate pathological from healthy tissues with high prediction values.

ACKNOWLEDGMENTS

This work was partially funded by the grant N° DM18604 – Bando Laboratori – DD MIUR 14.5.2005 n.602/Ric/2005 of the Italian Ministry of Instruction and Research.

REFERENCES

1. Villanueva FS. Molecular imaging of cardiovascular disease using ultrasound. J Nucl Cardiol 2008;15:576-586.
2. Pasqualini R, Arap W, McDonald DM. Probing the structural and molecular diversity of tumor vasculature. Trend Molec Med 2002;8:563-571.
3. Hobbs SK, et al. Regulation of transport pathways in tumor vessels: role of tumor type and microenvironment. Proc Natl Acad Sci 1998;95:4607-4612.
4. Maeda H, Wu J, Sawa T, Matsunama Y, Hori K. Tumor vascular permeability and the EPR effect in macromolecular therapeutics: a review. J Control Release 2000;65:271-284.
5. Liu J, et al. Nanoparticles as image enhancing agents for ultrasonography. Phys Med Biol 2006;51:2179-2189.
6. Wheatley MA, Forsberg F, Dube N, Patel M, Oeffinger BE. Surfacant-stabilized contrast agent on the nanoscale for diagnostic ultrasound imaging. Ultrasound Med Biol 2006;32:83-93.
7. Dayton PA, et al. Application of ultrasound to selectively localize nanodroplets for targeted imaging and therapy. Mol Imaging 2006;5:160-174.
8. Buchanan KD, Huang S, Kim H, MacDonald RC, McPherson DD. Echogenic liposome compositions for increased retention of ultrasound reflectivity at physiologic temperature. J Pharm Sci 2008;97:2242-2249.
9. Liu J, Li J, Rosol TJ, Pan X, Voorhees JL. Biodegradable nanoparticles for targeted ultrasound imaging of breast cancer cells in vitro. Phys Med Biol 2007;52:4739-4747.
10. Jin Y, Kannan S, Wu M, Zhao JX. Toxicity of luminescent silica nanoparticles to living cells. Chem Res Toxicol 2007;20:1126-1133.
11. Barbè C, et al. Silica particles: a novel drug-delivery system. Adv Mater 2004;16:1959-1966.
12. Piao Y, Burns A, Kim J, Wiesner U, Hyeon T. Designed fabrication of silica-based nanostructured particle systems for nanomedicine applications. Adv Funct Mater 2008;18:3745-3758.
13. Moulari B, Pertuit D, Pellequer Y, Lamprecht A. The targeting of surface modified silica nanoparticles to inflamed tissue in experimental colitis. Biomaterials 2008;29:4554-4560.
14. Masotti L, et al. FEMMINA: real-time, radio-frequency echo-signal equipment for testing novel investigation methods. IEEE Trans Ultrason Ferroelectr Freq Control 2006;53:1783-1795.
15. Massoptier L, Casciaro S. A new fully automatic and robust algorithm for fast segmentation of liver tissue and tumors from CT scans. Eur Radiol 2008;18:1658-1665.

The acoustic response of individual microbubbles in tubes

Mairead Butler[1], Aris Dermitzakis[2], David Thomas[1], Steve Pye[3], Vassilis Sboros[1]

1. Medical Physics, Centre for Cardiovascular Research, University of Edinburgh, UK
2. University of Patras, Greece
3. Medical Physics, NHS Lothian, Edinburgh, UK

There are no specific ultrasound imaging techniques which allow the differentiation between microbubbles in small vessels and large vessels *in vivo*. It is known that the presence of a tube wall influences the acoustic response of microbubbles (Garbin 2007). Data describing the acoustic response of individual, free microbubbles have previously been obtained using specifically designed experimental equipment (Sboros 2003, Thomas 2009). The existing experiment system was modified to allow the acoustic interrogation of microbubbles in mounted tubes. Cellulose based tubes of 200um diameter and acrylic tubes of 180um and 50 um diameter were used with contrast agents Definity (Lantheus Imaging) and BiSphere (Point BioMedical). Data for free bubbles subject to the same acoustic field as the tube was also available and used for comparison. The transmit frequency was 1.6 MHz and the pulse 6-cycles. The acoustic pressure ranged from 160 to 1000 kPa

For all microbubbles the fundamental and harmonic RMS backscattered pressure was calculated. In all tube sizes differences in the response of free microbubbles and microbubbles in tubes were observed, with the difference becoming more pronounced in the narrower tubes.

For rigid shelled biSphere, in the 200um tube, the lifetime of the microbubbles, i.e. number of consecutive pulses for which an echo was detected, was less than free biSphere microbubbles subject to the same acoustic pressure, e.g. at 550 kPa insonation, 33% of biSphere microbubbles in the 200um cellulose tube gave no echo after 7 consecutive insonations (1ms interval) whereas 7% of the free microbubbles gave no echo. In the 200um tube at 550 kPa the mean fundamental RMS pressure was 2.1 $\pm$ 1.3 Pa compared to 4.7 $\pm$ 3.7 Pa for free. In the 180um and 50um tube the harmonic response of the biSphere was higher than in the 200um tube and for free microbubbles. For biSphere, microbubble destruction increased with reducing tube diameter.

For lipid shelled Definity, there was an increase in the harmonic content of the microbubbles with decreasing tube size. The mean fundamental RMS pressure for free microbubbles was 5.69 $\pm$ 5.4 Pa and 2.72 $\pm$ 1.35 Pa in the 50um tube. In 200 um diameter tubes, more microbubbles survived consecutive

pulses, e.g. at 300kPa, after 7 consecutive pulses, no signal was detected from 33% of Definity microbubbles compared to 8% of microbubbles in the tube.

The size distributions of the microbubbles were assessed with the median value for free biSphere microbubbles being 3.15 $\pm$ 0.1 um and microbubbles in the 200um tube being 3.43 $\pm$ 0.1 um in diameter. This may explain part of the change in the observed acoustic behaviour.

Apart from the observed changes in the data presented here, the acoustic setup has shown that very small changes in the microbubble population acoustic behaviour are possible to record. This work provides valuable insight into the acoustic behaviour of microbubbles in tubes and might be useful for further developing pulse sequences for detecting microbubbles in tubes.

References

- Garbin V. et al., "Changes in microbubble dynamics near a boundary revealed by combined optical micromanipulation and high-speed imaging," *Appl Phys Lett* 90 (11): 114103 (2007).
- Sboros V. et al., "The behaviour of individual contrast agent microbubbles," *Ultrasound in Medicine & Biology* 29 (5): 687-694 (2003).
- Thomas D.H. et al., "Single Microbubble Response Using Pulse Sequences: Initial Results," *Ultrasound in Medicine & Biology* 35 (1): 112-119 (2009).

Investigating the nonlinear response of individual lipid encapsulated microbubbles at high frequencies

Brandon Helfield[1,2], Emma Huo[2], Emmanuel Cherin[2] and David Goertz[1,2]

[1]Department of Medical Biophysics, University of Toronto, Toronto, Ontario, Canada
[2]Sunnybrook Health and Sciences Centre, Toronto, Ontario, Canada

Microbubbles have been extensively employed in diagnostic ultrasound (f < 5MHz) to enhance the signal from blood and thereby increase the contrast between blood and tissue. Recently, there has been increasing interest in contrast imaging at higher frequencies; applications ranging from intravascular imaging, ophthalmology and small animal imaging. It has been established that populations of small lipid encapsulated microbubbles respond non-linearly at frequencies above 20 MHz. Despite these advances, the underlying behavior of these small microbubbles and their individual acoustic response is not well understood at these higher frequencies. Further understanding of these responses can lead to better optimization of contrast agents, improved contrast detection strategies and to enable quantitative data analysis of contrast images at high frequencies.

In this study, the acoustic response of individual bubbles from four types of lipid encapsulated agents was investigated: Definity (Lantheus Medical Imaging), Micromarker (Bracco Research), and two in-house fabricated agents. The former two agents were selected as they are widely used to perform nonlinear imaging at high frequencies. The latter two agents were used to investigate the potential role of shell microstructure on nonlinear microbubble behaviour and were prepared according to previously reported procedures[1] to have either a heterogeneous shell microstructure (comprised of larger condensed phase domains) or a macroscopically homogeneous structure. Experiments were conducted on individual microbubbles adjacent to an agar surface. Bubbles were optically sized and insonified at 25 MHz to examine their subharmonic response. Peak negative pressure ranged from 28 KPa to 1.28 MPa with either 10% bandwidth Gaussian enveloped pulses or tapered rectangular pulses. The echoes were then compared to simulations to gain insight into characteristics of nonlinear oscillations, particularly with regard to the symmetry of bubble oscillations.

Micromarker was found to be highly effective at generating nonlinearities, with 100% of bubbles with diameters between 1 and 3 μm (n=31) undergoing nondestructive subharmonic oscillations. Definity was found to have a more heterogeneous response with 66% for bubbles sized between 1 and 2 μm, and

[1] Borden et al., "Lateral Phase Separation in Lipid-Coated Microbubbles," **Langmuir** 22, 4291-4297 (2006)

33% for bubbles between 2 and 3 μm showing subharmonic behaviour (n=50). In addition, the pressure threshold for the onset of subharmonic generation was found to differ between these two agents. 71% of the Micromarker bubbles that generated subharmonics had onset pressure levels between 89-119 KPa to initiate subharmonics, while the majority of Definity (87%) had onset pressures between 147-473 KPa. For the in-house agents, it was found that 44% of the coarse microstructure bubbles were non-linearly active over a range of 1 to 3 μm (n=24), whereas only 15% of the homogeneous microstructure bubbles were over the same range (n=59). The propensity for subharmonic generation and variability in pressure thresholds for small lipid encapsulated microbubbles was therefore found to be highly sensitive to the specific microbubble formulation. The results also suggest that shell microstructure may be an important factor responsible for causing these heterogeneous responses. The phase relationship between the fundamental and subharmonic components of the received nonlinear signals was then examined and was found to be generally consistent between bubbles. A comparison of the measured and theoretical phase relationships indicates that subharmonics at these frequencies are associated with highly asymmetric oscillations.

Wideband Harmonic imaging of ultrasound contrast agent with a CMUT Probe

Anthony Novell and Ayache Bouakaz

UMR INSERM U930, CNRS ERL 3106 and Université François Rabelais, Tours, France

Aim: Upon suitable excitation, microbubbles generate different nonlinear components such as 2nd harmonic, superharmonic or subharmonic components. Currently, due to the limited frequency bandwidth of PZT transducers, only a single nonlinear component is selected and imaged. Today, advantages of Capacitive Micromachined Ultrasonic Transducers (CMUTs) such as wide frequency bandwidth could be used in nonlinear contrast imaging. However, the driving electrostatic force induces a nonlinear behavior generating thus undesirable harmonic components. Thanks to compensation methods, it is possible to considerably reduce these unwanted components by modifying the excitation waveform and exploit CMUTs for nonlinear contrast imaging. Compensation methods consist in transmitting, in addition to the fundamental excitation component, another frequency component in order to suppress the nonlinearities from the source. These methods allow recovering only the nonlinearities of the explored media and discriminating the harmonic generated by CMUT. We propose in this study the exploitation of the wide CMUT bandwidth to enhance the response from microbubbles by selective imaging of the 2nd harmonic and the subharmonic components concomitantly. This wideband imaging technique should improve both contrast to tissue ratio (CTR) and signal to noise ratio (SNR).

Methods: Experiments were performed using a 128 elements CMUT linear array probe centered at 4 MHz. The measured CMUT bandwidth at -6 dB was higher than 120%. The probe was connected to an open scanner with arbitrary waveform transmitters (M2M, France). A 2-cycle excitation Gaussian pulse of 2 MHz at 700 kPa and 60% bandwidth was transmitted. First, optimal parameters for compensation of the nonlinearities of the probe (e.g, phase or amplitude) were estimated using hydrophone measurements in order to reduce the 2nd harmonic component generated by the CMUT probe. Then, contrast agent harmonic imaging was performed using a 1/2000 diluted solution of SonoVue® microbubbles in a flow phantom. Selective imaging at a wide frequency band including both the second harmonic (at 4MHz) and the subharmonic (at 1MHz) components was performed. Imaging performances were evaluated in terms of CTR and SNR.

Results: Hydrophone measurements show that the CMUT generates a 2nd harmonic level only 6 dB below the fundamental level at 2MHz. After compensation, we achieve a 16 dB reduction of the 2nd harmonic component. Applying the compensation technique showed that the CTR at the 2nd harmonic band increased by 11 dB. Taking advantage of the wide band of the probe, the compensation procedure was applied to image both the 2nd and the sub harmonic concomitantly. Compared to subharmonic imaging alone, the addition of the 2nd harmonic component provides an increase of the SNR by 6.53 dB. The results are shown in the figure below.

Conclusion: These results demonstrate the ability to increase both CTR and SNR when wide band imaging is performed in combination with CMUT probes.

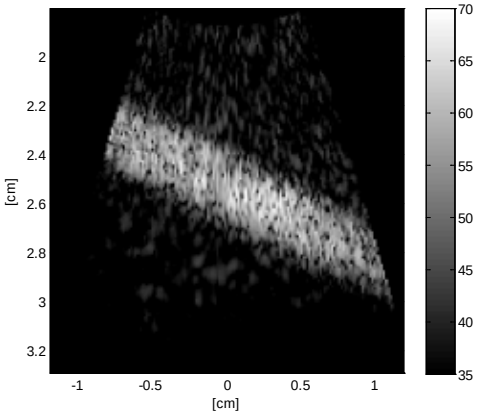

2nd harmonic imaging (2/4 MHz) without compensation

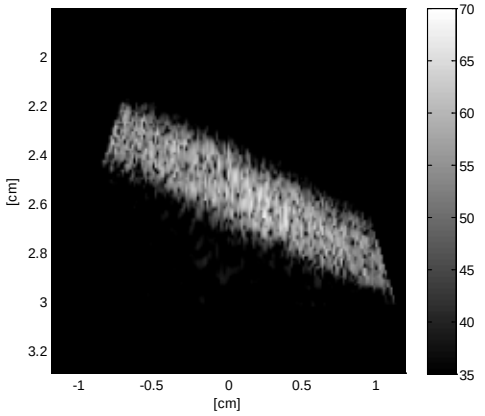

2nd harmonic imaging (2/4 MHz) after compensation

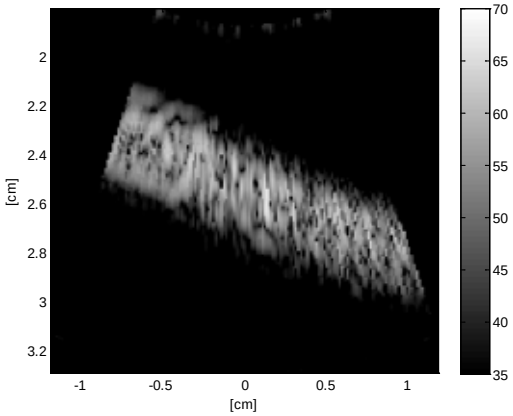

Subharmonic imaging (2/1 MHz)

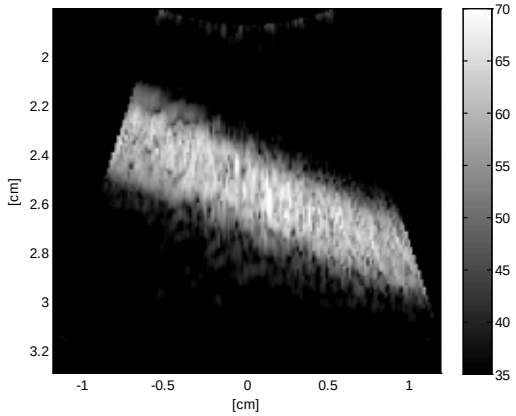

Wideband nonlinear imaging (2nd harmonic + subharmonic)

Subharmonic spectroscopy of ultrasound contrast agents

Telli Faez, Margreet Docter, Nico de Jong

Biomedical Engineering, ErasmusMC, the Netherlands
t.faez@erasmusmc.nl

Introduction

Atherosclerosis leads to the formation of multiple plaques within the arteries. Rupture of vulnerable plaque causes thrombosis, which rapidly slow or stop blood flow leading to a heart attack or stroke. The aim of this research is the early detection of vulnerable plaque by 3D ultrasound. For this reason a 2D matrix probe is designed with the frequency bandwidth of 5 to 10 MHz. Contrast agents are used to enhance the intensity of blood over tissue for better resolution and the subharmonic mode is chosen due to higher contrast to tissue ratio (CTR) [1]. In this study, the behavior of contrast agents was investigated for our specific frequency range, which is outside the commonly used range [2].

Material and methods

A highly diluted portion of BR14 contrast agent microbubbles (Bracco Research S.A., Geneva, Switzerland) was insonified with a transducer at frequency range of 2-7 MHz with step size of 200 kHz. The experiment was repeated in three acoustic pressures at focus: 50, 100 and 120 kPa. The response of the bubbles was recorded with the ultrafast recording camera (Brandaris 128). 30 single bubbles with approximate diameters between 1.5 to 5 μm were recorded. The diameter of the bubbles as a function of time (DT-curve) and the corresponding power spectra were determined. From the DT-curves the amplitude of excursion at transmitted frequency and half that frequency was calculated. The results were fitted to the response of a harmonic oscillator and the resonance frequency of corresponding bubble was extracted.

Results

30% of studied bubbles showed subharmonic scattering. These bubbles had the diameter between 2.5 and 4.5 μm. Figure (1) shows the resonance frequency of a 4.4 μm bubble at 2.7 MHz at 50 *kPa* and the shift towards lower frequencies by increasing the pressure.

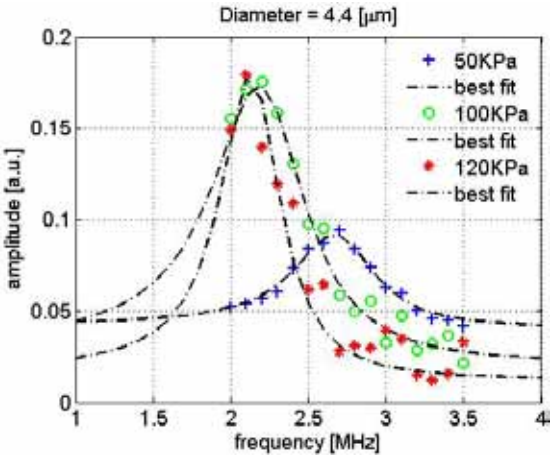

Fig 1- *Resonance curve (Amplitude vs. frequency) of 4.4 μm diameter bubble and fit with the resonance curve for a dumped harmonic oscillator driven by a sinusoidal forcing (Lorentzian function)* f_{res} *= 2.7, 2.23 and 2.15 MHz for 50, 100 and 120 kPa respectively.*

Discussion

In order to study subharmonic signal of this contrast agent in the frequency range of designed 2D probe (5-10 MHz) the experiments have to be repeated for transmitting frequencies double the bandwidth of the transducer. At the moment we are limited with the speed of Brandaris to reach this goal. Although, similar experiments on smaller bubbles at higher frequencies up to 12 MHz are in progress.

References

1. Shankar, US Med&Bio 24, p395, 1998
2. Steven B. Feinstein, Am J Physiol Heart Circ Physiol 287:450-457, 2004

Ultra high-speed fluorescence imaging of ultrasound-triggered local drug release

Erik Gelderblom[a], Klazina Kooiman[b], Marcel Böhmer[c], Nico de Jong[ab], Detlef Lohse[a], and Michel Versluis[a]

[a] Physics of Fluids Group, University of Twente, Enschede, The Netherlands
[b] Biomedical Engineering, Erasmus MC, Rotterdam, The Netherlands
[c] Philips Research, Eindhoven, The Netherlands
e.c.gelderblom@utwente.nl

Background

Detailed knowledge on the complex dynamics of ultrasound contrast agents has been gained through the use of the Brandaris 128 high speed imaging facility[1]. The non-linear behavior of coated bubbles, including an enhanced subharmonic response and 'compression-only' behaviour[2] as a result of shell buckling[3] were discovered by combining bright field microscopy with high-speed imaging at frame rates at a tenfold of the driving ultrasound frequency. A major drawback of such a visualization method is the poor contrast of the bubble wall due to a complex interplay of refraction and scattering of the light transmitted in back-illumination. In addition, bright field imaging lacks the ability to distinguish between liquid media with similar refractive index, which is crucial for the visualization of drug release.

Fluorescence microscopy does not suffer from the above shortcomings. Figure 1 shows a microcapsule (Philips Research[5]) imaged both in bright field and in fluorescence. The latter shows a distinct delineation of the wall boundaries and in addition a high contrast is achieved between the fluorescent liquid core and its surroundings. However, the nanoseconds timescales at which bubble oscillations, rupture and release take place makes time-resolved fluorescence imaging extremely challenging.

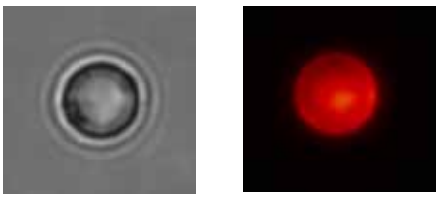

Figure 1 – Microcapsule imaged in bright field and in fluorescence (radius 2.5 μm).

Experimental setup

The excitation light source is a high power CW laser to maximize the fluorescence signal. An acousto-optic modulator controls the pulse length and avoids overexposure and heating of the (biological) sample. The fluorescence emission is captured by the objective and is coupled into the camera. The

microcapsules were recorded with a frame rate of up to 10 million frames per second, giving a unique insight into the physical mechanisms of local intravascular drug delivery.

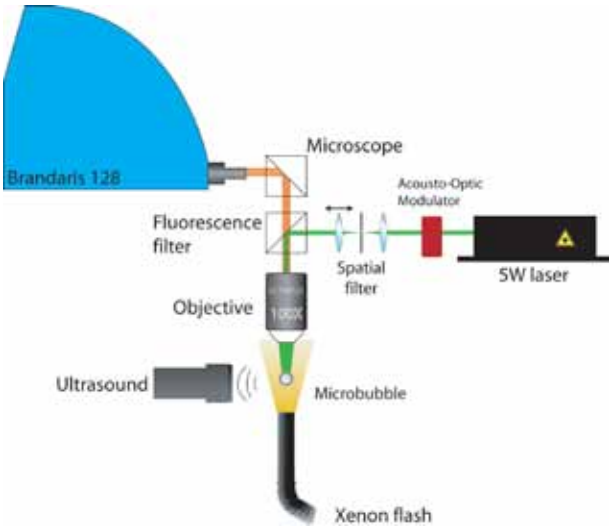

Figure 2 – Schematic of the experimental setup.

Results

Phospholipid-coated microbubbles with a perfluorobutane gas core were produced in-house (method described by Klibanov et al.). The fluorescently labeled microbubbles were driven by ultrasound at a frequency of 500 kHz and were recorded at a frame rate of 2 million frames per second. The fluorescence recordings show a higher contrast and enhanced details of the shell, as compared to the bright field recordings.

Oil-filled polymeric microcapsules (Philips Research[5]) with a high dye concentration mixed in the hexadecane liquid core demonstrate a photo-acoustic effect when excited with a laser intensity of just 1 MW/cm^2. The dye molecules absorb the laser light leading to intense heating of the liquid core. Rapid vaporization leads to expansion and finally the vapor starts to oscillate with a typical frequency of 200

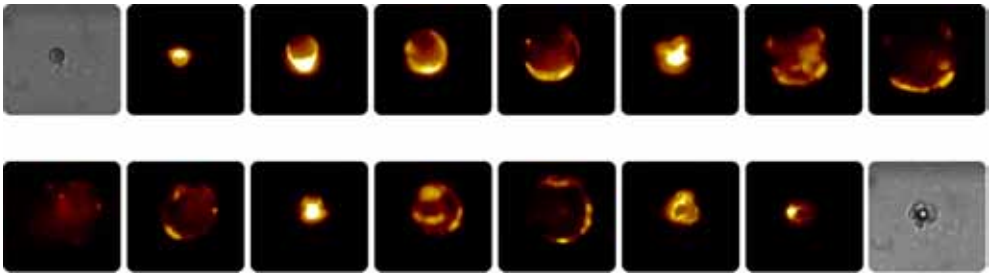

kHz. Figure 3 shows several frames from the fluorescence recording of the vapor bubble dynamics.

Figure 3 – Fluorescence recording (3 Mfps) of the photo-acoustic effect of an oil-filled microcapsule. Bright field images show the initial and final state.

Conclusion

Ultra high-speed fluorescence imaging is a powerful tool for the visualization of the instantaneous dynamics of coated bubbles. Drug release, its flow and resulting transfection can be observed at nanoseconds timescales.

References

1. Chin CT, Lancee C, Borsboom J, Mastik F, Frijlink M, de Jong N, Versluis M, Lohse D. Rev Sci Instru, 74 (2003).
2. N. de Jong, C.T. Chin, A. Bouakaz, F. Mastik, D. Lohse, and M. Versluis, Ultrasound Med.Biol. **33**, 653 (2007).
3. P. Marmottant, S. van der Meer, M. Emmer, M. Versluis, N. de Jong, S. Hilgenfeldt, D. Lohse, J. Acoust. Soc. Am. **118** (2005).
4. A.L. Klibanov, P.T. Rasche, M.S. Hughes, J.K. Wojdyla, K.P. Galen, J.H. Wible, and G.H. Brandenburger, Detection of Individual Microbubbles of Ultrasound Contrast Agents: Imaging of Free-Floating and Targeted Bubbles, Invest. Radiol., vol. 39, pp. 187-95 (2004).
5. M.R.Böhmer, R. Schroeders, J.A.M. Steenbakkers, S.H.P.M. de Winter, P.A. Duineveld, J.Lub, W.P.M. Nijssen, J.A. Pikkemaat, and H.R. Stapert, Preparation of monodisperse polymer particles and capsules by ink-jet printing, Colloids and Surfaces A, 289, 96–104 (2006).

Parametric Ultrasound Contrast Imaging with a Micro-Ultrasound System: A Reproducibility Study in Mice

A. Needles[1], T. Coulthard[1], N. Rognin[2], M. Arditi[2], L. Mercier[2], P. Frinking[2], and F.S. Foster[1,3]

1. VisualSonics, Toronto, Canada
2. Bracco Research SA, Geneva, Switzerland
3. Sunnybrook Research Institute, Toronto, Canada

Introduction:

This study focuses on the reproducibility of microbubble kinetics quantification in small animals, as assessed by a new software program developed for that purpose. This quantification software uses image sequences from a newly developed nonlinear contrast imaging mode on a micro-ultrasound system (Needles et al. 2009), applies curve-fitting with a perfusion model function to the acquired image sequence, and displays parametric images which map various parameters related to blood flow in perfused tissues. This study was conducted on assessing renal blood perfusion in the kidneys of healthy adult mice using the new quantification software tools. This should ultimately provide a set of baseline results which pre-clinical researchers can use as a guide to assess reproducibility in their *in vivo* perfusion studies using contrast imaging in mice.

Methods:

A micro-ultrasound system (Vevo 2100, VisualSonics) was operated at 18 MHz in Nonlinear Contrast Mode, with a 256 element linear array transducer (MS-250, VisualSonics, f_c = 21 MHz, 70% -6dB two-way bandwidth). *In vivo* imaging was conducted with MicroMarker™ (VisualSonics) contrast agent in the kidneys of healthy adult mice. Five female mice (average weight = 23.2 ± 1.8 g) and five male mice (average weight = 33.8 ± 3.1 g) were administered a single 50-µl bolus of contrast agent ($1.2 \cdot 10^7$ bubbles per bolus). Heart rate (HR), body temperature (T), and respiratory rate (RR) were monitored throughout the injection of the contrast agent and after its subsequent washout to ensure they were within normal limits (HR = 400-500 bpm, T = 35-37 °C, RR = 1-2 Hz). The scan plane was oriented from the dorsal side of the mouse, through a long section of the kidney. The scan plane was chosen to encompass as much of the kidney cortex and medulla as possible for assessing the perfusion of the microcirculation, while avoiding the larger renal blood vessels. Regions of interest (ROI) were placed in the medulla and the cortex. Time intensity curves (TIC) of relative echo-power obtained by

linearization of video signals (Rognin et al. 2008) were fitted for the different regions with a dedicated bolus model, using prototype quantification software (Bracco Research SA, Geneva). Parameters related to blood volume and flow (Peak Enhancement (PE), Wash-In Rate (WiR) and Rise Time (RT)) were obtained from the model fits within each ROI. The values of these parameters were recorded for each ROI, as well as the ratios between the two ROI (cortex/medulla). The rationale for quantifying the ratio stems from the fact that many researchers are interested in relative cortical vs. medullary flow when assessing renal function and response to treatments (Franchini and Cowley 1996; Mattson and Meister 2005). The software also generated parametric images from the model fits, which depicted spatial distributions of calculated parameter values. These parametric images were generated by curve-fitting the TIC in each pixel with the model function, in order to generate one parametric image for each given parameter. The parametric images of RT were used to manually segment the ROI placement for the regions within the medulla and cortex, as clear delineation was possible due to the different kinetics within these two tissue types (see Fig.2d as an example). Finally, the Coefficient of Variation (CV) (i.e. the ratio of standard deviation to the mean) for each parameter was expressed as a percentage for the set of female mice, male mice, and all mice grouped together.

Results:

Fig. 1 shows representative Nonlinear Contrast images of a female mouse at various instants during a contrast bolus.

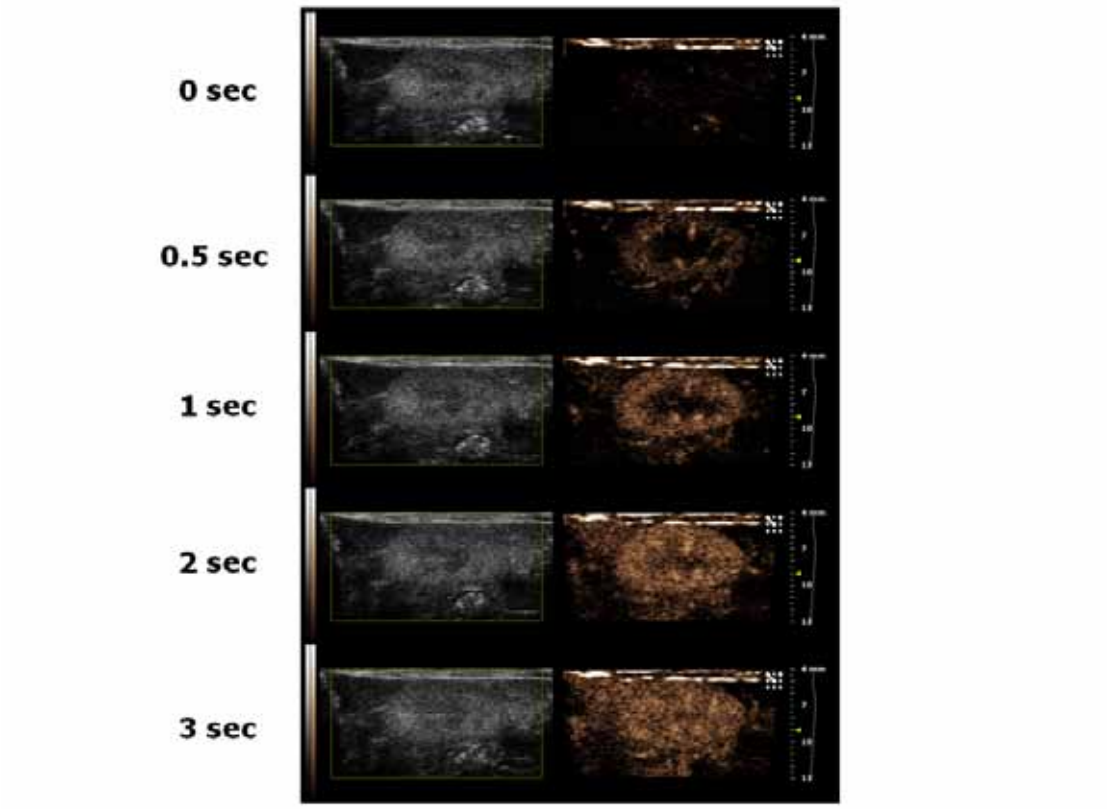

Fig. 1 – Nonlinear Contrast imaging sequence at various instants during a contrast agent bolus in a female mouse kidney. B-Mode images of the kidney (left) are displayed side-by-side with the Nonlinear Contrast images (right).

The TIC and parametric images of PE, WiR, and RT for the same animal are illustrated in Fig. 2 with the ROI shown on the parametric image of RT.

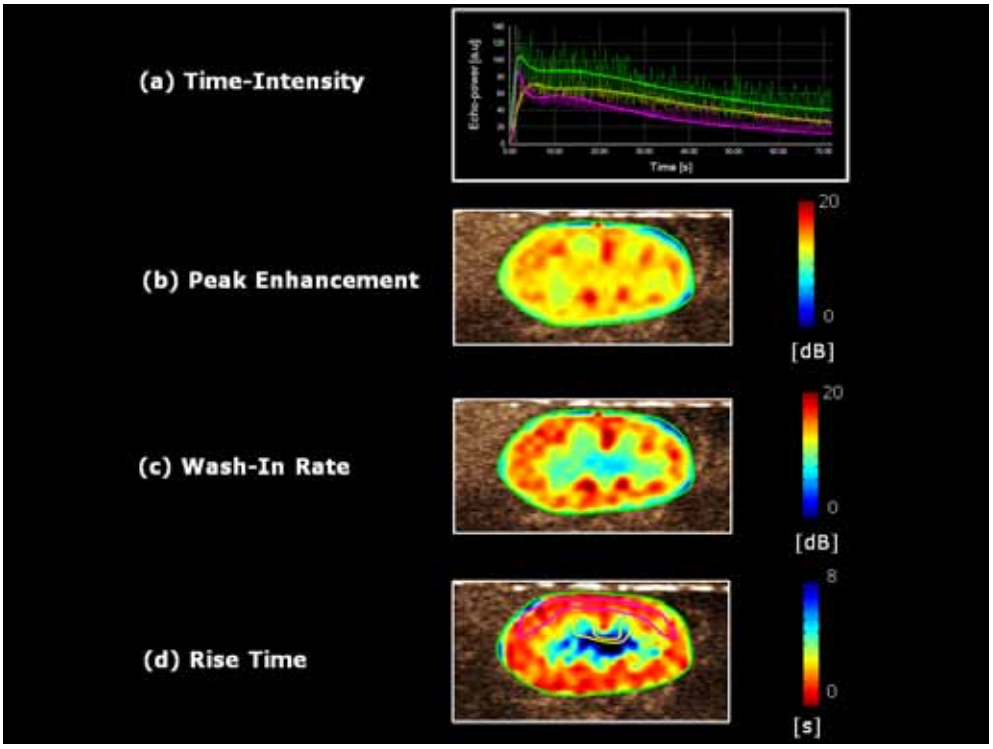

Fig. 2 – Time-Intensity curves (a) for a contrast bolus in a female mouse (from Fig. 1). The curves represent perfusion kinetics in the whole kidney (green), cortex region (magenta) and medulla region (yellow). Parametric images of the whole kidney depict spatial variations in Peak Enhancement (b), Wash-In Rate (c) and Rise Time (d).

In terms of reproducibility, the group of female mice had a CV < 30% in all regions and for all parameters, and in the case of RT the CV was < 20% (see Fig 3). For the male mice (Fig. 4), the CV of the amplitude-based parameters (i.e. PE and WiR) were higher in both the cortex and medulla (< 40%) than the female group. The RT in both the cortex and medulla was similar for both groups. Overall, when grouping all mice together, the worst-case CV was 30%, for the cortical WiR (see Fig. 5).

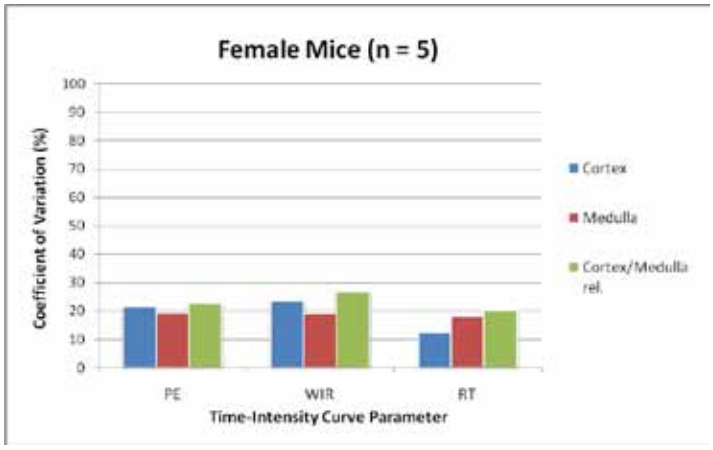

Fig. 3 – Coefficient of Variation (CV) for Peak Enhancement (PE), Wash-In Rate (WiR) and Rise Time (RT) for the group of female mice. CV is calculated for the cortex region (blue), medulla region (red) and the ratio of cortex/medulla regions (green).

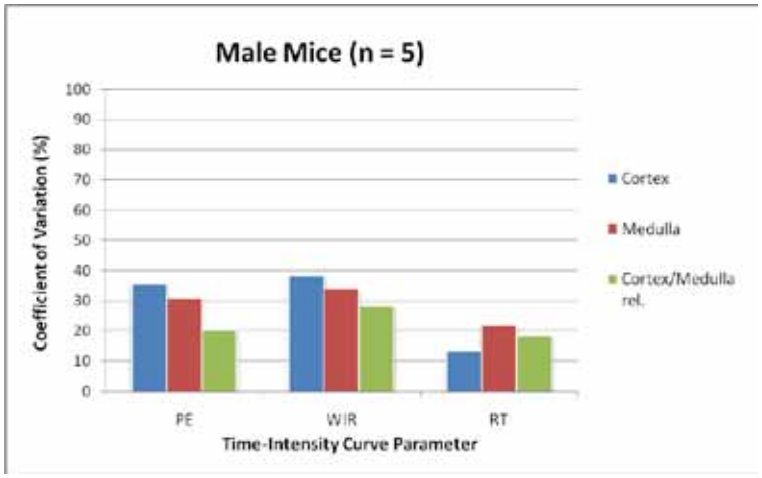

Fig. 4 – Coefficient of Variation (CV) for Peak Enhancement (PE), Wash-In Rate (WiR) and Rise Time (RT) for the group of male mice. CV is calculated for the cortex region (blue), medulla region (red) and the ratio of cortex/medulla regions (green).

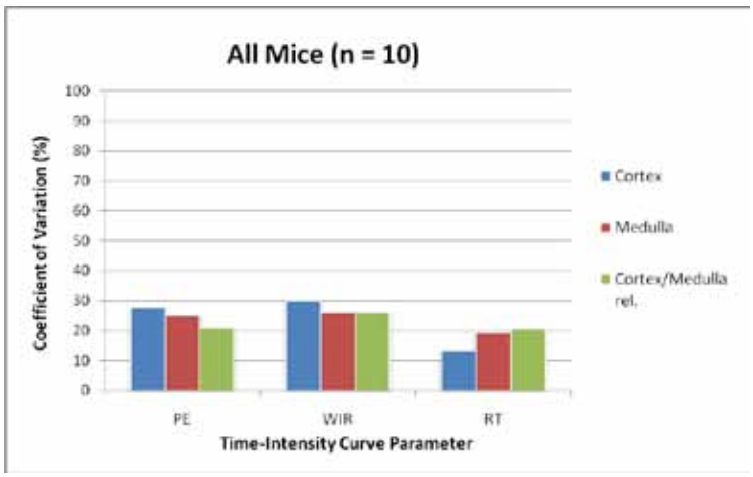

Fig. 5 – Coefficient of Variation (CV) for Peak Enhancement (PE), Wash-In Rate (WiR) and Rise Time (RT) for the group of all mice. CV is calculated for the cortex region (blue), medulla region (red) and the ratio of cortex/medulla regions (green).

Discussion and Conclusions:

In general, it is clear that the time-based parameter (RT) was the most reproducible quantity in all cases. This was also shown to be the case in a similar study in sheep (Strouthos et al. 2009). Utilizing the RT parameter as much as possible for *in vivo* quantification of blood perfusion is recommended for pre-clinical imaging in mice. An interesting finding was that the RT within the medulla showed more variability than within the cortex. On the contrary however, the amplitude-based parameters (PE and WiR) showed more variability in the cortex than in the medulla, and more variability in males than in females. This could perhaps be explained by the fact that the sizes of the kidneys for the female mice were much more consistent, leading to a more reproducible imaging plane. In the case of the males, the larger kidneys spanned a wider range of depths in the image, leading to a larger dependence on attenuation and beam profile effects. This was evident in the level of background tissue signal in the male mice which was more variable than in the females (not shown). This would lead to more

variability in the calculation of amplitude-based parameters. Finally, the variation in the ratios of the cortex to medulla parameters were all within 30%, a finding that will potentially be useful to researchers studying kidney function or targeting therapies designed specifically for either medullary or cortical flow. Knowing the variability in such studies is important for estimating the smallest changes in physiological parameters that can realistically and reliably be detected.

Important to note is that these experiments were conducted with a manual bolus injection. It is hoped that with improved experimental technique, specifically the implementation of a bolus injection pump, the reproducibility of the measured parameters could be improved even further. A second important aspect of this study, i.e. the investigation into the reproducibility of repeated injections within a single animal, is currently underway. This will help to determine what component of the variation presented here is intrinsic to the experimental technique (i.e. preparation and injection of the contrast agent), rather than caused by variability in the physiology of a particular animal. Finally, additional parameters such as Area Under the Curve (AUC), Time to Peak (TTP), Mean Transit Time (MTT) and Perfusion Index (PI), which have not been presented here, are currently being analyzed and will be discussed.

References:

- Franchini KG, Cowley AW. Renal Cortical and Medullary Blood Flow Responses During Water Restriction: Role of Vasopressin. Am J Physiol Regul Integr Comp Physiol 1996;270:R1257-R1264.
- Mattson DL, Meister CJ. Renal Cortical and Medullary Blood flow Responses to L-NAME and ANG II in Wild-type, nNOS Null Mutant, and eNOS Null Mutant Mice. Am J Physiol Regul Integr Comp Physiol 2005;289(4):R991- R997.
- Needles A, Mehi J, Arditi M, et al. Nonlinear Contrast Agent Imaging with a Linear Array Based Micro-Ultrasound System. Proc IEEE Ultrason Symp, 2009. In press.
- Rognin NG, Frinking P, Costa M, Arditi M. *In-vivo* Perfusion Quantification by Contrast Ultrasound: Validation of the Use of Linearized Video Data vs. Raw RF Data.
- Proc IEEE Ultrason Symp 2008:1690-1693.
- Strouthos C, Lambaskis M, Sboros V et al. Quantification of the Microvascular Blood Flow of the Ovine Corpus Luteum with Contrast Ultrasound. Proc IEEE Ultrason Symp, 2009. In press.

An *In Vivo* Model for Real Time Visualization of Microbubble-Mediated Sonothrombolysis in the Microcirculation

John Pacella, MS, MD; Francois Yu, PhD; Xucai Chen, PhD; Jonathan Leeman, BS; Linda Lavery, BS; and Flordeliza Villanueva, MD

Center for Ultrasound Molecular Imaging and Therapeutics, Cardiovascular Institute, University of Pittsburgh, Pittsburgh, PA

Background:

Occlusive coronary artery thrombus results in compromised myocardial perfusion and underlies myocardial infarction. Effective mechanical strategies for rapid clot removal from the epicardial coronary arteries have been developed. However, these approaches often result in distal microembolization of the thrombus, resulting in failure of microvascular reperfusion to the infarct zone despite restoration of epicardial coronary artery patency. Strategies for dissolution of diffusely dispersed thrombi from the microcirculation are limited, and ideally should be regionally targeted to the infarct territory. Ultrasound mediated microbubble destruction is a potentially attractive approach to achieving microvascular thrombolysis. However, optimal ultrasound parameters and microbubble properties have yet to be defined and an *in vivo* model for systematic assessment of such parameters is lacking. Furthermore, *in vitro* test systems do not reproduce the time-dependent endogenous fibrinolytic pathways that likely interact with the sonothrombolytic process. Herein, we propose a novel *in vivo* system that will not only allow for the pinpoint generation of microvascular thrombi, but will also allow application of contrast enhanced ultrasound during continuous direct observation of microvascular thrombi using intravital microscopy.

Methods:

We have performed 8 preliminary studies which demonstrate the feasibility of this approach. Our system is comprised of an Olympus BX 51 compound upright microscope with a Gibraltar stage. Rats were anesthetized and the cremaster muscle was exteriorized and placed on a customized stage for intravital microscopy. Various sized arteriolar thrombi were created by cannulating the vessel with a 2-5 μm tipped glass micropipette using a motorized Burleigh micromanipulator. Ultrasound was then applied to the preparation by positioning a 2 F ultrasound catheter (Ekos) within 2 mm of the microvascular thrombi. The catheter was driven by a pulse generator (Agilent) and a power amplifier

(Amplifier Research). Duty cycle (0.1-20%), pulse repetition frequency (PRF 1-10 Hz), and mechanical index (MI 0.07-1.0) were varied. Lipid encapsulated perfluorobutane microbubbles were intravenously infused during simultaneous application of ultrasound and intravital microscopic observation.

Results:

The system allowed for direct observation of the thrombus during administration of contrast enhanced ultrasound. The figure below depicts thrombus behavior in a single arteriole during one study. In the panel on the left, the thrombus was occlusive and large, and there was no flow in the arteriole. After the application of ultrasound during infusion of microbubbles (MI of 0.07, duty cycle of 20%, PRF of 1 Hz), thrombus dissolution and recanalization of the occluded artery were directly observed in real time (right panel). With manipulation of acoustic variables, other phenomena, such as reversible microvascular constriction, could be observed.

Conclusions:

This experimental model allows direct, real time observation of microvascular thrombi during the application of contrast enhanced ultrasound in a physiologic *in vivo* environment. Such an approach should help to guide the selection of optimal ultrasound and contrast parameters for successful microvascular thrombus dissolution, with the ultimate goal of restoring microvascular perfusion.

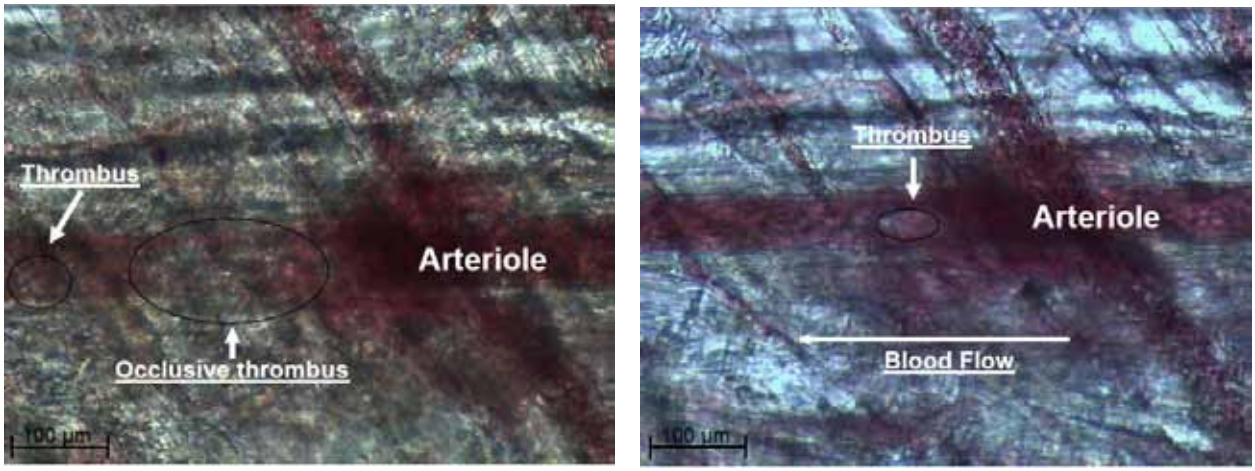

Ultrasound and Microbubble enhanced cell permeability through generation of transient sub-micron disruptions on the plasma membrane: Transmission electron microscopy studies

Raffi Karshafian [1]***, Peter N. Burns*** [2]

Department of Medical Biophysics, University of Toronto [1] *Department of Physics, Ryerson University, Canada* [2] *Imaging Research, Sunnybrook Health Sciences Centre, Canada*

The application of ultrasound with microbubbles increases cell membrane permeability and allows molecules to cross the otherwise-impermeable plasma membrane and enter the intracellular space of cells, a phenomenon referred to as *sonoporation.* Studies have been performed with the aim to optimize ultrasound and microbubble parameters to improve the delivery of drugs/genes into cells. As part of that effort, our group have identified exposure conditions which resulted in enhanced permeability in ~70% of the cells while maintaining cell viability (as assessed with propidium iodide marker). The primary mechanism underpinning sonoporation has been demonstrated to be the formation of non-lethal and transient pores on the cell membrane. However, in addition to the transient membrane disruption mechanism, endocytosis, which is a biological internalization process, has been shown to facilitate intracellular delivery at low ultrasound exposure conditions. In this study, the underlying mechanism associated with enhanced permeability was investigated under high MI ultrasound exposure conditions with the objective of quantifying the distribution of disruptions generated by ultrasound and microbubbles on the cell membrane.

KHT-C cells in suspension were exposed to ultrasound pulses of 500 kHz centre frequency, 570kPa peak negative pressure, 32μs pulse duration, 3kHz pulse repetition frequency and 5s insonation time with and without Definity microbubbles (3.3% v/v). Cell permeabilisation was assessed with 70kDa FITC-dextran. Plasma membrane morphology was observed with electron microscopy. Cell permeability of 71% was achieved by ultrasound and microbubbles with the FITC-dextran added 60s before ultrasound exposure. Permeability similar to control (0.5%) was achieved with ultrasound alone (2%), and with FITC-dextran added 60s following termination of ultrasound and microbubble treatment (0.6%). Untreated cells exhibited continuous plasma membrane morphology as assessed with transmission electron microscopy (TEM). TEM images of cells treated with ultrasound and microbubbles revealed disruptions on the plasma membrane generally ranging from 30 to 100 nm and as large as 400 nm, immediately (i.e., within 2s) following termination of ultrasound. No disruptions were observed on cells one minute after termination of ultrasound and microbubble treatment, and on

cells treated with ultrasound alone. The presence of disruptions on the cell membrane was consistent with the intracellular uptake of FITC-dextran molecules. This study demonstrated that the biological mechanism underpinning sonoporation is the generation of transient sub-micron disruptions on cell membranes by ultrasonically stimulated microbubbles.

Acoustic sizing of an ultrasound contrast agent

David Maresca [1], Marcia Emmer [1], Paul L. M. J. van Neer [1], Hendrik J. Vos [1], Michel Versluis [2], Marie Muller [1, 3], Nico de Jong [1, 4], Antonius F.W. van der Steen [1, 4]

[1] Department of Biomedical Engineering, Thoraxcenter, Erasmus MC, Rotterdam, the Netherlands
[2] Physics of Fluids group, Twente University, the Netherlands
[3] Institut Langevin, Université Paris Diderot, ESPCI ParisTech, Paris, France
[4] Interuniversity Cardiology Institute of the Netherlands, Utrecht, the Netherlands

Ultrasound contrast imaging depends largely on the harmonic behavior of bubbles. It is acknowledged that bubble size has a great impact on the amount of harmonic generation. However the size distribution of the contrast bubbles after administration to patients is largely unknown. High above resonance, bubble responses depend on their physical cross section only [1]. Our objective is to take advantage of this feature to measure single bubble sizes with ultrasound.

A 25 MHz single element focused transducer (2.6 cm focus) was mounted in a water tank. A highly diluted population of the ultrasound contrast agent Definity™ was injected in a 200 µm diameter cellulose capillary that crossed the transducer beam focus inside the water tank. A microscope equipped with a 40x water immersion lens and a CCD camera was added to record images of the capillary region of interest where the acoustic beam is focused. The pressures scattered by single bubbles responding to 400 kPa pulses (MI < 0.1) were acquired. The transducer was calibrated both in transmission and reception so that real pressure values could be derived from the measurements. At a frequency high compared to the bubble resonance frequencies, the backscattered pressure p_s relates to the bubble radius R as $p_s = R \cdot p_i / z$, where z is the transducer-bubble distance and p_i the incident pressure hitting the bubble.

We sized one by one 88 Definity™ bubbles from the same vial both acoustically and optically. The size distribution obtained acoustically showed a mean diameter (2.5 µm) and a standard deviation (0.9 µm) in agreement within 8% with the optical reference measurement (Figure 1). Both results are in agreement with the size distribution claimed by the manufacturer (Table 1).

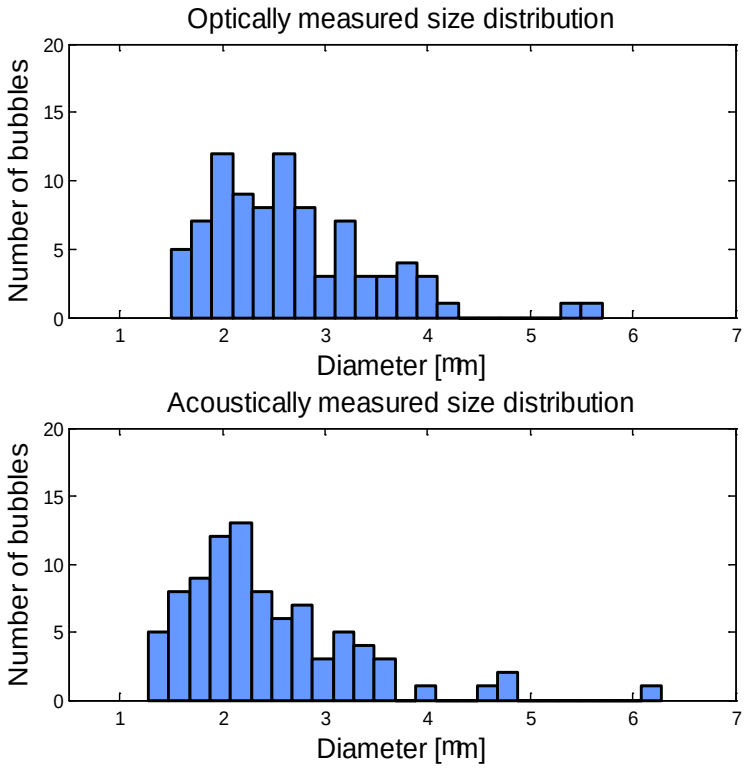

Table 2. Definity™ size distribution, Lantheus Medical Imaging®

Table 1: Microsphere Size Distribution	
	Microsphere particle size parameters
Mean diameter range	1.1 µm – 3.3 µm
Percent less than 10 µm	98%
Maximum diameter	20 µm

The acoustically determined size distribution is comparable in shape with the optically determined distribution and only appears very slightly shifted to lower radii. The 12% uncertainty of the hydrophone used to calibrate the transducer could be a reason for the observed shift. The random disparities between the two distributions may originate from the different position each bubble had within the transducer focal spot. We expect as well that the capillary affects the transducer pressure field, creating hot pressure spots within the tube. An application of our method could be to analyze bubbles administered in superficial arteries (e.g. carotid artery) as it potentially estimates the size distribution of a bubble population noninvasively.

[1] J Sijl, et al., "Acoustic characterization of single ultrasound contrast agent microbubbles", *JASA*, 2008

Towards an ultrasound contrast method for imaging extavascular molecular targets

Tom H. Shorrock and Jeffrey C. Bamber

Joint Department of Physics, Institute of Cancer Research and Royal Marsden Hospital, Downs Road, Sutton, Surrey, SM2 5PT, UK

The use of resonant and non-linear scattering from micron-sized bubbles insonated at frequencies in the low megahertz range has worked well for adding contrast to depict vasculature in clinical ultrasound images and improve the measurement of blood flow. Such bubbles may also be functionalised to target specific molecular markers but are restricted to the vasculature due to their size, which is hard to change. This limitation will prevent ultrasound from developing into a full molecular imaging modality. If it could be overcome, ultrasound would have a major role to play in molecular imaging, because of its cost effectiveness, its excellent temporal and spatial resolution, and its potential for extremely high sensitivity to the contrast agent.

Here we report preliminary studies of a combined contrast agent and imaging concept, based on a perfluorocarbon emulsion with a drop-size small enough (less than about 150 nm) to leave blood vessels, and who's drops can be transiently vaporised acoustically to create bubbles on the other side of the blood vessel wall. The method relies on two synchronised acoustic waves, one at a low-frequency to vaporise the oil and manipulate the resulting bubbles for imaging, and one at a high-frequency that images them. The use of a relatively short activating/manipulating wave and its accurate synchronisation with the imaging wave resembles in some respects the technique of SURF imaging[1], and it distinguishes this work from previous perfluorocarbon droplet vaporisation-based imaging studies[2,3].

Experiments were carried out with a novel arrangement where the low frequency and high frequency transducers face each other to produce co-axial and co-focal beams of waves travelling in opposite directions. The two acoustic waves, the vaporising/manipulating wave at 0.5 MHz and the imaging wave at 20 MHz, pass though each other in the sample at the same time, at a position and over a distance determined by the synchronisation and the low frequency burst length (between 5 and 40 cycles). If the low frequency wave has induced bubbles to appear, the high frequency imaging pulse (2-3 cycles) will interact with them at different sizes for different depths. Thus, with data from a single pair of pulses, the depth dependence of the echo signal allows the high frequency acoustic backscatter to be studied as a continuous function of phase of the vaporising/manipulating wave. This arrangement

was implemented with two systems. First, both transducers were stationary, so that the time evolution of the high frequency backscatter along a single line could be studied. Second, a Cortex Dermascan™ ultrasound scanner was used to scan the high frequency transducer mechanically, to produce about 4 pairs of B-scans per second, within which a central region was illuminated by the low frequency beam; the pairs of images were formed by pulsing the high frequency transducer twice for each image line, once with the synchronised low frequency burst on and once with it off.

Preliminary studies were carried out with commercial microbubbles (Levovist™ and Sonovue™), to determine whether in the above experiment an influence could be observed of the low frequency wave pressure on the high frequency scattering cross-section. As the pressure of the manipulating wave was increased, evidence of very high frequency harmonic forward scattering was observed, as too was bubble destruction/cavitation, but no clear evidence of a pressure dependent scattering cross-section was immediately obvious at 20 MHz.

This prompted a number of theoretical studies. In particular, the Keller-Miksis equation was used to calculate the time variation of the microbubble radius for free gas bubbles, and hence the depth dependence of the 20 MHz scattering cross-section in the above experiment. It was found that for a single resting bubble size, pronounced increases in 20 MHz scattering cross-section were predicted during the compression phase of the manipulating wave, as the bubbles pass through resonant size, whereas when the calculations were repeated for a realistic weighting of bubble sizes this resonance effect was smoothed out so that only a small residual increase in the 20 MHz scattering cross-section remained, now at the rarefaction phase of the manipulating wave and apparently due only to the change in geometrical scattering cross-section. This may explain the above experimental results.

Samples of water and a perfluoropentane (boiling point 28 deg C) emulsion manufactured by sonicating the oil in lecithin and degassed water before passing it through a 200nm filter, were also studied in the above experiment. Vaporisation of this simple emulsion was demonstrated, as observed by transient but bright signals on the 20 MHz images appearing at the focus of the low frequency wave. Interestingly, in the first of the above experimental arrangements, bands of highly localised high frequency echo signals were also found, at the spatial period of and in the rarefactional regions of the low frequency wave. These echo signals were observed at lower drive pressures for the emulsion than for water, and they co-existed with audio frequency emissions that were similar to those observed for cavitation. The echoes themselves were short duration events, appearing to have poorer temporal and spatial correlation than would be expected from the 20 MHz point spread function.

These preliminary results extend previous work on perfluorocarbon droplet vaporisation, suggesting that exceptionally short duration droplet cavitation events may be induced and that a SURF imaging approach may have potential for imaging them. Further work will aim to confirm and quantify the above observations and improve understanding of their variation with experimental conditions through further modelling and experiment, and to extend the experiments using a multifrequency transducer that will allow the vaporising/manipulating wave and the high frequency imaging wave to be launched from the same location, as needed for eventual in vivo evaluation of the method.

References

1. Hansen R, Angelsen BAJ. SURF imaging for contrast agent detection. IEEE Trans UFFC, 2009;56:280-290.
2. Asami R, Azuma T, Yoshikawa H, Kawabata K. Tumor enhanced imaging and treatment with targeted phase-change nano particles, pp. 1973-1976 in: Proc 2007 IEEE Ultrasonics Symp, 1051-0117, New York, IEEE, 2007.
3. Matsuura N, Gorelikov I, Williams R, Wan K, Zhu S, Booth J, Burns P, Hynynen K, Rowlands JA. Nanoparticle-tagged perfluorocarbon droplets for medical imaging, Proc Mat Res Soc, 2008; DOI: 10.1557/PROC-1140-HH03-05

Phase-shift nanoemulsion/microbubble platform for ultrasound-mediated drug delivery

Natalya Rapoport

Department of Bioengineering, University of Utah, Salt Lake City, Utah, USA
Co-authors: Kwon-Ho Nam, Anne M. Kennedy, Jill Shea, Courtney Scaife

During the last decade, nanomedicine has evolved as a new field of oncology that holds promise of solving hard problems of current cancer chemotherapy. Various drug nanocontainers and delivery modalities have been suggested for increasing stability and aqueous solubility of chemotherapeutic drugs and decreasing their systemic toxicity. Properly designed nanoparticles avoid extravasation to normal tissues and recognition by reticulo-endothelial system cells, which prolongs their circulation time and allows passive tumor targeting. Passive targeting is based on the enhanced permeability of defective tumor microvasculature that allows extravasation of drug-loaded nanoparticles through large inter-endothelial gaps; it was shown that in a variety of tumors, characteristic pore cutoff size ranges between 380 and 780 nm, though in some tumors it may reach up to 2 μm. In contrast to tumors, blood vessels in normal tissues have tight inter-endothelial junctions that don't allow extravasation of nanoparticles. In addition to enhanced vascular permeability, tumors demonstrate poor lymphatic drainage; this positive effect provides for a long retention of the extravasated particles in tumor tissue. This effect is called enhanced permeability and retention, or EPR.

An alternative approach to tumor targeting consists of developing stimuli-responsive nanoparticles that release their drug load only in response to environmental or physical stimuli, such as pH, hyperthermia, light, or ultrasound. Ultrasound as a component of a drug delivery modality is especially attractive for reasons of cost-effectiveness and prospects for combining ultrasonic imaging and therapy. Ultrasound may be applied with a variety of drug carriers. Ultrasound may be directed toward deeply located body sites in precise energy deposition patterns. Sonication may be performed non-invasively or minimally invasively through intraluminal, laparoscopic or percutaneous means.

For many decades, microbubbles have been used in clinical practice exclusively as ultrasound contrast agents in ultrasound imaging. During the last decade, microbubbles have attracted attention as drug carriers and enhancers of drug and gene delivery and are now being widely investigated for this application. However, these systems present inherent problems. Their very short circulation time (minutes) and micron size do not allow effective extravasation into tumor tissue, which is an essential prerequisite for effective drug targeting.

The way to solve above problems may consist in developing drug-loaded, nano-scaled microbubble *precursors* that would effectively accumulate in tumor tissue by passive or active targeting and then convert into microbubbles in situ after tumor accumulation. With this in mind, we have recently developed block copolymer stabilized echogenic perfluorocarbon nanoemulsions. The core of nanoemulsions was formed by either perfluoropentane (PFP) with a boiling point of 29 ºC at atmospheric pressure or perfluoro crown ether-10 (PFC) with a boiling point of 140 ºC at atmospheric pressure. The shell of nanodroplets was formed by biodegradable block copolymers poly(ethylene oxide)-co-poly(lactide) (PEG-PLA) or poly(ethylene oxide)-co-polycaprolactone (PEG-PCL). Here, we describe acoustic and therapeutic properties of these nanoemulsions that were explored in breast, ovarian, and pancreatic cancer models.

Due to high mismatch between acoustic impedances of perfluorocarbon and water (or tissue), both PFP droplets (~0.3 MRayl) and bubbles (<<0.3 MRayl) manifest echogenic properties; however bubbles manifest much higher echogenicity than droplets, which creates better contrast in ultrasound images. Even more importantly, only bubbles undergo high-amplitude oscillation and inertial cavitation in an ultrasound field, which concentrates ultrasound energy and substantially enhances ultrasound-mediated drug delivery. Though drug delivery from micelles, liposomes, or emulsions may be ultrasonically enhanced even without microbubbles, presence of microbubbles dramatically increases intracellular uptake of drugs or genes. Therefore nanodroplet vaporization to generate bubbles would be highly desirable for both ultrasonography and drug delivery.

We have identified three major factors that induced droplet-to-bubble transitions in PFP nanoemulsions, namely heat, injection through thin needles, and ultrasound. In the presentation, these factors will be discussed in detail for the droplets inserted in liquid emulsions or gels. Among those listed, ultrasound was the most effective. Thermal transition was significantly hampered even for PFP nanodroplets in liquid emulsions due to high Laplace pressure inside droplets. An example of dependence of boiling temperature on droplet size for a PFP nanoemulsion is presented in Figure 1. At physiological temperatures, PFP droplets with a diameter smaller than about 4 μm will not vaporize and therefore will circulate as liquid droplets, which is important for their extravasation and tumor accumulation. On the other hand, after ultrasound-triggered droplet-to-bubble transition, the bubbles with a size larger than 4 μm will not condense back into the liquid state and will be preserved as microbubbles, which is important for ultrasound imaging and drug release. If PFP were an ideal gas, these bubbles would be formed from droplets of a diameter equal or larger than 800 nm.

The data presented in Figure 2 show that after systemic injections in vivo, drug (paclitaxel, PTX) encapsulated in nanoemulsion was tightly retained by nanodroplets without ultrasound, but was effectively released under the action of therapeutic ultrasound.

Examples of therapeutic efficacy of the proposed combined tumor therapy by drug-loaded nanoemulsions and ultrasound are presented in Figures 3-5. The data of Figure 6 suggest nanodroplet

accumulation in tumor after systemic injection. The data of Figure 7 show injection-induced droplet-to-bubble transition in vitro and in vivo.

Advantages and limitations of the prospective clinical application of the described technique will be discussed.

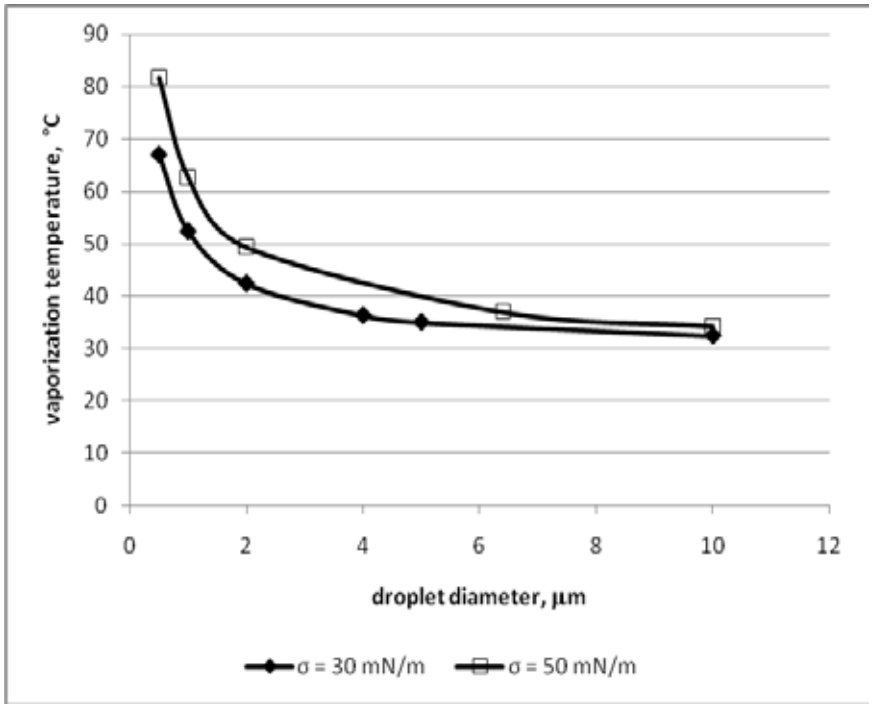

Figure 1. Dropler vaporization temperature as a function of droplet size for the surface tension values of 30 mN/m and 50 mN/m.

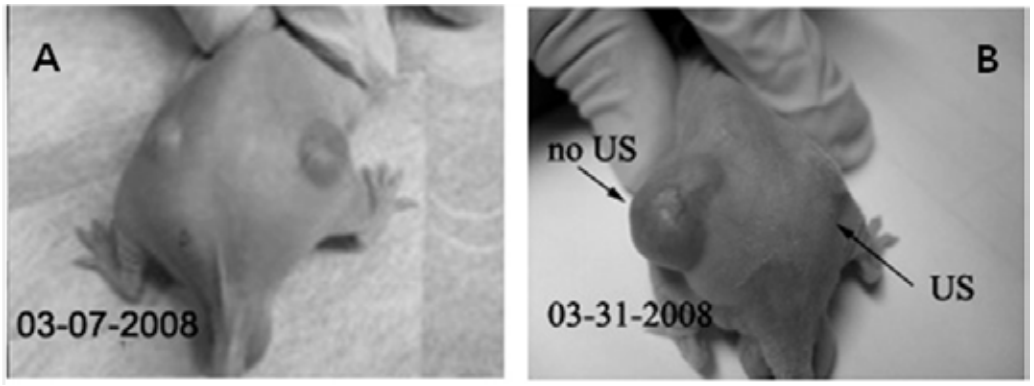

Figure 2. Photographs of a mouse bearing two ovarian carcinoma tumors (A) - immediately before and (B) - three weeks after the treatment; a mouse was treated by four systemic injections of nanodroplet-encapsulated PTX, nbGEN (20 mg/kg as PTX) given twice weekly; the right tumor was sonicated by 1-MHz CW ultrasound (nominal output power density 3.4 W/cm^2, exposure duration 1 min) delivered 4 hours after the injection of the drug formulation. Ultrasound was delivered through a water bag coupled to a transducer and mouse skin by Aquasonic coupling gel.

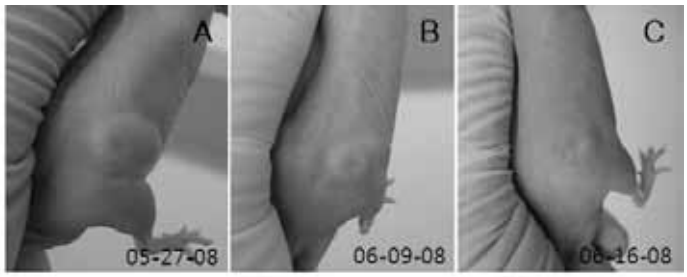

Figure 3. Regression of ovarian carcinoma treated by the proposed technique as described for Figure 2.

The first photograph was taken before the start of the treatment, the second – two weeks later, i.e. immediately after the completion of the treatment. The third photograph was taken one week after the completion of the treatment.

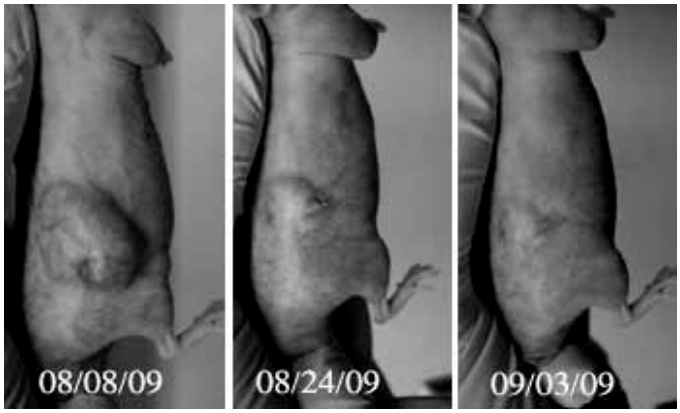

Figure 4. Regression of the breast tumor treated by paclitaxel-loaded PFC nanoemulsion and focued 1-MHz ultrasound at a nagative pressure of 1.5 Mpa.

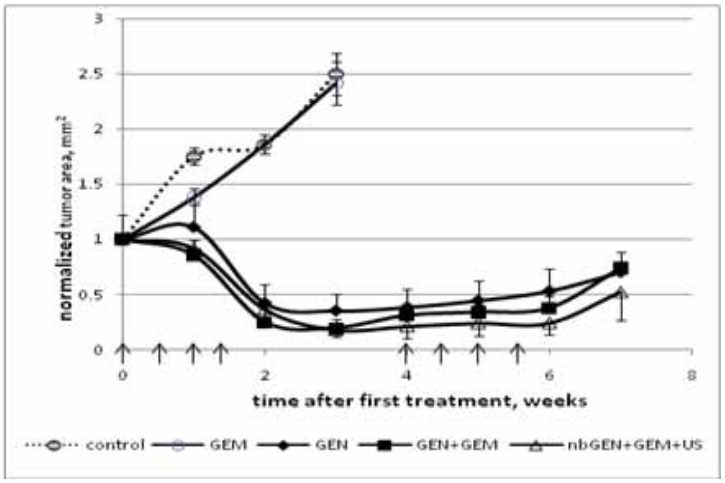

Figure 5. Growth/regression curves of pancreatic cancer treated by micelle or nanodroplet encapsulated paclitaxel and unfocused 1-MHz ultrasound.

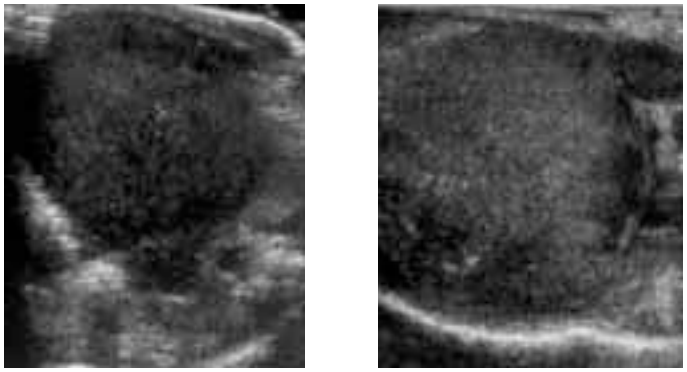

Fig. 6. Ultrasound images of a pancreatic tumor before (left) and 5.5 h after systemic injection of paclitaxel-loaded PFP nanoemulsion (right).

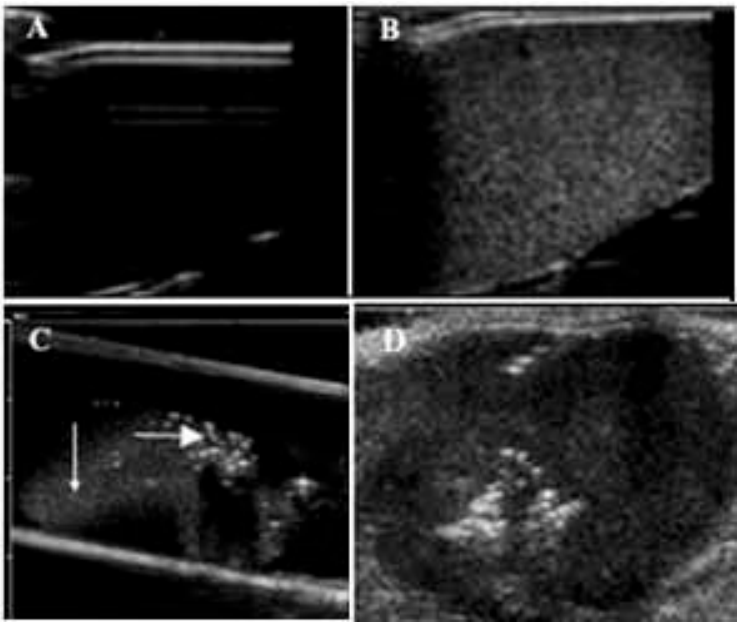

Figure 7. Ultrasound images of nanodroplets/microbubbles;
A – water in a test tube; B - PFP/PEG-PCL nanodroplets in a test tubes,
C – PFP/PEG-PCL nanodroplets injected into agarose gel through a 26 G needle;
D - PFP/PEG-PCL nanodroplets injected into a subcutaneous pancreatic tumor through a 26 G needle.

New developments in therapeutic applications of microbubbles: an update

Raffi Bekeredjian

Gas filled microbubbles have emerged as a new tool for site specific gene and drug delivery. This is based upon two distinct characteristics of microbubbles exposed to ultrasound: the ability to unload a previously loaded bioactive substance and the ability to transiently increase capillary permeability. We have used specifically designed microbubbles to create a gene and doxorubicin delivery system.

Previously, we had loaded microbubbles with naked DNA to be delivered to rat hearts. While this technique does work, despite systemic intravenous injection of loaded microbubbles, the transgene expression time is too short and efficiency is too low. Therefore, we developed a new system using adeno associated virus particles that can be transfected into the heart, using ultrasound targeted microbubble destruction. This allows a more efficient and very long transgene expression in the myocardium. Using this technique, we were able to deliver both reporter genes to rat hearts, as well as an oxygen stable HIF1-alpha mutant, that would induce significant angiogenesis in the heart. This technique is presently transferred to a large animal model using retroperfusion of virus loaded microbubbles into the coronary veins.

In a different work a novel microbubble carrier for doxorubicin has been developed and characterized in-vitro. The newly developed doxorubicin-loaded microbubbles possess a soft but stable phospholipid monolayer shell. Importantly, the active drug is embedded in the microbubble shell and is complexed to the phospholipids by both electrostatic and hydrophobic interactions. Despite their drug load, these novel microbubbles retained all important physical characteristics for ultrasound targeted microbubble destruction, comparable with the commercially available ultrasound contrast agents. In cell culture studies doxorubicin-loaded microbubbles in combination with ultrasound demonstrated a 3.2 fold increase of the anti-proliferative activity compared to free doxorubicin and doxorubicin-loaded liposomes.

Ultrasound-Mediated Drug Delivery using Echogenic Liposomes

Christy K. Holland, Jonathan Kopechek, Kathryn Hitchcock (Biomedical Engineering, Univ. of Cincinnati, Cincinnati, OH, USA), Danielle Caudell, Gail Pyne-Geithman (Dept. of Neurology, Univ. of Cincinnati, Cincinnati, OH), Shao-Ling Huang, Ph.D., David D. McPherson, M.D. (Dept. of Internal Medicine, Univ. of Texas Health Science Center, Houston, TX, USA)

Due to the prevalence of thrombo-occlusive and atherosclerotic disease worldwide and the need for improved clinical treatments, pulsed ultrasound in combination with drugs have been investigated to improve recanalization in patients with these diseases. Acceleration of clot removal is particularly critical in the treatment of acute ischemic stroke. Echogenic immunoliposomes are under development to enable ultrasound-controlled drug delivery. Mechanistic studies *in vitro* have revealed that stable cavitation is correlated with enhanced penetration of recombinant tissue Plasminogen Activator (rt-PA) into clot and with enhanced drug delivery across the vascular endothelium. A review of *in vitro* sonothrombolysis studies utilizing a commercial ultrasound contrast agent or echogenic liposomes loaded with rt-PA to nucleate stable cavitation will be presented. Strategies to harness bubble activity using infusions of echo contrast agents and image-guided, targeted drug delivery schemes will be reviewed. This work was supported by NIH 2RO1 NS047603, NIH 1RO1 HL074002, and NIH 2R01 HL059586.

Drug uptake by endothelial cells through targeted microbubble sonoporation

Klazina Kooiman[1], Miranda Foppen-Harteveld[1], and Nico de Jong[1-2-3]

1- Dept. of Biomedical Engineering, Thoraxcenter, Erasmus MC, Rotterdam, the Netherlands
2- Interuniversity Cardiology Institute of the Netherlands, Utrecht, the Netherlands
3- Dept. of Applied Physics, Physics of Fluids, University of Twente, Enschede, the Netherlands

Background

Molecular imaging using ultrasound makes use of targeted ultrasound contrast agents that consist of encapsulated gas microbubbles. Until now, targeted microbubbles have only been used for imaging, not drug delivery. Drug uptake using microbubbles can be induced by sonoporation, a method that induces transient cell membrane pores by oscillating or jetting microbubbles so that therapeutics can enter the cell. So far, sonoporation has only been induced using non-targeted microbubbles [1,2]. Due to the blood flow, there may be insufficient microbubble-cell contact *in vivo*. A microbubble targeted to the cell membrane may overcome this, but it is not known whether sonoporation can still be induced. This study focuses on inducing sonoporation with CD31-targeted microbubbles in endothelial cells at low acoustic pressures. CD31 was chosen since this adhesion molecule is expressed constitutively on the surface of endothelial cells [3].

Method

Biotinylated lipid coated microbubbles with a C_4F_{10} gas core were made by sonication [4]. After CD31 antibody conjugation [5], microbubbles were added to human umbilical vein endothelial cells grown in an Opticell. The microbubbles were allowed to adhere to the cells by flotation for 5 min. The Opticell was then reversed and mounted in the set-up such that the bound microbubbles were on top of the cells. Microbubble-cell behavior upon insonification at 1 MHz (6x 10 cycle sine-wave bursts) at 80, 120 and 200 kPa peak negative acoustic pressure was studied with the Brandaris 128 high-speed camera [6] (frame rate ~12 MHz). Microbubble diameter (D) – time curves were extracted from the recordings and the relative vibration $D_{max} - D_{min}$ normalized to the resting diameter D_0 were determined. The cell-impermeable propidium iodide (PI; 25 μg/ml) was used as indicator for increased cell membrane permeability due to sonoporation. PI uptake was detected using fluorescence and recorded with a high sensitivity CCD camera (LCL-902K, Watec, Orangeburg, NY, USA).

Results

A total of 31 cells were studied that all had one microbubble attached per cell. After insonifying the targeted microbubbles at 80 kPa, PI uptake was observed in six cells (30%). Fourteen cells (70%)

showed no PI uptake. At 120 kPa, one cell (20%) had taken up PI whereas four cells (80%) showed no PI uptake. At 200 kPa, five cells (83%) had taken up PI whereas one cell (17%) showed no PI uptake. Overall, PI uptake was observed in 12 cells (39%). Brandaris 128 high-speed camera recordings revealed the behavior of the targeted microbubbles upon insonification. The figure shows the relation between the relative vibration of the adhered microbubbles $(D_{max} - D_{min})/D_0$, the resting size of the microbubbles D_0 and the induction of PI uptake. The relation suggests that when a microbubble adhering to an endothelial cell is larger than 3.0 μm or the relative vibration is greater than 0.5, sonoporation is most likely induced for insonification at 1 MHz. Interestingly, this is irrespective of the peak negative acoustic pressure the microbubbles were insonified at. Ultrasound treatment alone did not induce sonoporation at all three studied peak negative acoustic pressures.

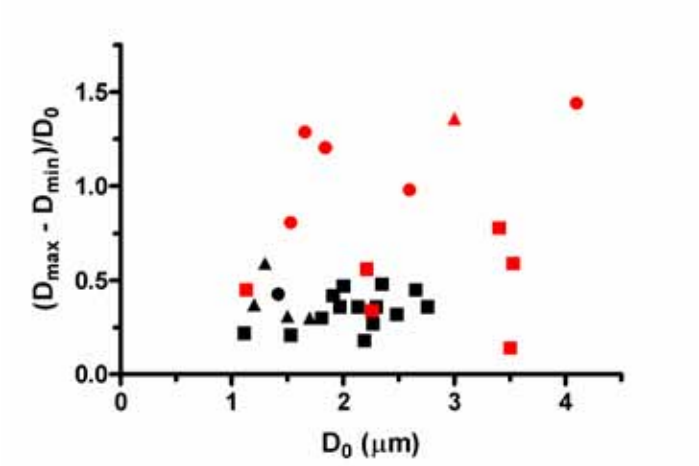

Figure. Relation between relative vibration of microbubbles $(D_{max} - D_{min})/D_0$, resting size of microbubbles D_0, and induction of sonoporation. Targeted microbubbles were insonified at 1 MHz (6x 10 cycle sine-wave bursts) at 80 kPa (squares; n=20), 120 kPa (triangles; n=5), and 200 kPa (spheres; n=6) peak negative acoustic pressure. Black symbols: no propidium iodide uptake by endothelial cell; red symbols: propidium iodide uptake by endothelial cell.

Conclusion

This study reveals that targeted microbubbles can induce sonoporation. This feature may now be used in molecular imaging using ultrasound, thereby combining imaging and drug delivery.

Acknowledgments: This project is supported by innovation subsidies collaborative projects by the Dutch Ministry of Economic Affairs under number IS042035. The authors would like to thank A.L. Klibanov from the University of Virginia, Cardiovascular Division, Charlottesville, Virginia, USA for discussions about the microbubble preparation.

References

[1] van Wamel et al, J Control Rel 2006; 112: p. 149
[2] Schneider, J Endourol 2008; 22: p. 795
[3] DeLisser et al, Immunol Today 1994; 15: p. 490
[4] Klibanov et al, Invest Radiol 2004; 39: p. 187
[5] Lindner et al, Circulation 2001; 104, p. 2107
[6] Chin et al, Rev Sci Instru 2003, 74: 5026

Tumor therapy by microbubbles and ultrasound: mechanism of tumor growth control

A.L. Klibanov, T.I. Shevchenko, B. Kundu, Z. Du,
M. Bohmer, B.I. Raju, R. Seip, C.T. Chin.

University of Virginia, Charlottesville VA, 22908-0158
Philips Research, Eindhoven NL and Briarcliff Manor NY.

Introduction. Destruction of microbubbles in the vasculature by medical ultrasound is known to induce non-thermal bioeffects, such as petechial hemorrhaging [1,2], enhancement of nanoparticle extravasation [3], opening of blood-brain barrier [4], therapeutic angiogenesis [5] and antivascular action [6]. We have hypothesized that destruction of microbubbles in the tumor vasculature would cause vascular endothelium destruction and direct contact of pro-thrombotic tissue factor with the blood, leading to clotting and reduction of tumor blood supply. Contrary to this initial hypothesis, our preliminary experiments showed only brief reduction of the tumor blood flow after microbubble+ultrasound treatment, yet tumor growth could be inhibited and even reversed. This study was performed in order to investigate the potential mechanisms of the observed tumor therapy effect.

Methods. Decafluorobutane microbubbles stabilized with a monolayer of phosphatidylcholine and PEG stearate (mean particle size <2.5 um) were prepared in house and stored refrigerated in sealed vials under decafluorobutane atmosphere. MC38 mouse colon adenocarcinoma cells (courtesy Dr. J. Schlom, NIH) were subcutaneously grafted in the left hind leg of C57BL/6 female mice. After tumor could be visually detected and its size measured with a caliper, therapy was initiated.

Animal study was performed in accordance with a UVA ACUC-approved protocol; all animal experiments were performed under isoflurane gas anesthesia. Microbubble dispersion in normal saline (50.106 bubbles in 50 ul) was administered intravenously in the tumor-bearing mice. It was immediately followed by insonation of tumor using TIPS system (Philips Research) operated in the intermittent mode (1 Hz, 1.2 MHz, 100,000 cycles, 5MPa peak negative acoustic pressure). Imaging guidance for TIPS treatment was provided by intra-operative high frequency scanhead (HDI 5000 or iE33 ultrasound imaging systems were used). Imaging transducer was mounted laterally on the side of TIPS probe water standoff assembly. Microbubble & ultrasound treatment was repeated twice daily, for a period of two weeks. Tumor size was measured daily with a caliper. As per ACUC protocol, mice were euthanized if tumor load reached 10% of the animal body mass. The animal body mass and general mouse appearance and behavior were assessed for signs of side effects. Seven tumor-bearing animals were used in each of the experimental and control groups.

For evaluation of tissue metabolism, 18F-fluorodeoxyglucose (FDG) administration combined with

microPET imaging was performed in a separate set of experimental animals, a day before and a day after microbubble-ultrasound treatment. Frozen section histology was used to evaluate control and insonated tissues for the presence of leukocytes. Tumor temperature increase during insonation was evaluated with a needle thermocouple; it was minimal, always under3oC.

Results. Circulating microbubbles could be clearly observed by ultrasound imaging in the tumor vasculature. Microbubble destruction in response to TIPS treatment was observed; brief (up to several minutes) reduction of tissue perfusion after TIPS treatment pulses was clearly detected.

Untreated animals, as well as mice from control groups which only received either microbubbles or ultrasound separately, demonstrated rapid tumor growth, resulting in the necessity to perform euthanasia. The group of animals receiving the combination microbubble+ultrasound treatment demonstrated significant inhibition of tumor growth and in some instances a reduction of tumor size; no euthanasia was required for those animals for the duration of the study.

Tumor-bearing hind leg tissue insonated after microbubble administration demonstrated significant accumulation of FDG as compared with non-insonated tumors, indicating an increase in metabolic activities. Such increase of FDG uptake cannot be explained by the increase of tumor cell metabolism, because tumor growth is inhibited. However, it can be attributed to the leukocyte accumulation in the insonated tissues. Histology of the muscle tissue insonated after microbubble administration showed significant accumulation of leukocytes in the tissue 24 hours after treatment; leukocytes may be responsible for the enhancement of FDG uptake in the insonated tumors.

Conclusion. Destruction of microbubbles in the tumor vasculature results in the reduction of tumor size and inhibition of tumor growth. Direct tumor cell killing by either mechanical or thermal effects should not be significant and cannot explain the therapeutic effects; likewise, it is unlikely to be caused by the brief (minutes) reduction of the tumor blood flow. A more promising hypothesis is the induction of inflammatory response subsequent to cavitation events in close proximity to vascular endothelium, leading to the accumulation and activation of leukocytes that may provide antitumor effect.

Acknowledgment. This study was supported by NIH R21/33 CA102880 to A.L. Klibanov.

References.

1. Skyba DM, Price RJ, Linka AZ, Skalak TC, Kaul S. Direct in vivo visualization of intravascular destruction of microbubbles by ultrasound and its local effects on tissue. Circulation. 1998;98:290-293.

2. Wible JH Jr, Galen KP, Wojdyla JK, Hughes MS, Klibanov AL, Brandenburger GH. Microbubbles induce renal hemorrhage when exposed to diagnostic ultrasound in anesthetized rats. Ultrasound Med Biol. 2002;28:1535-1546.

3. Price RJ, Skyba 39DM, Kaul S, Skalak TC. Delivery of colloidal particles and red blood cells to tissue through microvessel ruptures created by targeted microbubble destruction with ultrasound. Circulation. 1998;98:1264-1267.

4. Hynynen K, McDannold N, Vykhodtseva N, Jolesz FA. Non-invasive opening of BBB by focused ultrasound. Acta Neurochir Suppl. 2003;86:555-558.

5. Chappell JC, Song J, Klibanov AL, Price RJ. Ultrasonic microbubble destruction stimulates therapeutic arteriogenesis via the CD18-dependent recruitment of bone marrow-derived cells. Arterioscler Thromb Vasc Biol. 2008;28:1117-1122.

6. Bunte RM, Ansaloni S, Sehgal CM, Lee WM, Wood AK. Histopathological observations of the antivascular effects of physiotherapy ultrasound on a murine neoplasm.Ultrasound Med Biol. 2006;32:453-461.

Review of vascular imaging with Contrast-enhanced ultrasound (CEUS)

Steve Feinstein, MD, FACC

Professor of Medicine,Rush University Medical Center,Chicago, Illinois USA

Proliferation of the arterial adventitial vasa vasorum presages the early atherosclerotic development and plaque vulnerability. Recent advances using CEUS provides direct visualization of the vasa vasorum and intra-plaque neovascularization. This CEUS methodology serves as a new surrogate marker for the detection and monitoring of premature and advanced atherosclerosis. This presentation will review the clinical value of CEUS for identifying and quantifying carotid artery vasa vasorum and intra-plaque neovascularization. The presentation will provide a road map for developing and validating the CEUS techniques ranging from in vitro calibration to 3D representation and quantification. Once clinically validated, the uses of CEUS may provide a method to non-invasively monitor therapeutic interventions. And importantly, the therapeutic ultrasound will be discussed focused on the use of ultrasound-directed, site-specific therapy for drug and gene delivery systems. These combined applications for diagnosis and therapy provide unique opportunities for clinicians to image and direct therapy for individuals with vulnerable lesions.

Plaque Imaging

Professor Edward Leen, Dr David Owen, Dr Jo Shalloup & Professor Alun Davies

Imperial College London, Hammersmith and Charing Cross Campus, London

Traditionally, stroke risk stratification has been based on the degree of internal carotid artery luminal narrowing, and the presence of recent focal neurological symptoms related to the ipsilateral cerebral hemisphere. Results of the European Carotid Surgery Trial (ECST) and the North American Symptomatic Carotid Endarterectomy Trial (NASCET) highlights the importance of accurate assessment of the degree of internal carotid artery stenosis. Extensive work had been undertaken in the generation of reliable and reproducible criteria for the calculation of internal carotid artery stenosis using conventional duplex ultrasonography measuring peak velocities. Duplex ultrasonography remains the first line imaging modality in this context.

However, it is now evident that the degree of stenosis alone is a relatively poor predictor of future stroke in asymptomatic patients. Indeed, the Asymptomatic Carotid Surgery Trial (ACST) highlighted the need to identify the subgroup of asymptomatics that would benefit from intervention. In order to define this subgroup, research has been focused on the evaluation of the morphology of plaques *in vivo* using imaging modalities. Histological and functional techniques have determined the features of such vulnerable plaques, including: inflammation; extra-cellular matrix degradation; neovascularisation; intra-plaque haemorrhage; and apoptosis. Imaging intra-plaque inflammation, neovascularisation, haemorrhage and apoptosis have been attempted with some success using MRI and/or PET scanning. However, the high prevalence of carotid disease and expense associated with these imaging techniques preclude them from replacing ultrasound as first line investigation.

Conventional ultrasound has been used to identify plaque constituents with “Gray-Scale Median” (GSM) evaluation. Studies have consistently demonstrated that plaques, which are echo-lucent on ultrasound, with a low GSM, have high lipid, haemorrhage and macrophage on histology. Conversely, echogenic plaques, with a high GSM, have a higher fibrous content. GSM is also associated with clinical findings: evidence of cerebral infarction on CT is more common in the presence of echo-lucent plaques rather than echogenic ones, regardless of symptomatic status. Echogenicity on ultrasound has also been shown to predict ipsilateral ischaemic stroke; patients with echo-lucent plaques are at increased risk compared with those with echogenic plaques. However, hazard ratios for development of stroke that are associated with differing echogenicity scores are not sufficiently great enough to warrant translation into clinical practice. Furthermore, studies investigating the use of GSM in selection for carotid artery stenting (CAS) have had conflicting results.

However ultrasound imaging intraplaque neovascularisation may be a means to identify the high-risk plaque. It is now known that plaques bearing the hallmarks of vulnerability, including inflammation, haemorrhage, lipid accumulation and thin fibrous caps, are also associated with increasing neovascularisation. Neovascularisation appears to be an early feature of atherosclerosis, predating macrophage infiltration, and as the plaque progresses so too does intimal neovascularisation. Carotid plaques retrieved at endarterectomy have many more microvessels and transcripts known to promote neovascularisation when they originate from symptomatic, compared with asymptomatic patients. Furthermore, symptomatic plaques have been shown to contain abnormal, immature vessels that may precipitate plaque instability through their acting as sites of vascular leakage and inflammation.

Contrast enhanced ultrasound imaging of the plaque neo-vascularisation has been shown to correlate with histological findings. Feinstein and colleagues reported a moderate correlation value of 0.64; Coli et al reported an increase in neovascularisation in patients demonstrating extensive enhancement; Giannoni *et al* reported diffuse contrast uptake in plaques from symptomatic patients, all of whom had increased number of microvessels confirmed on histology. The latter group described the common presence of small vessels within plaque underlying ulcerations. Up until that point, these three groups used subjective visual assessment made by human readers to ascribe binary or discreet scores to the imaging findings. Using a quantitative method, Xiong and colleagues who studied 104 carotid stenoses, revealed that plaque enhanced intensity and the intensity normalised against carotid luminal intensity were both significantly greater in symptomatic versus asymptomatic atheromata. Current CEUS methodologies for plaque imaging will be addressed as well as novel methods of identifying plaque vulnerability will be discussed in this presentation.

Late Phase Contrast Enhanced Ultrasound to Assess Inflammation within Carotid Atherosclerotic Plaque

David R.J. Owen

INTRODUCTION

The carotid atherosclerotic plaques most vulnerable to rupture are those with a large inflammatory infiltrate (1-5). Hence there has been considerable interest in imaging inflammation within atherosclerotic plaques with PET and MRI, but given the prevalence of atherosclerosis, costs grounds alone prohibit these techniques from being translated into routine clinical practice.

Late phase contrast enhanced ultrasound (LP-CEUS) may represent a low cost means of detecting plaque inflammation. Ultrasound contrast agents (microbubbles) are phagocytosed by monocytes *in vitro* and remain acoustically active for up to 30 minutes (6;7). Furthermore, preclinical studies show that microbubbles can be detected within monocytes which are attached to the endothelium of inflamed tissue (8). It has also been demonstrated that microbubbles adhere directly to the surface of damaged endothelium (9).

The purpose of this study was to determine whether non-targeted microbubbles are retained in human carotid plaque in sufficient number to be detected by late phase contrast enhanced ultrasound.

MATERIALS AND METHODS

This prospective study was approved by the local Research Ethics Committee. Informed consent was obtained from all subjects prior to their examination. Between December 2008 and May 2009 we recruited subjects aged 18 years or over who presented to the vascular clinic for a carotid duplex ultrasound scan at our institution, and whose scan showed an atherosclerotic plaque of > 30% stenosis by velocity criteria.

Plaques were defined as symptomatic if symptoms consistent with stroke, transient ischaemic attack (TIA) or amaurosis fugax had occurred within 12 months of entry into the study, in the neurovascular territory of the plaque studied. Plaques were defined as asymptomatic if no such events had ever occurred within their neurovascular territory. There was no significant difference between the symptomatic and asymptomatic groups in age, gender, or history of diabetes mellitus, hypertension, presence of an HMG-CoA reductase inhibitor (statin) on their prescription, and smoking.

The examination was performed with the subject in the supine position using a Philips (Bothel, WA) iU22 ultrasound scanner equipped with a high frequency linear array L12-5 MHz probe. The contrast agent used was SonoVue™ (Bracco spa, Milan, Italy). 2mL of this preparation was injected as an intravenous bolus into an antecubital vein. CEUS was performed with flash-imaging at intermediate

mechanical index of the carotid bifurcation and internal carotid artery, using a non-linear imaging (power modulation) contrast mode, 6 minutes following the bolus contrast injection. Six flash frames were acquired in less than 1 second in the axial orientation at the level of greatest stenosis. The cine-loop of the acquisition was saved on the hard-drive and QLAB software (Philips; Bothel, WA) was used to quantify echo intensity of the plaque using raw linear data. All regions of interest (ROIs) were drawn by an ultrasonologist with 17 years experience (EL) who was blinded to the medical history. Using the fundamental B mode image, a single ROI was drawn on the outline of the plaque. The ROI is automatically mapped to the same position on the contrast image, and QLAB calculates the signal intensity of each pixel within the ROI. The mean signal intensity is then automatically calculated. A second ROI was drawn around the residual lumen to calculate mean signal intensity in the lumen.

The data was log transformed for statistical analysis. The signal intensity of the plaque was normalised by dividing the plaque signal intensity by the lumen signal intensity (because the data was log transformed, normalisation required subtracting the lumen signal intensity from the plaque signal intensity). The normalised signal was compared between the two groups (symptomatic and asymptomatic) using the t-test, assuming unequal variances.

RESULTS

The LP-CEUS normalised plaque intensity was significantly greater in the symptomatic group 0.3899 (95% CI: -0.1056 to 0.8854) than the asymptomatic group -0.6869 (95% CI: -1.036 to -0.3380), (P=0.0005). Of note, the lowest signal intensity from the symptomatic group was derived from the subject who had the longest event to scan time (of nearly 1 year). For this subject, the signal fell below the mean of the asymptomatic group.

There was no correlation between normalised LP-CEUS plaque intensity and percentage luminal stenosis (P=0.27).

There was no evidence of a relationship between diabetes, smoking history, or statin dose with LP-CEUS signal, nor of differential LP-CEUS signal between those subjects in the symptomatic group with TIA versus CVA.

Figure 1
Normalised Plaque LP-CEUS signal Intensity

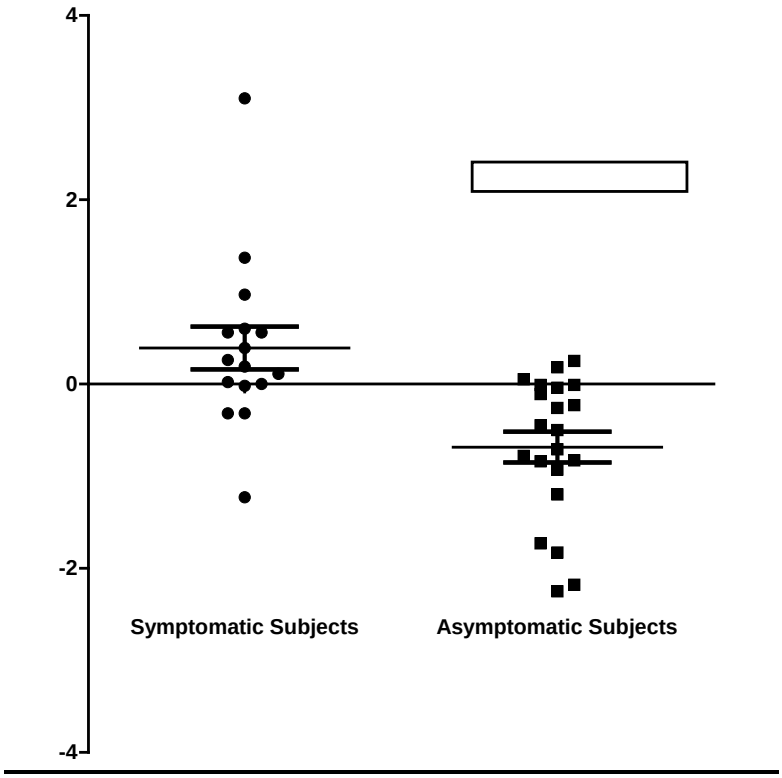

The figure shows mean and standard error of mean

DISCUSSION

Our study has demonstrated that the LP-CEUS signal intensity of carotid plaques is greater from plaques which are symptomatic (ie within the neurovascular territory of a recent cerebrovascular event), compared those which are asymptomatic. This suggests that plaques responsible for cerebrovascular events are those that tend to have late sonographic enhancement. This finding may merely represent the fact that symptomatic plaques have more intraplaque blood volume than asymptomatic plaques, and thus contain more circulating microbubbles in the late phase, just as they do with dynamic contrast enhanced ultrasound (10). But this is unlikely because, during the dynamic phase, the signal from the lumen is approximately two orders of magnitude greater than the signal from the plaque. Were the late phase plaque signal purely a result of circulating microbubbles, it should only represent a small fraction of the late phase lumen signal. The fact that the late phase signals of plaque and lumen are of similar magnitude, implies that microbubbles have accumulated within the plaque. Biological plausibility of this theory is provided by preclinical work demonstrating that microbubbles are passively targeted to tissue with activated endothelium and/or inflammation (6;8;9). We therefore suggest that by detecting retained untargeted microbubbles, LP-CEUS has the potential to detect inflammation and/or endothelial activation within carotid plaque *in vivo*.

CONCLUSION

By quantifying intraplaque inflammation, LP-CEUS is able to distinguish groups of symptomatic from asymptomatic patients. LP-CEUS may therefore represent a tissue specific marker of inflammation.

Reference List

(1) Virmani R, Burke AP, Farb A, Kolodgie FD. Pathology of the vulnerable plaque. J Am Coll Cardiol 2006 Apr 18;47(8 Suppl):C13-C18.

(2) Schaar JA, Muller JE, Falk E, Virmani R, Fuster V, Serruys PW, et al. Terminology for high-risk and vulnerable coronary artery plaques. Report of a meeting on the vulnerable plaque, June 17 and 18, 2003, Santorini, Greece. Eur Heart J 2004 Jun;25(12):1077-82.

(3) van der Wal AC, Becker AE, van der Loos CM, Das PK. Site of intimal rupture or erosion of thrombosed coronary atherosclerotic plaques is characterized by an inflammatory process irrespective of the dominant plaque morphology. Circulation 1994 Jan;89(1):36-44.

(4) Boyle JJ. Association of coronary plaque rupture and atherosclerotic inflammation. J Pathol 1997 Jan;181(1):93-9.

(5) Moreno PR, Falk E, Palacios IF, Newell JB, Fuster V, Fallon JT. Macrophage infiltration in acute coronary syndromes. Implications for plaque rupture. Circulation 1994 Aug;90(2):775-8.

(6) Lindner JR, Dayton PA, Coggins MP, Ley K, Song J, Ferrara K, et al. Noninvasive imaging of inflammation by ultrasound detection of phagocytosed microbubbles. Circulation 2000 Aug 1;102(5):531-8.

(7) Yanagisawa K, Moriyasu F, Miyahara T, Yuki M, Iijima H. Phagocytosis of ultrasound contrast agent microbubbles by Kupffer cells. Ultrasound Med Biol 2007 Feb;33(2):318-25.

(8) Lindner JR, Coggins MP, Kaul S, Klibanov AL, Brandenburger GH, Ley K. Microbubble persistence in the microcirculation during ischemia/reperfusion and inflammation is caused by integrin- and complement-mediated adherence to activated leukocytes. Circulation 2000 Feb 15;101(6):668-75.

(9) Tsutsui JM, Xie F, Cano M, Chomas J, Phillips P, Radio SJ, et al. Detection of retained microbubbles in carotid arteries with real-time low mechanical index imaging in the setting of endothelial dysfunction. J Am Coll Cardiol 2004 Sep 1;44(5):1036-46.

(10) Xiong L, Deng YB, Zhu Y, Liu YN, Bi XJ. Correlation of carotid plaque neovascularization detected by using contrast-enhanced US with clinical symptoms. Radiology 2009 May;251(2):583-9.

In vivo targeting of mouse carotid artery endothelium using echogenic perfluorohexane loaded macrophages

Kornmann LK, Zernecke A, Curfs DM, van der Made I, Janssen BJ, De Winther MP, Reneman RS, Hoeks AP, Reesink KD

Background

Molecular imaging of the microcirculation using ultrasound contrast agents is shown to be successful. Targeting the endothelium of large arteries, however, is difficult due to demanding adherence requirements as a result of a high wall shear stress.

Aim

To investigate the potential of monocytes to act as ultrasound contrast agent, providing selective adhesion to activated murine carotid artery endothelium and echo signal enhancement.

Methods

Murine bone marrow derived macrophages (BMM) were incubated for 3h with different concentrations of perfluorohexane (PFH) emulsions (Fig. A). Effects of PFH loading on BMM adhesion molecule expression (i.e., PSGL-1, VLA-4, Mac-1, LFA-1) were analyzed by flow cytometry. Static (no flow) adhesion of PFH loaded BMM to TNF-α stimulated b.End5 endothelial cells was assessed *in vitro* by microscopy. Echogenic potential was evaluated in an experimental setup (agar wells) using a medical ultrasound scanner. The size distribution of loaded and unloaded BMM was compared to native murine blood leukocytes by microscopy (N=200 per group). *In vivo*, echogenicity of the BMM in blood was evaluated with an ultrasound scanner for small animals. The interaction of the BMM with TNF-α stimulated endothelium in the carotid artery was assessed by intravital microscopy.

Results

In vitro, incubation of BMM with PFH emulsions resulted in dose-dependent uptake and echogenicity (5-17 dB). Flow cytometry showed no down-regulation of BMM adhesion molecule expression due to PFH loading. Static adhesion to b.End5 endothelial cells was preserved, although PFH loading tended to attenuate the number of adherent cells. Both loaded and unloaded BMM (medians 17.3 and 16.6 μm, no difference in size, p=0.051) were significantly larger than blood monocytes (14.0 μm), but distributions were overlapping in the 12-16 μm range. After intravenous injection, PFH loaded BMM did enhance blood echogenicity *in vivo*, but unloaded BMM did not (Fig. B). Moreover, the injected

macrophages exhibited rolling and adhesion behaviour on the TNF-α stimulated carotid artery endothelium, similar to native blood leukocytes (Fig. C). Rolling behaviour was not different (p=0.33) between PFH loaded and unloaded BMM (Fig. D). Similarly, there was no difference in the number of adherent loaded and unloaded BMM (p=0.25).

Conclusion

Our findings demonstrate that, *in vivo*, perfluorohexane loaded macrophages enhance the echogenicity of circulating blood. Moreover, the loaded macrophages roll and adhere selectively to carotid artery endothelium under physiological flow conditions, which substantiates their potential to act as contrast agent.

Figure: see below

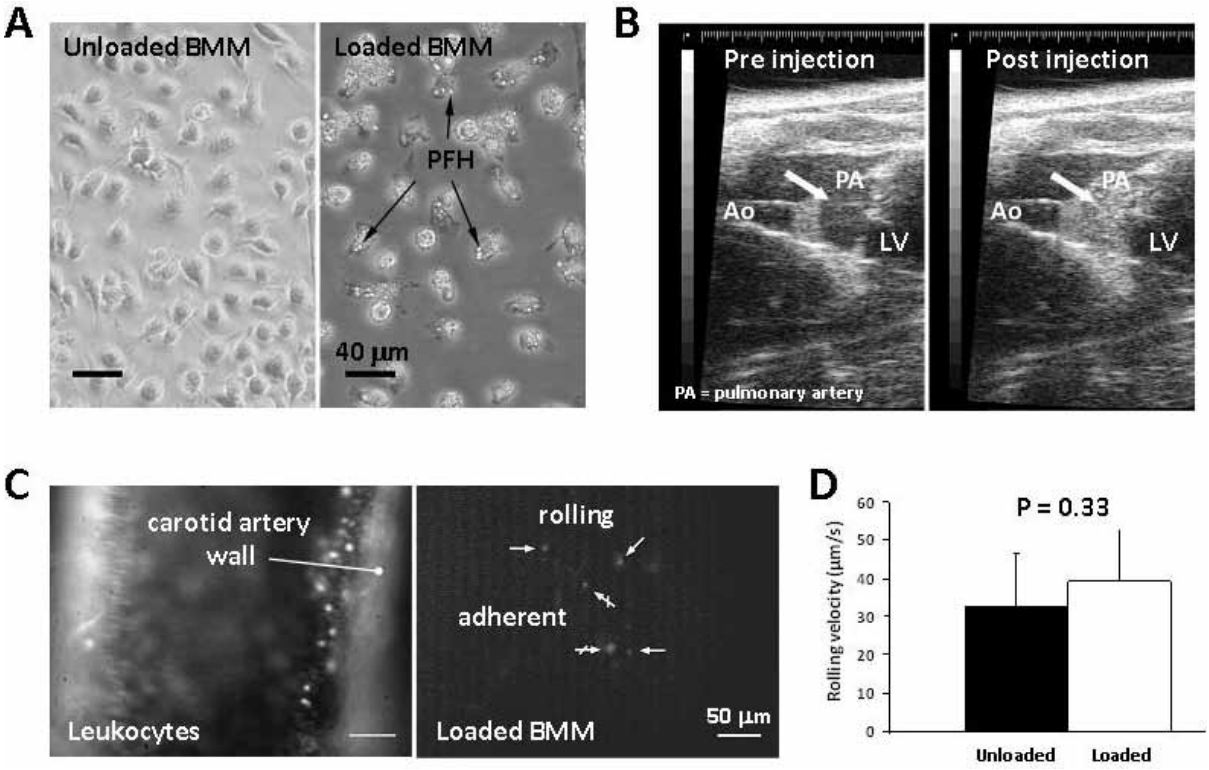

Imaging Angiogenesis with Cyclic Peptide Microbubbles

C. Anderson, X. Hu, J. Tlaxca, A.L. Klibanov, M. Lawrence, K. Ferrara, J. Rychak

Ultrasound molecular imaging of angiogenesis has strong potential for both clinical use and as a research tool in tumor biology and development of anti-angiogenic therapies. In the current study, we describe the development and characterization of microbubbles bearing cyclic peptides. Such small peptides offer the advantages of low cost and ease of synthesis relative to conventional protein ligands, although the target specificity of small ligands can be sub-optimal. Two ligands were examined: 1) a cyclic RGD peptide, which is known to bind alpha-v beta-3 and other integrins that are up-regulated on angiogenic endothelium, and 2) a control cyclic RAD peptide which was not expected to exhibit any integrin adhesion. Peptides were bound to the microbubble surface using covalent conjugation chemistries, and conjugation efficiency was assessed fluorometrically. We measured the adhesion of targeted microbubbles under laminar flow conditions on a surface of recombinant murine alpha-v beta-3 integrin. Significant adhesion of cRGD, but not cRAD, microbubbles was observed; binding was reduced by >90% upon blocking with an anti-alpha- v beta-3 integrin antibody. We next assessed microbubble adhesion on confluent murine endothelial cells that express alpha-v beta-3, and observed approximately 10-times greater adhesion of cRGD compared to cRAD or naked microbubbles. However, pre-incubating the endothelial cells with blocking antibodies against the alpha-v, beta-3, or both subunits of the integrin resulted in 80%, 44%, and 75% reduction in cRGD microbubble adhesion, respectively. This data suggests that although the cRGD peptide is able to bind alpha-v beta-3 integrin with affinity sufficient to mediate microbubble adhesion, endothelial cells may express other targets that may account for up to ~20% of the observed microbubble retention. We assessed cRGD and cRAD microbubble adhesion in two mouse models of tumor angiogenesis: a syngeneic model of gastrointestinal cancer and a human xenograft model of breast cancer. We observed approximately 15-20 times greater signal from cRGD microbubbles relative to non-targeted control microbubbles in both models. Interestingly, we observed a significant signal from cRAD microbubbles in both models, although at different magnitudes. Our results suggest that microbubbles targeted with a cyclic RGD-containing peptide are able to bind to alpha-v beta-3 integrins, although other targets are expressed in vitro and likely in vivo. The correlation between these unknown targets and angiogenesis is not yet known. Additionally, cRGD microbubbles exhibit significant accumulation and contrast enhancement in mouse models of tumor growth.

The 15th European Symposium on Ultrasound Contrast Imaging Rotterdam is sponsored by:

GE Healthcare
Mrs. Julie Woodland
Senior Brand Manager
MR and Ultrasound
Medical Diagnostics
Amersham Place
Little Chalfont Bucks HP7 9NA - UK

SIEMENS AG - Ultrasound Division
Mr. Richard Medley, Product Manager
H WS ES US CRM Operations
Sir William Siemens Square
Newton House
Frimley, Camberley, SY GU16 8QD - UK

PHILIPS Medizin Systeme GmbH
Mr. Janusz Bielczynski
CV Ultrasound Marketing Manager
Hewlett Packard Str.2
D-71034 Boeblingen
Germany

ZonMw
Mr. H.J. Smid
Research and Innovation
Postbus 93245
2509 AE Den Haag
The Netherlands

Oldelft BV
Mr. R. 't Hoen
Elektronicaweg 10
2628 XG Delft
The Netherlands

BRACCO International BV
Mr. Marco Graf, Congress Manager
GCO Global Strategic Marketing
Centro Galleria 2
Via Cantonale
CH-6928 Manno
Switzerland

KNAW
Dr. R.J.H. Trienes
Manager International Research Grants
P.O. Box 19121
1000 GC Amsterdam
The Netherlands

Erasmus Trustfonds
Drs. R. Rijntjes
Eendrachtsweg 41
3012 LD Rotterdam
The Netherlands

Visualsonics
Mr. Anil K K Amlani
Acting President and CEO
3080 Yonge Street
Toronto, Ontario
M4N 3N1 - Canada

Coeur
Mr. J.W. Deckers
Erasmus MC - Thoraxcenter
Dr. Molewaterplein 50
3015 GE Rotterdam
The Netherlands

The 15th European Symposium of Ultrasound Contrast Imaging, Rotterdam is sponsored by: